The Gaia Mission and the Asteroids. A perspective from space astrometry and photometry for asteroids studies and science.

D. Hestroffer, Aldo Dell'Oro, Alberto Cellino, Paolo Tanga

The Gaia Mission and the Asteroids.

A perspective from space astrometry and photometry for asteroids studies and science.

Daniel Hestroffer[1], Aldo dell'Oro[2,1], Alberto Cellino[2], Paolo Tanga[3]

[1] IMCCE, CNRS, Observatoire de Paris, 77 avenue Denfert Rochereau, 75014, Paris, France
e-mail:hestroffer@imcce.fr

[2] INAF-Osservatorio Astronomico di Torino, strada Osservatorio 20, 10025 Pino Torinese, Italy
e-mail: delloro@oato.inaf.it, cellino@oato.inaf.it

[3] Cassiopée, CNRS, Observatoire de la Côte d'Azur, France
e-mail: Paolo.Tanga@oca.eu

Summary. The Gaia space mission to be operated in early 2012 by the European Space Agency (ESA), will make a huge step in our knowledge of the Sun's neighborhood, up to the Magellanic clouds. Somewhat closer, Gaia will also provide major improvements in the science of asteroids, and more generally to our Solar System, either directly or indirectly. Gaia is a scanning survey telescope aimed to perform high accuracy astrometry and photometry. More specifically it will provide physical and dynamical characterization of asteroids, a better knowledge of the solar system composition, formation and evolution, local test of the general relativity, and linking the dynamical reference frame to the kinematical ICRS. We develop here the general aspects of asteroid observations and the scientific harvest in perspective of what was achieved in the pre-Gaia era. In this lecture we focus on the determination of size of asteroids, shape and rotation, taxonomy, orbits and their improvements with historical highlight, and also the dynamical model in general.

Key words: Gaia ; astrometry ; photometry ; asteroid physical properties ; dynamic ; orbit determination

In memoriam of Jacques Henrard (1940–2008). We dedicate this article to this wonderful colleague from the FUNDP (Namur), who was—as long as possible—an assiduous participant to such winter schools of the CNRS, and did always share his bright mind and high excitement in science and research.

Foreword

This paper is a compulsion of several of this CNRS school courses given in Bad-Hofgastein completed by some additional material. It is not intended to give a complete review of the Gaia capabilities for asteroids science, or of the treatment of orbit determination and improvement since the beginning of orbit computation. Neither will it cover each of the different techniques used for any particular problem. We hope however that it gives an overview of the Gaia mission concept, astrometry and photometry of asteroids (and small bodies) in particular from space, and current developments in this research topic. Besides, this school being in French in a German speaking place, some French and German bibliography have sometime been favoured or added.

1 Introduction

Before entering into the description of the Gaia mission observations and the discussion of the expected results for asteroids science, we will briefly remind the basic principles from the Hipparcos mission, and then give an overview of the Gaia objectives (§2). We will present the Gaia satellite and instruments as well as its operational mode (§3), and expected scientific results for the Solar System (§4). In the next sections we will develop more specifically three aspects: the astrometric CCD signal yielding the fundamental astrometric position and marginal imaging capabilities (§5), the photometric measure yielding physical properties of asteroids (§6) and the dynamical model from the asteroids astrometry (§8). This provides a solid overview of what can be achieved in the domain of planetology and dynamical planetology of asteroids. The following sections are more general and not exclusively related to Gaia. There we develop the general problem of orbit determination and improvement for the case of asteroids orbiting around the Sun (§9), we give a short description of both historical and modern methods. Finally we treat the case of orbit determinations of binaries (§10) focusing mainly on resolved binaries. But since the problem of orbit reconstruction for extra-planetary systems appeared to be of importance for this school it has been briefly addressed here through the problem of astrometric binaries (§10.4). Extra-solar planets is another topic actually addressed by Gaia, but this is out of the Solar system, and out the topic of the present lecture.

2 Gaia – The context

2.1 Before Gaia – The Hipparcos legacy

Ten years have passed now since the publication of the Hipparcos catalogue in 1997. This space mission did provide a scientific harvest in many fields of astronomy and even, indirectly, in Earth science [85]. The Hipparcos mission provided a homogeneous astrometric catalogue of stars with more sources and more precise than were the Fundamental Katalog series during the 20^{th} century. The acronym "HIgh Precision Parallax COllecting Satellite" –in honour of the Greek astronomer Hipparchus—recalls that the basic output is of course the measure of the parallax of

stars and their proper motions. In fact there were two programmes or instruments on board the satellite: Hipparcos and Tycho. Both provide astrometry and photometry of the celestial sources that were observed over the period 1989-1993, and two catalogues of stars were derived as well, the Hipparcos and Tycho catalogues. The Tycho data is based on the "sky mapper" which gives the detection of sources and triggers the main astrometric field observations for Hipparcos. It is hence less precise than Hipparcos but has more targets (about 2,500,000 stars in its version second version Tycho2 in the year 2000) than Hipparcos (about 120,000), and provides two-dimensional astrometry as well as photometry in two bands close to the Johnson B and V. Additional treatment of the raw data has been undertaken [117]. Further details on the Hipparcos/Tycho mission and instrumentation can be found in e.g. [57, 58] in the context of high accuracy global astrometry, and [43, 47, 84, Vol. 1, Sec. 2.7] for all details on the solar system objects observations and catalogues. The Hipparcos and Tycho Solar System Annex files (`solar_ha, solar_hp,solar_t`) are available on the CDS data-base[4]. While Hipparcos and Tycho were designed to observe stars, they nevertheless could also provide data for solar system objects: 48 asteroids, 5 planetary satellites and 2 major planets[5]. There were different limiting factors depending on the programme instrumentation: for Hipparcos, magnitude brighter than $V \leq 12.4$ and size smaller than $\phi \leq 1$ arcsec, for Tycho magnitude brighter than $V \leq 12$ and size smaller than $\phi \leq 4$ arcsec. But the more stringent one was that Hipparcos could only observe a very limited number of objects in its field of view (FOV), both for stars or asteroids.

The basic principle of the mission was to derive relative positions of targets observed simultaneously in two well separated fields of view. The measure principle consists basically in observing the target while it crosses the field of view with a photometer and to record the photon flux as modulated by a periodic grid. In addition to the relative astrometry given by the grid, the photometers also recorded the total flux, providing the magnitudes in the broad $Hp \approx V_J + 0.3035\,(B - V)$ system for Hipparcos, and in two (red and blue) bands for Tycho. The Tycho astrometric and photometric data are less precise than their Hipparcos counterpart, and concern only 6 asteroids compared to 48 asteroids observed within the Hipparcos mission.

The Hipparcos measure of position and magnitude of these selected solar system objects provided many scientific outcomes. We list a few showing the diversity of the applications:

- From the observed positions of the satellites, and taking one model for their ephemerides, one can derive the (pseudo-)position of the system barycenter, and/or the center of mass of the planet, as well. Such positions are model dependant since one uses the theory for the orbits of the satellites, but they are far more precise than direct observations of the planets themselves [73].
- The particular photometry derived by one of the data reduction consortium (FAST) comprises the classical apparent magnitude together with an additional one that is biased for non point-like sources. This allowed to indirectly resolve the object and derive information on its size and light distribution [46].

[4] URL: http://webviz.u-strasbg.fr/viz-bin/VizieR?-source=I/239/

[5] Pluto was not observed which spare us the trouble of having to name this object observed in the past, before last IAU resolution.

- Hipparcos astrometry enabled the determination of the mass of (20) Massalia from a close encounter with the asteroid (44) Nysa [4].
- High accuracy astrometry of asteroids enabled to improve their ephemerides [50], and also to detect small systematic effects due to the photocentre offset[44].
- High accuracy astrometry of asteroids enables to link the dynamical inertial frame to the catalogue [101, 5, 22].
- The stellar astrometric catalogue, mostly Tycho2, has an indirect consequence on science for the Solar System. Such stars provide better astrometric reductions for modern CCD observations of solar system objects, as well as re-reduction for older plates (the problem is still the low density when compared to e.g. UCAC2); they also provide much better predictions for stellar occultation path [26, 102, 28].

Compared to Gaia observation and science of solar system objects, Hipparcos was most a (nice) prototype, or a precursor. They still have many common points:

- obviously space-based telescopes are exempt from all many atmosphere-related problems (seeing, refraction, ...) and provide better stability (mechanical thermal) and a better sky coverage (not limited to one hemisphere);
- scanning law with a slowly precessing spin axis (going down to solar elongations $\approx 45^\circ$);
- simultaneous observation of two fields of view for global astrometry;
- astrometric and photometric measurement, the colour-photometry being mandatory for correction to the astrometry.

The main difference between the two missions arise from the use of CCD device for Gaia instead of a photo-multiplier channel with Hipparcos/Tycho, and to a lesser extent the capabilities of onboard data-storage as well as data transmission to the ground-segment. Albeit CCD observations were already in use in astronomy and astrometry in particular during the 80's, Hipparcos could not benefit of this technique: CCDs were still not validated for use in space (which requires a higher quality and robustness) and in any case the design of the satellite had to be set long before the beginning of the mission (often satellites are launched with outdated material). The consequences are dramatic in terms of number of celestial bodies observable and general astrometric and photometric accuracy: Gaia is not an Hipparcos-II. The limiting magnitude of Tycho was $V \leq 12$, but the catalogue is far from being complete[6] at that level; in comparison the limiting magnitude of Gaia will be $V \leq 20$. The border of Hipparcos is at 200 kpc, while Gaia will reach a large part of the Milky Way up to the Magellanic clouds.

In this respect also Gaia is different from the SIM mission [98, 99] (USA) which will provide very accurate parallax but for a very limited number of targets. The smaller Japanese mission Jasmine has more common points but, observing in the infra-red, the scientific goals are orthogonal and complementary. Last, the two European satellites differ in their location in space, Hipparcos missed its geostationary orbit and was on an eccentric one, Gaia will be at the L2 Sun-Earth Lagrangian point. Gaia will also observe a large number of solar system objects (mainly asteroids) which data will provide new insights and scientific results as developed in the next sections.

[6] Hipparcos with its larger-band filter can reach slightly fainter magnitudes, 12.5, but is anyway much less complete than Tycho.

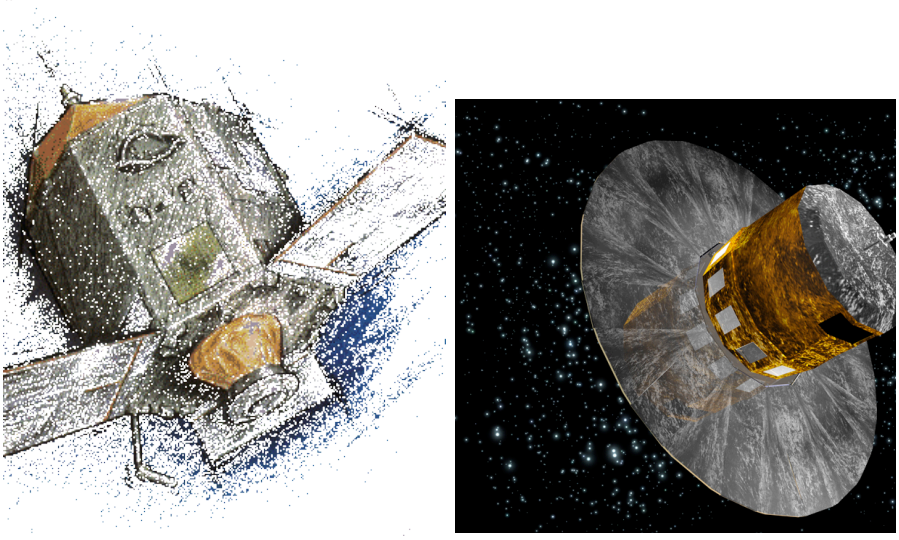

Fig. 1. The Hipparcos (left) and Gaia (right) satellites in a pictorial view. Hipparcos: one sees above the thruster and solar arrays one of the telescope baffle, for one of the observing direction. Gaia: the large, circular sunscreen will be deployed after launch and cargo to L2, it protects the instruments and permit their thermal stability. The telescopes, detectors and associated circuitry are situated inside the hexagonal or cylindrical housing.

2.2 What is Gaia?

The Gaia mission was designed to provide a renewed insight in the Galaxy structure, through a homogeneous set of very accurate measurements of stellar positions, motions and physical properties [69, **?**]. However, the independence from any input catalogue grants that a very large number of non-stellar sources will be additionally observed. In fact, Gaia will automatically select observable sources with a criteria mainly based on a single parameter, the magnitude threshold ($V < 20$).

During the preliminary study of the mission, the community of planetologists realised that the observations of asteroids by Gaia may have a strong scientific impact, allowing a general improvement of our view of the Solar System of the same order as in the case for stars [**?**]. Of course, the reasons are similar and are built on the unprecedented astrometric accuracy of Gaia and on its spectro-photometric capabilities.

One will note, however, that the strongest quality of the Gaia data—beside accuracy—will reside in homogeneity. In fact, no other single survey have produced an equivalent wealth of data for 300,000 Solar System objects, as is expected for

Gaia [70]. As we will illustrate in the following, a complete characterisation of the small bodies of the Solar System will be possible.

We can also compare Gaia to other forthcoming deep surveys, such as the very important Pan-STARRS[7], expected to map the whole observable sky 3 times per month at greater depth (V∼24, for the single observation at SNR=5). In this case, even more objects will be detected, and this will constitute a serious advantage to feed investigations of smaller or more distant and fainter asteroids. However, the astrometric and photometric accuracy—despite being optimised—will remain limited by ground-based conditions, and spectro-photometry will not be of the same level as in the case of Gaia. Other typical observational constraints for ground-based investigations also apply to Pan-STARRS, including the minimum Sun elongation that will be reached, severely limiting its capabilities for the investigation of peculiar asteroid categories, like Earth crossers or the Inner Earth Objects. Last the sky coverage is limited to one hemisphere and *global astrometry* is hardly achieved with such systems (on the other hand they will benefit of the Gaia catalogue of stars).

For these reasons, and despite the limitation in brightness to V∼20, we believe that Gaia is rather unique and really has the potential to have a major impact in Solar System science. In this lecture, we will try to focus on the kind of data that the mission will provide, and on the corresponding data treatment that is being conceived in order to extract the relevant information. Hopefully, the observer will appreciate the techniques allowing to reach an exceptional accuracy, and the theoretician will find interesting new problems that must be solved to fully exploit the data scientific content.

3 The Gaia mission

3.1 Launch and orbit

The Gaia satellite will fit into the payload bay of a Soyuz fregat vector, that will be launched from the European base of Kourou (French Guyana). After a ∼1-month travel, it will reach the L2 Lagrangian equilibrium point, that is situated 1,5 million km from Earth, opposite to the Sun. The satellite will then deploy the solar panels, fixed on a large, circular sunscreen (diameter: 10 m) that lies on a plane perpendicular to the spin axis (Fig. 1). The visibility of the satellite and the data link are reduced when compared to a geostationary orbit, but the environment is quieter. The L2 point is a dynamically unstable equilibrium location, requiring firing the satellite thrusters to apply trajectory corrections every ∼1 month. Gaia will thus be maintained on a Lissajous orbit around L2, allowing it to avoid eclipses of the Sun in the Earth shadow. The location thus appears as an optimal choice for constant sunlight exposure, and for maximum thermal stability. The planned operational lifetime of the mission will be 5 years.

3.2 The spacecraft

The beating heart of the satellite is enclosed in an approximately cylindrical structure, including all the relevant parts: the thrusters openings and their fuel tanks,

[7] http://pan-starrs.ifa.hawaii.edu/public/

the electronic equipment, and of course the optical train. Since we are interested in the observations, we will just give some fundamental design principles concerning the latter component [**?**].

The optical bench structure is based on an octagonal toroid built in silicon carbide. This is a critical component, supporting all the optics and the focal plane. The measurement principle—being similar to that of Hipparcos—requires two different lines of sight, materialised by two Cassegrain telescopes. The primary mirrors are rectangular and measure 1.45×0.50 m^2. Five additional mirrors are required to fold the optical path, obtaining an equivalent focal length of 30 m. The light beams are combined and focused on a single focal plane, composed by a matrix of 106 CCDs. The extreme rigidity of the toroidal structure (actively monitored during the mission) ensures that the angle between the two telescopes (also called "basic angle") remains constant at 106.5 degrees.

The CCD array constitutes a large, 1-Gpixel camera, that can be compared (in pixel number) to the Pan-STARRS cameras. However, it remains unrivalled in surface, since it extends over 0.93×0.46 m, by far the largest CCD array ever conceived.

The resolution anisotropy due to the rectangular entrance pupil of the telescopes are matched by strongly elongated pixels, about three times larger along the direction in which the diffraction spot is more spread.

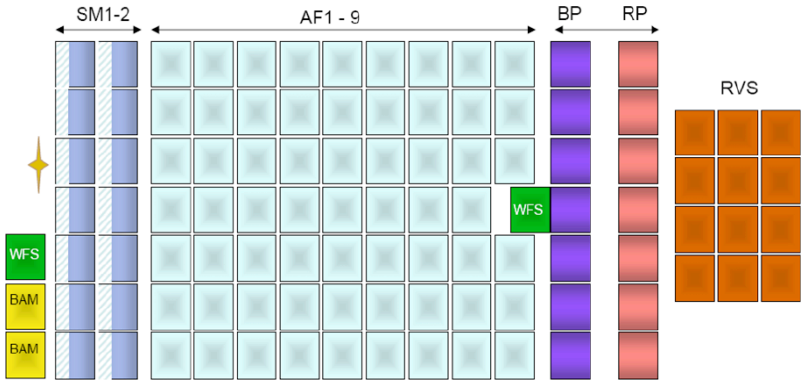

Fig. 2. The focal plane receives the light beams of both telescopes. While spinning, Gaia scans the sky in such a way that images of sources enter the focal plane from the left and cross it moving toward the right. The whole crossing takes about 1 minute. Each CCD is crossed in 3.3 seconds. See the text for instrument details. The Basic Angle Monitoring (BAM) and Wave-front Sensor (WFS) CCDs are used for monitoring tasks.

The general organisation of the focal plane is illustrated in Fig. 2. Different groups of CCDs are identified depending upon their functions, since they correspond in all respects to different instruments. The main Gaia instrument is the Astrometric Field (AF), receiving unfiltered light, which is devoted to produce ultra-precise

astrometry of the sources [**?**]. The other instruments are aimed at achieving spectral characterisation. The figure shows the Red and Blue Photometers (RP and BP), which will be receiving light dispersed by a prism, and have optimised sensitivity in two different, contiguous portions of the visible spectrum. The resolution of RP and BP is rather low, each portion being spread on ∼30 pixels. The Radial Velocity Spectrograph (RVS), on the other hand, provides a spectrum in a restricted wavelength range ($847 - 874\,\mathrm{nm}$) but with much higher resolution. It is aimed at sampling some significant spectral lines that can be diagnostic of stellar composition and can be used to derive radial velocities with a $\sim 1\,\mathrm{km.s}^{-1}$ typical uncertainty. Due to star crowding (superposition of spectra) and SNR constraints, RVS will have a limit magnitude at $V = 17$. This instrument will provide no scientific information for asteroids. On another hand the measures for the bright asteroids will be used to calibrate the kinematic zero point of the RVS, as a complement to the data from IAU standard stars.

Since Gaia is continuously spinning with a rotation period of 6 hours, the sources will drift on the focal plane, entering from the left in the scheme of Fig. 2 and travelling toward the right. The displacement will be compensated by a continuous drift of the photoelectrons on the CCD at the same speed; this technique (also used on fixed ground-based telescopes) is known as "TDI mode" (from "Time Delay Integration"). The resulting integration time (3.3 seconds) corresponds to the time interval required by a source to cross each CCD. Of course, this principle applies to all instruments. As a consequence, while an image of the source drifts on the AF CCDs, it will take the form of a dispersed spectra while moving on RP, BP and RVS.

An important part of the focal plane, the Sky Mapper (SM), requires some additional explanation. In fact, Gaia will neither record nor transmit to the ground reading values for all the pixels, due to constraints on the data volume. Conversely, only a reduced number of values ("samples"), representing the signal in the immediate surroundings ("window") of each source, will be processed and transmitted, and only for objects brighter than $V = 20$. These samples represent either the value of single pixels, or of some binning of couples of pixels, depending upon the star brightness. For stars with $V > 16$ (i.e., the largest fraction of sources) only 6 samples will be available, corresponding to the signal binned along 6 pixel rows in the direction perpendicular to the scan motion. These samples will be transmitted for each CCD in the AF field. Larger samples are required to accommodate the dispersion of RP, BP and RVS spectra.

As a consequence, the AF information on positions will be essentially one-dimensional, being very precise along the scanning circle, but very approximate in the across-scan direction. One should also note that the windows are assigned by the on-board algorithm after SM detection. Beside a confirmation of detection that is expected from the first AF column, no other controls are executed all along the focal plane crossing, and the window follows the object on each CCD, assuming that it shifts at the nominal scanning speed. While this is true for stars, we will see that Solar System objects will suffer measurement losses due to their apparent motion.

3.3 Observation principles: the scanning law

The accuracy requirements of the mission can be reached only if the sky coverage is fairly uniform. To obtain this result, the direction of the spin axis of the probe cannot obviously stay fixed, but it must change, slowly but continuously, to change correspondingly the orientation of the scanning circle on the sky.

Two additional rotational motions are thus added to the 4- revolutions-per-day satellite spin (Fig. 3). The first one is a precession of the spin axis in 70 days, along

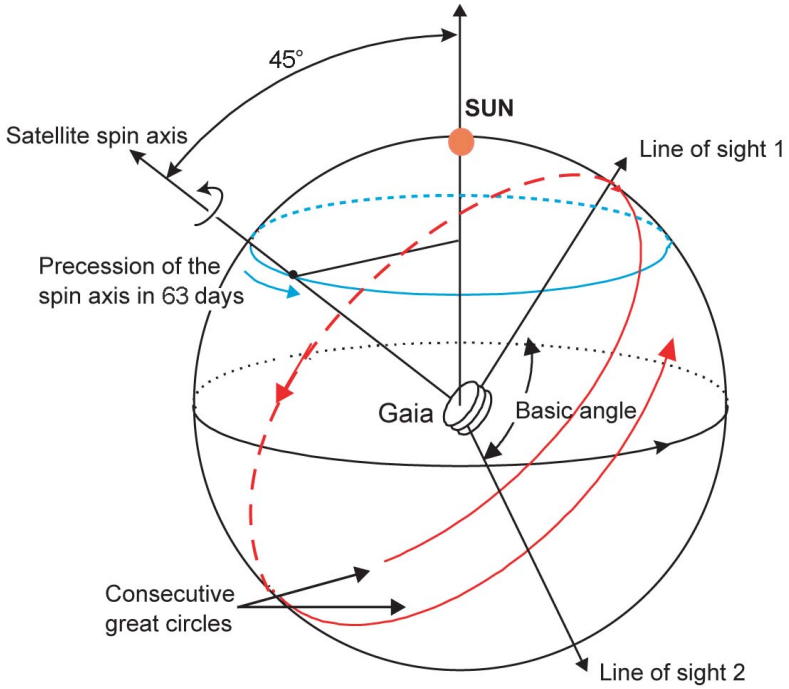

Fig. 3. The Gaia scanning law, composed by three rotations (spin, precession and orbital revolution) as explained in the text.

a cone whose axis points towards the Sun. The change in orientation of the latter, provided by the orbital revolution around the Sun in 1 year, is the last additional rotation.

The overall motion, beside being derived from the scanning law optimisation, is also compatible with the need of keeping the system in thermal stability, since the incidence angle of the Sun light on the solar screens remains constant, and the enclosure of the scientific instruments is always consistently shadowed.

The scanning law that results from the combination of the three rotations permits $60 - 100$ observations of any direction on the sky. Each one occurs with different orientations of the scan circle, allowing to reconstruct the full two dimensional

position of fixed sources from positional measurements that are essentially one-dimensional.

The availability of the observations in two simultaneous directions, and their multiplicity, has an important consequence: the star measurements contain both the information needed to map their position on the sky, and that needed to reconstruct the orientation of the probe at any epoch. For this reason, the process of astrometric data reduction—the so called "Global iterative solution"—is an inversion procedure allowing to retrieve at the same time the parameters that define star positions, their proper motion and the attitude of the probe. The applicability and performances of this strategy have been fully proved in the previous Hipparcos mission.

4 Solar System science

While scanning the sky, sources corresponding to Solar System objects (planets, dwarf planets, asteroids, comets, natural satellites, ...) will enter the Gaia field of view, and will be detected and recorded. The main difference with respect to stars will come from their motion. Their displacement on the sky have two main consequences: they will not be re-observed at the same position; their motion will not be negligible even during a single transit.

These two basic statements are sufficient to dictate the need of a special data treatment for these objects. Several specific problems can thus be identified at first order, deserving an appropriate data reduction chain; we cite here:

- image smearing during integration time;
- signal shape due to resolved size and/or shape;
- de-centering relative to CCD windows, or total loss during one transit;
- identification of new objects from detections at different epochs.

These issues are strictly related to the basic characteristics of the mission, but also other challenges are present when the science content to be extracted is considered. They will be discussed in the following sections.

A specific management activity for Solar System data reduction has been created in the frame of the DPAC (Data Processing and Analysis Consortium), as a part of the "Coordination Unit 4" devoted to process specific objects needing special treatment (double stars, exo-planet systems, extended objects, Solar System objects).

Following the most recent mission specifications, one can identify the categories of objects that will be really observed by Gaia. In fact, all sources that will appear larger than $\sim$ 200 milli-arcsecond (mas) will probably be discarded and have no window assigned. This selection automatically excludes from observations the major planets, some large satellites (such as the Galilean satellites of Jupiter, or Titan) and also the largest asteroids (or dwarf-planets) when closer to Earth (Ceres, Pallas, Vesta, in particular).

On the other hand, small planetary satellites very close to major planets will be accessible thanks to the low level of contamination from light scattered by the nearby planet. However, the vast majority of the observed objects will consist of asteroids of every category: mostly from the Main Belt, then small ones belonging to the Near Earth Object population, and some additional tens among Jupiter Trojans, Centaurs, and Trans-neptunians. Using the most recent survey data, we can

estimate a population of $\sim 300,000$ asteroids to be observable by Gaia, representing just 1/4000th of all the sources that Gaia will measure.

Each asteroid will be observed (by the AF) $\sim 60-80$ times during the nominal mission operational lifetime of five years, although the number of detections can be much lower for Near Earth Objects, sensibly depending upon the geometry of the observation. On average, we can estimate that no less than 1 asteroid/sec will enter the Gaia astrometric instrument when the viewing direction is close to the ecliptic.

Most asteroids will be known when Gaia will fly, so the discovery potential of Gaia remains low and does not constitute in itself a reason of special interest for the mission. One exception can probably be represented by specific object categories easily escaping most ground-based surveys, such as low elongation Inner Earth Objects.

In fact, the geometry of the observations relatively to the positions of the Sun and the Earth can be easily estimated since most of the Solar System objects orbit the Sun at very low ecliptic inclinations. It is thus straightforward to use the

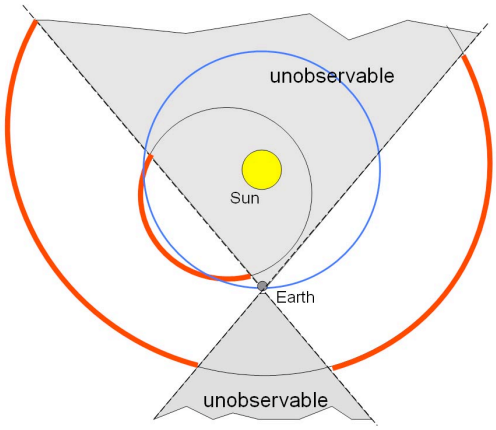

Fig. 4. At any given position along Earth orbit, the sky not accessible to the Gaia scan motion is delimited by two cones centered around opposition and conjunction with the Sun. When projected on the ecliptic, the unobservable region appears as the two grey regions in this picture. The observable portion of the orbit of a NEA and an MBA is enhanced.

relevant angles to identify the regions of the ecliptic plane that can be visited by the Gaia scanning circle. The result is shown in Fig. 4 where the dashed sectors represent the viewing directions that are compatible with the scanning law. As one can see, Gaia will never observe neither at the opposition nor toward conjunction, but mostly around quadrature.

More precisely, while quadrature represents the average direction, it won't be the most frequent one, since the intersection of the scan plane with the ecliptic spends most of the time preferentially close to the extremes of the accessible region.

The region at ∼45 degrees elongation from the Sun will thus be explored and could represent the most fruitful area for discovery purposes. Another poorly known population, not easily accessible from the ground, is the one represented by asteroid satellites. In fact, binaries larger than ∼120 mas will be seen as separate sources by Gaia, and today it is hard to estimate how many of them will be discovered.

However, we stress that the full physical and dynamical characterisation of known objects is the much more ambitious and rewarding goal that is expected from the Gaia mission. In fact, preliminary studies have shown that the precision of Gaia observations (both for photometry and astrometry) will be able to improve by more than 2 orders of magnitude the quality of asteroids orbits [104], to derive a mass from mutual perturbations for ∼150 asteroids [70], to derive for most of them a shape and the rotational properties by lightcurve inversion [20], to measure General Relativity PPN parameters [45], to directly measure asteroid sizes [**?**], to constrain non-gravitational accelerations acting on Earth crossers [105]. We will detail in the following the most relevant of these issues.

As a result, we can already guess today that Gaia will open new perspectives for a better understanding of the Solar System—of asteroids in particular—portraying in a self-consistent way both dynamical and physical properties. Subsequent studies will take profit of the situation, for example by rebuilding observational approaches that exploit better orbit and size and shape data (see e.g. the asteroid occultation case [103]).

5 Analysis of the astrometric signals

5.1 Introduction

The CCD signal of a minor body transiting in the field of view of Gaia is characterised by some features that make it different from the ideal signal produced by a fixed star, and for this reason it requires a special treatment with respect to the standard processing pipeline adopted for stars.

First, it is important to understand what we mean in this lecture when we speak of "fixed stars". A fixed star is an ideal point-like source whose motion on the celestial sphere can be considered nil during the time taken by the source to make a transit across the Gaia field of view (FOV). In practical terms, the celestial objects that most closely fit the above definition are not stars, but distant quasars.

It is obvious that the property of being a non-moving source refers to the celestial sphere and not to the Gaia focal plane, since the Gaia field of view continuously changes while the satellite makes its scan of great circles on the celestial sphere (as a first approximation). However, as we will see in the following discussion, it may be said that the apparent motion of a fixed star in the Gaia FOV is at least approximately cancelled out by the adopted process of signal acquisition.

In general, a point-like source produces a photon flux distribution across the focal plane that, for a rectangular pupil like that of Gaia, is essentially the Fraunhofer diffraction pattern corrected for the aberrations introduced by the instrument optics itself. It is not our intention to discuss here all the details of the optical configuration of Gaia, but it is necessary to point out at least a few basic concepts. First, the response of the instrument to the distribution of photons produced by a

point-like source is called Point Spread Function (PSF). The PSF is necessarily the starting point to develop any description of the astrometric performances expected from Gaia. More in particular, the diffraction pattern produced on the focal plane by a point-like source *not moving across the field of view* is known as the *optical* PSF. By "diffraction pattern" we mean the bi-dimensional spatial distribution of the incident photons on the focal plane per unit area per unit of time. This includes the aberrations introduced by the instrument optics, the transmittance of the instrument, the response of the CCD detectors, and it depends also on the spectral distribution of the source. In particular, if we call "quasi mono-chromatic optical PSF" the optical PSF produced by a source for which the spectral distribution of its emitted radiation is limited to a very small interval of wavelengths, then we may define a poly-chromatic optical PSF as the average of different mono-chromatic optical PSFs, each one weighted according to the spectral distribution of the source.

The situation is more complex if we consider the effects related to the actual area of the focal plane (that in the case of Gaia is quite large). Distortions introduced by the instrument aberrations depend on the position of the source in the field of view. Sources in different positions in the field of view produce PSFs centered in different locations in the focal plane. Then, PSFs detected in different points of the focal plane, even if produced by the same kind of source and spectral distribution, show different features.

Moreover, due to the fact that in the adopted Gaia instrument configuration the signals are detected by an array of distinct CCDs, each having a well defined quantum efficiency (QE) which is wavelength-dependent, it follows that the different spectral components of the PSF are detected with different efficiencies. For this reason, when we talk about the PSF, or in general the signal, of a generic source, it is more convenient and straightforward to refer to the number of photoelectrons produced by the CCD detectors per unit of time instead of the number of incident photons per unit time on the detector itself. In other terms, in the rest of this lecture we will call PSF the diffraction pattern including the effect of CCD quantum efficiency. It is worthwhile to point out that the QE of the CCDs in the Gaia astrometric focal plane is nominally the same for all of them, and that no additional filters are placed in front of them.

As a matter of fact, however, the PSF of fixed stars is even not observable in the sense explained above, due to two fundamental reasons. First of all, the spatial resolution of the detector is finite because so is the dimension of the CCD pixels. As a consequence, the detector does not give the number of photoelectrons generated in any arbitrary point of the CCD per unit area and unit time, but it gives the total (integrated) number of photoelectrons collected by each pixel during the integration time. In other terms, the optical PSF has to be integrated within the rectangular area of the pixel and within the duration of the integration time. The second reason why the optical PSF is not directly observable is that, due to the complex motion of the satellite which allows it to scan the celestial sphere, any source moves within the field of view during the time in which it produces photoelectrons in the focal plane (source transit in the Gaia FOV). As a consequence, the PSF moves on the focal plane. Accordingly, the PSF is collected by all pixels and CCDs on which the PSF itself transits. Due to the effect of the apparent motion of the source in the FOV, the detected PSF should be smeared along the path that the image follows on the focal plane. In order to avoid this very undesirable effect, a transfer of charges from

pixel to pixel towards the read-out register is done at the same velocity and along the same direction of the apparent image motion. This technique of read-out of the CCD is known as Time Delayed Integration (TDI) mode. In TDI, the generated photoelectrons "follow" the portions of the PSF that produced them. Ideally, if the motion of the charges followed exactly the same trajectory as that of the image in the focal plane and at the same continuous rate, the spatial distribution of the recorded photoelectrons would reproduce exactly the PSF. Unfortunately, this is not strictly true in practice, for the charge transfer is not a continuous process. What happens in practice is that the motion of the collected photoelectrons is produced by transferring all charges within one pixel into the adjacent one in the along-scan direction at regular time steps. The duration of the time step, indicated as the TDI period, is set in order to minimise the spread of the PSF due to the source motion. Nevertheless, the TDI mode cannot guarantee a perfect cancelation of the PSF smearing. The reason is that, even if the TDI period is kept constant and the charge transfer is done along the instantaneous scan direction, what happens is that the motion of the image is neither uniform nor aligned exactly in the along-scan direction. On one hand, this is simply due to the precession motion of the spin axis of the satellite, which is constantly changing the orientation of the along-scan direction. But even in the case that the motion of the image on the focal plane was perfectly uniform and exactly aligned with the along-scan direction, nevertheless the TDI mode could not correct completely the PSF smearing. The reason is that during each single TDI period the charges are not transferred, whereas the image moves and the signal is smeared. In this way, photons coming from the same point of the optical PSF may be collected by two different pixels. The final effect is that the PSF is broader and systematically displaced in the along-scan direction.

In principle, the TDI period should be equal to the along-scan dimension of the pixels divided by the image velocity. Non uniformity of the along-scan motion introduces further distortion due to deceleration and acceleration of the image with respect to the TDI mean motion.

The PSF including the finite size of the pixels and the effect of the TDI mode is called *total* or *effective* PSF. But the real signal is affected also by other sources of noise and distortion. First of all, the signal is produced by a stochastic process, corresponding to the random sequence of photon arrivals and photoelectron generation. Then, the final number of charges collected in a given pixel is a random number, typically governed by the Poisson statistics. Moreover, the signal is distorted by the effect of cosmic rays on the CCD, affecting also the Charge Transfer Efficiency (CTE) from one pixel to another. Some studies point out that some packets of charges can be entrapped and be released later without correlation with the regular TDI mode. All these effects introduce distortions of the final signal that are under investigation.

The treatment of the signals produced by Solar System objects (SSOs) is even more difficult than in the "simple" case of fixed stars described above. SSOs are differently from stars, in that they are characterized by a much faster apparent motion. When we say that SSOs move we intend that they display a motion with respect to the fixed stars. As a consequence, the trajectory of SSO images across the focal plane does not follow the same pattern of fixed stars in the same field of view and their motion is not properly corrected by the TDI mode.

SSOs have a residual velocity with respect to the apparent motion of a fixed star, and this residual velocity has components both on the along-scan and the across-scan direction. This fact has the consequence that their final signals are spread. Moreover, while we may expect that for fixed stars the time interval between the transit on a given CCD and the adjacent one in the along-scan direction is constant, being about equal to the number of pixels in the along-scan direction in a CCD multiplied by the TDI period, this is no longer valid for a SSO. The transit of a SSO image on a CCD is either delayed or anticipated with respect to that of stars, depending on the residual velocity.

Velocity is not the only one peculiar features of SSOs to be taken into account. Another effect is that these objects may appear in general, or very often, as extended sources. This means that the final signal is not simply due to the PSF as for the case of point-like stars, but each point of a SSO image produces an independent PSF, and the final signal is the sum of all these PSFs. This means that the signal of a SSO depends on the size, the shape and the brightness distribution of its image.

For all the above reasons the analysis of the signals of SSOs requires a special treatment with respect to the simpler one used for fixed stars.

5.2 Signal computation

Let be x and y the coordinates of a cartesian system associated to the focal plane, having the x-axis set along the scan direction and directed as the movement of charges of the TDI mode. Let $I(x, y)$ be the photoelectron distribution produced by the optical image of a non moving source, that is the number of photoelectrons generated per unit area and unit time around the point of coordinates (x, y). The function $I(x, y)$ contains information about both the PSF photoelectron distribution $f(x, y)$ and the apparent brightness distribution of the observed object $g(x, y)$. From a mathematical point of view, I is the convolution of f and g:

$$I(x, y) = \iint g(x', y') f(x - x', y - y')\, \mathrm{d}x' \mathrm{d}y' \tag{1}$$

For sake of brevity multiple integrals signs will be omitted in the following. Let now τ be the TDI period. The signal, that is the number of photoelectrons collected by a pixel whose centre has coordinates (α, β), during the interval of time τ, from a source image with centre located at coordinates (x_c, y_c), is given by:

$$S(\alpha, \beta) = \iiint I(x - x_c, y - y_c) \Pi\left(\frac{x - \alpha}{\Delta x}\right) \Pi\left(\frac{y - \beta}{\Delta y}\right) \Pi\left(\frac{t}{\tau}\right) \mathrm{d}x\, \mathrm{d}y\, \mathrm{d}t \tag{2}$$

where Δx and Δy are the along-scan and across-scan dimensions of the pixels, t is the time, and $\Pi(u)$ is the gate function equal to 1 for $-1/2 \leq u \leq 1/2$ and zero otherwise.

If now we assume that the image source moves with constant velocity, so that:

$$x_c = \dot{x}t + x_0 \qquad y_c = \dot{y}t + y_0$$

the signal becomes:

$$S(\alpha,\beta) = \int I(x-\dot{x}t-x_0, y-\dot{y}t-y_0)\Pi\left(\frac{x-\alpha}{\Delta x}\right)\Pi\left(\frac{y-\beta}{\Delta y}\right)\Pi\left(\frac{t}{\tau}\right)\mathrm{d}x\,\mathrm{d}\,\mathrm{d}t \quad (3)$$

Two comments are necessary at this point. For fixed stars it is assumed that $\Delta x = \dot{x}\tau$, but for SSOs this is not the case in general. In particular, if v_τ is the mean transfer velocity of the charges, so that $v_\tau = \Delta x/\tau$, the relevant parameter for SSOs is the residual along-scan velocity $\mu = \dot{x} - v_\tau$. Second, at every time interval of duration τ the charges in a pixel are moved to its immediate adjacent pixel. In this process, $\alpha \rightarrow \alpha + \Delta x$, while at the same time $x_c \rightarrow x_c + (\mu + v_\tau)\tau = x_c + \Delta x + \mu\tau$ and $y_c \rightarrow y_c + \dot{y}\tau$. For fixed stars we have $\alpha - x_0 =$ const., assuming an ideally perfect clocking, then in this case the total number of electrons recorded during the integration time T is simply T/τ times the number obtained over one pixel. This is not true for SSOs, and the computation of the integral has to be done for the entire integration time. For sake of simplicity the computation can be done under the assumption that the optical PSF is locally constant, or in other words that we may use the same PSF over one whole CCD.

In practical terms, the preferred option to attack the problem of signal computation has been so far based on a different, numerical ray-tracing approach. Let us then come back to consider the incoming photons from the source, before they start to interact with the optical system to produce the recorded image. We may imagine a coordinate system following the moving object and with origin in (x_c, y_c) and axes parallel to the along and across-scan directions. In this reference system, the photons coming from the source would produce an image in an hypothetic detector, and the coordinates of a given point belonging to this (static) image would be x' and y'. Now, we can easily compute the corresponding coordinates (x, y) in the moving Gaia focal plane of the the photons coming from the (x', y') point just defined above. These are:

$$\begin{aligned} x &= x' + \dot{x}t + x_0 \\ y &= y' + \dot{y}t + y_0 \end{aligned} \quad (4)$$

In the adopted method of image simulation, based on a Monte Carlo algorithm, all the quantities x', y' and t are randomly generated. The time t is uniformly generated between $-T/2$ and $T/2$ where T is the integration time, while x', y' are randomly generated according to a given surface luminosity distribution $g(x, y)$ of the object (chosen *a priori*), using a ray tracing algorithm which takes also into account an assumed light scattering law characterising the object's surface. For the details of the numerical algorithm of generation of the sampling positions x' and y' see [**?**]. The number N of sampling points (x', y') depends on the magnitude of the object and on instrument characteristics including the CCD quantum efficiency. In particular, we have that $M = -2.5 \log N + C$, where M is the apparent magnitude and C is a suitable constant. At magnitude 12, corresponding to the saturation limit of the CCD in astrometric focal field, the number of collected photoelectrons are about one million. The nominal magnitude limit of detection is $V \approx 20$ and corresponds to about one thousand photoelectrons [83]; see also §5.4.

Of course, the above optical image, or in other words the (x, y) distribution of incoming photons from the observed object, is not yet the final recorded signal. We have still to take into account the fact that each photon incident on the optical system suffers an angular deviation δx and δy, respectively, in the along-scan and

across-scan direction due to the diffraction of the instrument aperture. The numerical model reproduces the instrument diffraction effect by generating δx and δy randomly, but according to a parent distribution given by the PSF of the system. In other words, the probability of a given deviation is proportional to the value of the PSF $f(\delta x, \delta y)$ for this particular deviation. In order to obtain the real arrival position of a single photon on the focal plane we have then to add δx to x and δy to y. Obviously all the quantities x', y', δx and δy are expressed with the same unit.

As mentioned in the previous section, the spreading of the recorded photoelectrons in the along-scan direction on the focal plane due to the scanning motion of the satellite, is reduced by the Time Delayed Integration (TDI) read-out mode. For this reason we introduce a moving coordinate system (X, Y) synchronised with the TDI charge transfer. Obviously $Y = y$ because no TDI correction is performed in the across-scan direction. In this way, the "effective" position of the photoelectron inside the CCD image turns out to be:

$$\begin{aligned} X &= \theta(x' + \delta x + \dot{x}t + x_0, t) \\ Y &= y' + \delta y + \dot{y}t + y_0 \end{aligned} \tag{5}$$

where θ is a special function accounting for the step by step TDI translation, and depending on time t explicitly, according to the phase of the TDI charge transfer. In practical terms, however, TDI blurring is included in the adopted PSF, so that the θ function reduces to a simple continuous translation (see [**?**] for details). In this case, we may simply write down the following:

$$\begin{aligned} X &= x' + \delta x + \dot{x}t + x_0 \\ Y &= y' + \delta y + \dot{y}t + y_0 \end{aligned} \tag{6}$$

where $\dot{x}$ and $\dot{y}$ represent the residual velocity of the object with respect to the TDI motion. For SSOs, this corresponds in practice to the apparent motion with respect to the fixed stars.

The final step of the numerical procedure is the allocation of the photoelectrons into the corresponding pixels. The Gaia CCD detectors have rectangular pixels with smaller side $\Delta X = \Delta x$ in the along-scan direction, and larger side $\Delta Y = \Delta y$ in the across-scan direction. Each pixel is labelled with integer indexes i and j and corresponds to the rectangular region defined by the points (X, Y) such that:

$$X_i \leq X < X_i + \Delta X\,;\; X_i = i\Delta X \qquad Y_j \leq Y < Y_j + \Delta Y\,;\; Y_j = j\Delta Y \tag{7}$$

in this way the origin of the coordinates system coincides with the the left-hand, lowest corner of the pixel labelled as $i = 0$, $j = 0$.

In the astrometric focal plane of Gaia only a limited region of the CCD grid is actually read-out. This window is, again, a rectangular $n \times m$ one, with a number n of pixels in the along-scan direction and m pixels in the across-scan direction. In this way $0 \leq i \leq n-1$ and $0 \leq j \leq m-1$. Following the sampling scheme proposed by [52], 12×12 pixels windows should be used for stars between 12 and 16 magnitude (in the G-band of Gaia), and 6×12 windows for stars between 16 and 20 magnitude. We indicate by N_{ij} the number of photoelectrons in the i-th pixel of the window in the along-scan direction and the j-th in the across-scan direction.

It is important to note that in general the recorded signal is binned, that is the numbers of pixels in the across-scan direction are integrated (summed up), so that the final signal consists of the n numbers:

$$N_i = \sum_{j=0}^{m-1} N_{ij} \qquad 0 \leq i \leq n-1 \tag{8}$$

In the following, we will assume that CCD window is always binned, and what we call "signal" is actually given by the set of discrete photoelectron counts just defined above.

5.3 CCD processing

In general terms, we call "CCD processing" a sequence of numerical procedures aiming at extracting from the recorded signal N_i all possible information of interest. In particular, in the case of SSOs, four parameters are of great importance: the position of the object, its angular size, its velocity and its apparent magnitude. Basically, both for stars and SSOs, the adopted method of determination of all the relevant parameters is based on a best-fit procedure.

It is assumed that a mathematical model of the signal is at disposal, or in other terms that we are able to compute the numbers N_i for any set of values of the unknown parameters. This computation can be done analytically or throughout numerical codes. In addition to a signal model, one has to decide a criterion of comparison between the computed (C) and the observed (O) signal, in order to minimising or maximising some target function expressing the mathematical distance between C and O.

We note that, in principle, an alternative approach, based on a full reconstruction of the image, could also be adopted. A number of refined techniques of image reconstruction have been actually developed in the literature in several situations. On the other hand, it seems that such kind of approach can hardly be applied with success to poorly sampled signals covering only a few pixels, like those from faint, nearly point-like sources detected by Gaia. For this reason, we focus on the approach based on the determination of a limited number of relevant unknown properties of the sources by means of a signal best-fit approach.

For sake of simplicity, in order to focus on a few fundamental concepts rather than on unnecessary technical details, let us limit now to a one-dimensional case. Let L be the model function used to fit the recorded signal. For a fixed star this reduces to the PSF integrated in the across-scan direction and convoluted with the Π function describing the shape of the pixel. This leads to derive the so-called Line Spread Function (LSF). For fixed stars, this depends only on the position c in pixels of the star and on its apparent magnitude, or, in other words, on the total number of collected photoelectrons. The signal is proportional to the flux and can be reproduced by translating the centre of the LSF into the star position. If we call L the LSF per unit of flux (that is, normalised to one collected photoelectron) the expected number of photoelectrons in the pixel i, $E(N_i)$, is given by:

$$E(N_i) = r^2 + b + NL(i - c) \tag{9}$$

where N is the total number of photoelectrons produced by the source, and r is the RMS readout Poisson noise in electrons. The term b is the contribution of the background in electrons per sample. We assume that $r^2 + b$ is known with sufficient accuracy.

If N_i is the number of electrons really collected in the sample i, a method of estimation of the unknown parameters c and N, corresponding to the unknown photocentre position and apparent magnitude of the source, can be based on a maximum likelihood criterion. More precisely, c and N are varied in order to maximise the probability of collecting the observed counts N_i, assuming the signal model L. For Poisson statistics this probability is given by the likelihood function:

$$f(c,N) = \prod_{i=0}^{m-1} \frac{[r^2 + b + NL(i-c)]^{N_i}}{N_i!} \exp\left[-(r^2 + b + NL(i-c))\right] \tag{10}$$

The numerical problem is then to find the values of c and N that maximise $f(c,N)$.

Without entering in too many details, let us take into account the case of a SSO. In this case, the signal model does not depend only on the parameters c and N. Assuming that the object has a known shape and brightness distribution, we have to introduce as additional parameters its size s in pixels and its velocity v. As we have already discussed above, the meaning of v is the difference between the velocity of the image on the focal plane and the mean TDI transfer velocity of the electrons. In this case the likelihood function becomes:

$$f(c,s,v,N) = \prod_{i=0}^{m-1} \frac{[r^2 + b + NL(i-c,s,v)]^{N_i}}{N_i!} \exp\left[-(r^2 + b + NL(i-c,s,v))\right] \tag{11}$$

For fixed stars the TDI motion is set according to the image motion, so on the average the position c is at rest. In the case of a moving source, however, this is no longer true. For this reason it is necessary to specify what we mean by c for a moving source. In particular, the meaning of c must be that of the position of the image at a particular epoch, for example at the epoch of the signal read-out.

We have just assumed that the brightness distribution of the source is known and the only parameter to be determined is its size s. This can be a critical point for some applications to SSOs and in particular to asteroids. In general, each asteroid has its own shape, spin axis orientation and rotation period. Moreover, when it is observed at some given epoch it is seen under some illumination condition, quantified by the value of the so-called phase angle. The phase angle is defined as the angle between the directions to the observer and to the Sun, as measured from the asteroid barycenter. We note that Gaia will never observe asteroids at zero phase angle, corresponding to object opposition from the Sun, but at phase angles larger than 10 degrees, as a rule. This means that, due to the defect of illumination, the position of the "photocentre" of the collected signal will not be coincident with the position of the (sky-projected) barycenter of the object. This effect will have to be taken into account for the purposes of using Gaia astrometric measurements of asteroids to obtain refined orbital elements.

In addition to the above problems, the surface of any asteroid is characterised by its own reflectance properties, that may well be different for different objects, and also may vary, in principle, from point to point of the same object, determining an apparent brightness distribution which will vary depending on the observing circumstances. Finally, other problems may also arise in the cases of non-resolved binary systems, and of objects characterised by the presence of some kind of cometary activity (and Gaia will certainly observe comets).

Of course, the above mentioned effects make the CCD processing of SSOs a quite challenging task. As opposite to other kind of sources, the signal of any asteroid transiting in the field of view is inherently different with respect to the signals collected for the same asteroid during different transits, corresponding to different observing circumstances. All this makes SSOs completely different for what concerns the CCD processing and reduction of the collected astrometric signals, with respect to the case of fixed, point-like stars.

5.4 Accuracy estimation

In order to estimate the accuracy of the measurement of the most important parameters, that for asteroids include apparent magnitudes, motions, positions and sizes, it is necessary to take into account all the disturbing factors that affect the generation of the recorded signal. The main sources of noise include photon statistics, CCD read-out noise (RON), dark current, the noise introduced by the background, errors in the calibration of the PSF, perturbation of the electronic devices due to the satellite's environment, like the radiation damage of the CCDs produced by cosmic rays.

Some of these noise sources are still under investigation, including PSF calibration and CCD radiation damage, whereas for others an estimation is already available. For what concerns the RON, its total amount should be about 4 photoelectrons (e^-). Including also the dark noise and other electronic disturbing factors, the total detection noise (TDN) should be of the order of $6 - 7$ e^- for each CCD in the focal plane. This means that in the signal acquisition process the counted numbers N_i are affected by an uncertainty of this order.

Background contribution to the signal deserves a separate discussion. Sky brightness does not introduce an error in the photoelectrons read-out, but rather an additional contribution of some number of photoelectrons to be added to the number of photoelectrons produced by the source. According to the HST/WFPC2 Instrument Handbook, the sky brightness at high ecliptic latitudes should be around 23.3 mag.arcsec^{-2}, while it is around 22.1 mag.arcsec^{-2} on the ecliptic plane, because of the zodiacal light ([83]). According to the most updated configuration of the instrument ([96]), taking into account the size of the CCD pixels in the astrometric field (10×30 μm), the focal length of the telescope (35 m), the pupil aperture (1.45×0.50 m), and the CCD integration time (4.42 sec), we expect a background contribution of about 2 e^-/pixel on the ecliptic, and 0.6 e^-/pixel at high latitude. These two values should be considered as the extreme limits of background contribution per CCD.

The major source of noise is certainly due to photon statistics. According to the most updated mission design, the integration time T should be equal to 4.42 sec for CCDs in the astrometric field. The total number N of collected photons depends on the source's magnitude M, and $M = -2.5 \log N + C$, where C is a constant (neglecting the effect of the windowing cut-off). Visual magnitude $M = 0$ corresponds to an energy flux of 2.52×10^{-8} Wm^{-2}. Considering a mean wavelength of collected photons about 550 nm, this energy flux corresponds to a photon flux around 7×10^6 photons/cm^2/sec. Taking into account an integration time of 4.42 sec and an aperture of 1.45×0.50 m^2, the number of incoming photons should be around $1.6 \times 10^{11} 10^{-M/2.5}$, or $N_s \sim 10^{11} 10^{-M/2.5}$ including a factor 1/2 due to

CCD quantum efficiency. So we expect about 10^6 photoelectrons at magnitude 12, corresponding also to the saturation level of the CCDs, and about 10^3 at magnitude 20, that is the nominal detection limit.

A quick estimation of the error in the position measurement can be done in the following way. Let us assume for simplicity the case of the signal from a nearly point-like, non moving source. Its signal corresponds more or less to the instrument LSF. As we have explained above, the signal can be regarded as the distribution over a few pixel rows of the recorded photoelectrons. Then, the mean value of the photoelectrons' positions can be used as an estimator of the image position. As it is well known from statistics, the standard deviation of the mean is equal to the standard deviation of the distribution divided by the square root of the number of samples, that is in this case, the number of the collected photoelectrons. The standard deviation of the LSF is about $2-3$ pixels. Thus, at magnitude 12, which gives 10^6 electrons as seen above, we expect that the standard deviation of the mean is about $2-3\times10^{-3}$ pixels ($\sim 0.1-0.2$ mas). In the same way, at magnitude 20, when we expect to collect more or less 10^3 electrons, the accuracy of the mean should be about $0.05-0.1$ pixels ($\sim 3-6$ mas).

We note that the above values for the effective uncertainty in the photocentre determination of SSOs are much higher than the final, end of mission uncertainty in the determination of the positions of single stars. The reason is that for SSOs, which move and are seen in different observational circumstances in different transits on the Gaia focal plane, we cannot merge together the results of different detections, and we are forced to limit ourselves to derive separately the positions of the objects at different transits based on signals collected at these single transits. As opposite, the determination of the position of the stars will be performed by cross-matching the information derived from the measurements of tens of different transits. For this reason the final accuracy for stars at magnitude 12 is expected to be of the order of 10^{-4} pixel (see [83]), corresponding to about 0.004 mas.

The accuracy in the determination of the angular size of SSOs may be estimated by means of some numerical tests based on a simplified method of measurement. We have seen that the position of the object is related to the *mean* of the spatial distribution of the recorded photoelectrons. In the same way, the angular size of the source is related to the *standard deviation* of the same photoelectron distribution. Let us assume for simplicity that the shape of the object of whom we want to measure the angular size is a perfect sphere with a uniform brightness distribution. Let us assume also that the object is observed at zero phase angle. In other words, we assume that the object appears as a flat, uniform disc in the sky. In order to avoid complications with the truncation of the signal, we assume also that the object's residual velocity is zero. This means that the final signal is well centered and it is not truncated. If the number of collected photons was infinite, then a deterministic relationship between the standard deviation σ of the signal and the diameter D of the disc would exist. So, by computing the expected standard deviation for each possible value of the disc's size, it should be possible to obtain the corresponding value of the size from the observed signal. In the real world, however, due to the fluctuations of the numbers N_i caused by photon statistics, to each value of the measured size of the disc may correspond different values of D. The distribution of these possible values is characterised by a mean and a dispersion around it. An example is given in Fig. 5, obtained by means of a numerical Monte Carlo

simulation. The figure shows that a given value of σ can be produced by some interval of possible values of D. Using this kind of plot we can assess the expected accuracy in size determination.

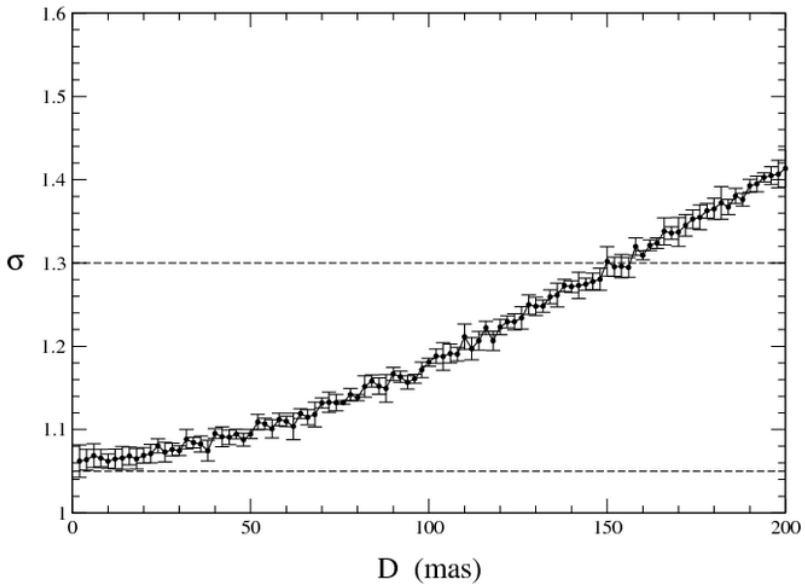

Fig. 5. Standard deviation σ (in pixels) of signals produced by an ideal spherical and homogeneously emitting object seen at zero phase angle, as a function of its apparent diameter D. The bar corresponds to the standard deviation of σ. due to photon statistics.

In particular, the dispersions of the values of σ for a single value of the size D depends on the magnitude of the source, and it increase as the magnitude increases (or the flux decreases). Moreover, the relation between σ and D is not linear, but rather it can be written as:

$$\sigma^2 = \frac{D^2}{16} + \sigma_0^2$$

where the first term is introduced by the angular distribution of the incoming photons and σ_0^2 is the variance introduced by the LSF. It follows that if we wish to estimate the value of D from the measured value of σ, the error $\mathrm{d}D$ is given by:

$$\mathrm{d}D = \frac{16\,\sigma\,\mathrm{d}\sigma}{D} \tag{12}$$

where $\mathrm{d}\sigma$ is the error, mainly due to the photon statistics, in the measurement of the standard deviation σ of the signal. So, for a given value of $\mathrm{d}\sigma$, the uncertainty of the size estimation increases as the size itself decreases. In other terms the slope $\mathrm{d}\sigma/\mathrm{d}D$ of the function $\sigma(D)$ decreases as D decreases, as it is clear from Fig. 5.

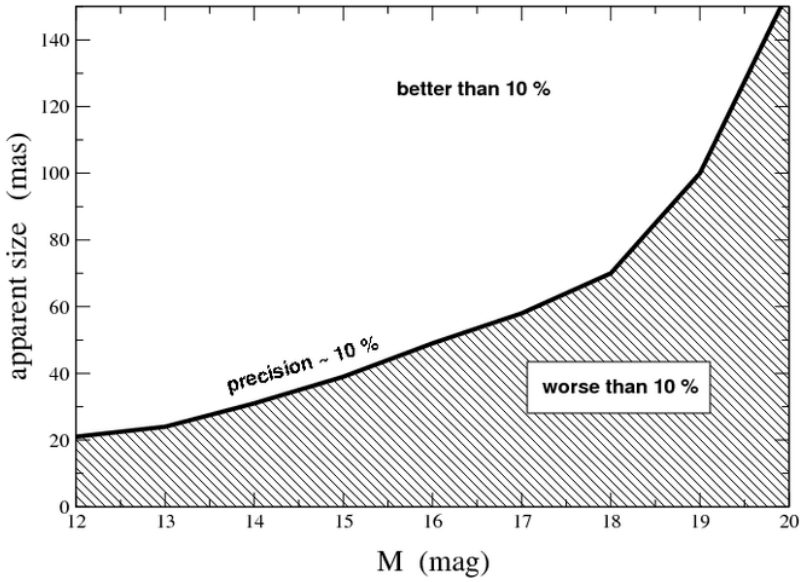

Fig. 6. The smallest size measurable with a precision of 10 % plotted as a function of the object apparent magnitude.

Since dσ is magnitude-dependent, it is possible to associate to any possible magnitude value a corresponding critical value of the size D for which the resulting relative error dD/D is equal to some given limit, like 10 %, as an example. The result of this exercise is shown in Fig. 6. In the figure, the size limit corresponding to a relative size determination accuracy of 10 % is plotted *versus* the magnitude. The domain of this plot below the 10 % line corresponds to observational circumstances in which the image cannot be distinguished from that of a point-like source. At magnitude 12 it is possible to appreciate the apparent size for objects with a diameter of 20 mas, but at magnitude 20 this limit raises up to 150 mas. In conclusion, points below the 10 %-line in the figure correspond to observational circumstances for which the object is too far or is too faint for its angular size to be measured with an accuracy better or equal to 10 %.

5.5 Size measurement of Main Belt asteroids

In order to assess the capabilities of Gaia in measuring the sizes of Main Belt asteroids, we take advantage of existing simulations of observations of these objects by GAia during its operational lifetime ([**?**]). These simulations provide the list of the transits of Main Belt objects on the field of view of the instrument, specifying the distance r from the satellite and its apparent magnitude M. Among the full set of simulated observations, we selected only those of objects for which a value of diameter d is available (taken from the most recent issue of the IRAS catalogue of asteroid sizes and albedos, [108]), and for which the apparent magnitude should

range between 12 and 20. We assumed for sake of simplicity that the objects are spherical. The apparent size of the objects for each of the above observations will be obviously $D = d/r$. Having at disposal such a set of simulated observing circumstances for a large sample of objects (about 2,000), it is possible to assess whether for each single detection the object's size can be determined with a precision better (*good observation*) or worse (*bad observation*) than 10 % on the basis of the diagram in Fig. 6.

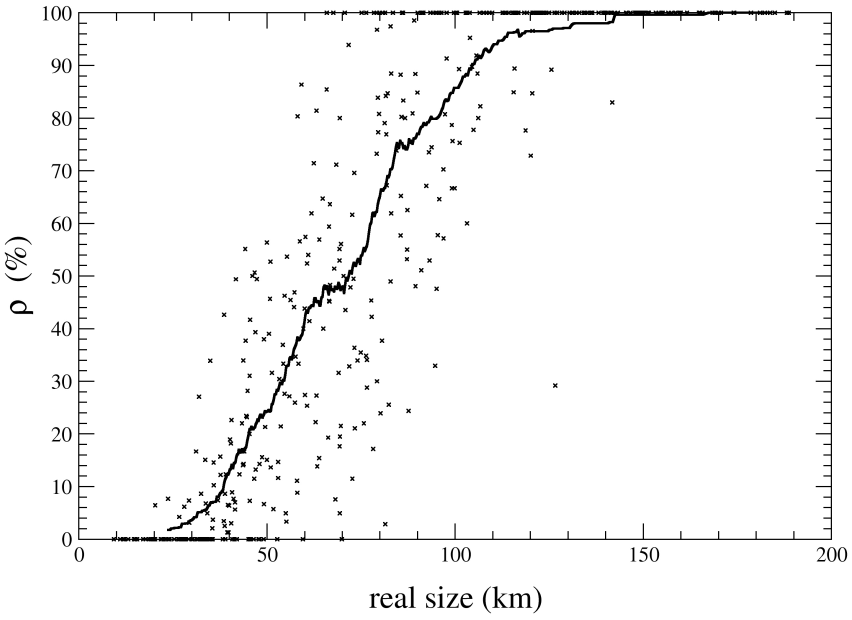

Fig. 7. Efficiency of Gaia in measuring the diameters of the Main Belt asteroids.

For any object, in general some observations will be good and others will be bad, according to the observing circumstances. Let S be the total number of observations of one single asteroid, and let s be the total number of *good* observations of the object, in the sense explained above. The resulting ratio $\rho = s/S$ can be taken as an evaluation of the efficiency of Gaia in measuring the size of this asteroid.

We show in Fig. 7 the result of this exercise. Each asteroid is plotted as a small cross in the efficiency - diameter plane. The solid line is the average value of the efficiency versus real diameter resulting from a running-box analysis. For asteroids having a size larger than 100 km the measurement efficiency is well above 50 %, and almost all observations are good. Below 20 km no good observation is

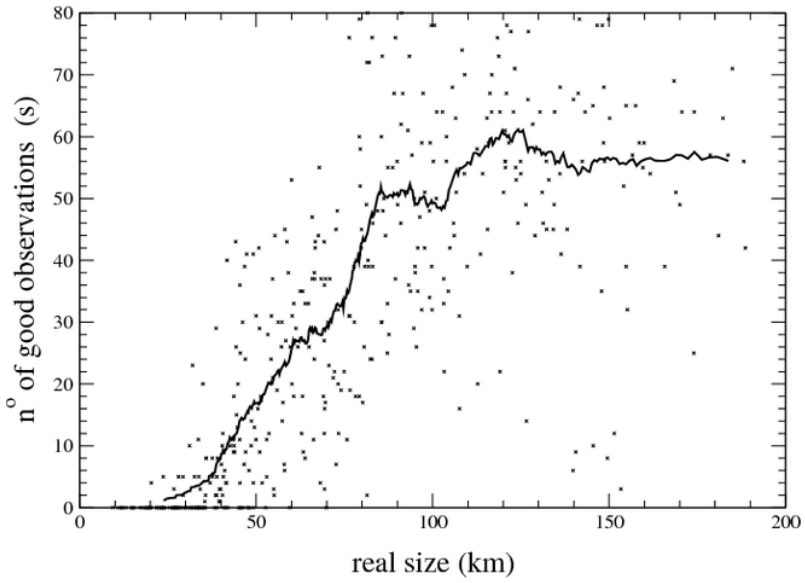

Fig. 8. Number of observations of Main Belt asteroids of different sizes, allowing a size measurement with an accuracy of 10 % or better.

possible, because the objects are either too small or too faint or both (note the group of crosses with $\rho = 0$ %). At the limiting size of $20 - 30$ km, the measurement efficiency is only a few percent.

A slightly different plot is shown in Fig. 8, where the number of good observations s is plotted against the real diameter for each asteroid. Again, the solid line is a running-box average. The crosses are rather scattered meaning that apart from the average scenario there are very different situations, depending on the individual orbital and physical properties of the objects. We note that in the case of very large asteroids the observation efficiency can decrease due to the paradoxical fact that in many cases they are too bright, and they reach the CCD saturation limit of magnitude 12 (examples are the group of crosses in Fig. 8 at $D \simeq 150$ km and $s \leq 10$ corresponding to the asteroids 11 Parthenope, 18 Melpomene, 20 Massalia, 39 Laetitia, 89 Julia, 349 Dembowska).

5.6 Limits and Margins of Improvement

The results discussed in the previous sections have been obtained under some simplifying assumptions. In particular, we assumed that the objects had spherical shapes, and that the optical properties of the emitting surfaces were homogeneous. Or, in other words, we made the assumption that the surface albedo of the objects was homogeneous throughout the surface. Moreover, even if we did not mention this explicitly, the results shown in Figs. 5 to 8 were based on simulations in which some assumptions concerning the diffusive properties of the object surfaces were

made. In fact, a well defined light-scattering law was assumed when running the ray-tracing part of the signal simulator. Without entering into details, the assumption was that of surfaces scattering the incident sunlight according to a composition of a Lambertian and a Lommer Seeliger scattering law.

Now, we can ask ourselves whether the above simplifying assumptions are reasonable, and if there is some way to possibly improve the model. In this respect, the answer seems to be yes, and the way of improving the model is based on ancillary information that is expected to become available when the full set of recorded signals from each object at all transits collected during the Gaia operational lifetime will be available. In particular, the idea is that of taking profit of the analysis of the disk-integrated magnitude measurements performed at each object transit. The measurement of the apparent magnitude at each transit on the Gaia focal plane is a less complicated task with respect to the determination of the astrometric position and apparent size of the object, as seen in the previous section. Given the full set of measured apparent magnitudes of an object, it will be possible to derive from that a big deal of information concerning the rotational properties (spin rate and direction of the spin axis) and overall shape, assumed for simplicity to be that of a triaxial ellipsoid. The derivation of the above parameters is described in another section of this lecture. Having at disposal the object's pole direction and a more realistic triaxial shape, it will be possible to compute for each transit the corresponding observational circumstances in terms of apparent shape and orientation of the illuminated part of the body visible from Gaia at the epoch of the observation. In this way, a much improved object's model, with respect to that of a simple homogeneous sphere, will be adopted and used to derive refined estimates of the object's size and also of the offset between the position of the barycenter and that of the photocentre during the transits for which the object becomes resolvable.

As for the choice of the scattering law, the situation is intrinsically more difficult, yet not completely hopeless. In particular, it will be possible to take profit of the fact that at least for a few objects (433 Eros, 243 Ida, 951 Gaspra, 253 Mathilde, and probably in the near future 1 Ceres and 4 Vesta) we have at disposal data taken *in situ* by space probes. For these objects, we have very detailed information about size, shape, spin and surface properties. The idea is then that of using this ancillary information to possibly improve the adopted scattering laws in the reduction of Gaia data. In particular, the most correct scattering law, at least for the objects of the above list, should be the one producing a better agreement between the Gaia results and the known properties of the objects.

6 The Determination of asteroid physical properties

6.1 Introduction

The determination of asteroid physical properties will be one of the fundamental contributions of Gaia to Planetary Science. As we have seen in §5, asteroid sizes will be directly measured for a number of objects that should be of the order of 1,000, according to current signal simulations. This spectacular result, however, will be only one of a longer list that includes:

– the measurement of about 150 asteroid masses;

- as just mentioned above, the direct measurement of about 1,000 asteroid sizes;
- based on the measured masses and volumes, the determination of the average densities for about 100 objects belonging to practically all the known taxonomic classes;
- the determination of the rotational properties (spin period and polar axis orientation) and overall shapes for a number of the order of 10,000 objects;
- a new taxonomic classification based on reflectance spectra (including wavelengths in the blue region of the spectrum) obtained for several tens of thousands of objects;
- the measurement of the Yarkovsky acceleration for some tens of near-Earth objects.

To the items of the above list, we have to add, of course, the derivation of much improved orbits for a data-set of about 300,000 objects, taking profit of the unprecedented astrometric accuracy of the Gaia mission. A detailed description of the expected performances of Gaia in the determination of orbits, masses and Yarkovsky acceleration is given in §8.

In what follows, we will focus on the remaining items of the above list, namely spin properties and taxonomy.

6.2 Inversion of disk-integrated photometric data

Historically, photometry has been one of the first observing techniques applied to obtain information on some physical properties of the asteroids.

Due to the fact that these objects have non-spherical shapes and their apparent brightness is due to solar photons scattered by the illuminated surface, there is a periodic modulation of the brightness due to the object's rotation. Photometric observations over a sufficiently long interval of time to cover a full rotation cycle, produce then what is usually called a *lightcurve*, namely a plot of the apparent brightness as a function of time, which shows the periodic variation in magnitude due to rotation. Lightcurves provide thus in a straightforward way one of the many physical properties of an object, namely its rotation period.

The morphology of a lightcurve at a given epoch is the complex result of the shape of the object, the orientation of its rotation axis (the "asteroid pole"), and the light scattering properties of the surface. The difference in magnitude between the maximum and the minimum brightness of the object during a rotational cycle is called *lightcurve amplitude*.

The fact that asteroids are moving objects on the celestial sphere has the consequence that the geometric configuration Sun - asteroid - observer changes for observations carried out at different epochs. The observing circumstances at a given epoch are characterized by different values of the heliocentric and geocentric distances, of the illumination conditions, which are described by the so-called phase angle described in §5.3, and by two quantities that describe the orientation of the asteroid spin axis with respect to the direction to the observer and to the Sun. These two quantities are two angles: the *aspect angle*, normally indicated as ξ, and the *obliquity angle*. The aspect angle is the angle between the directions of the spin axis and the direction to the observer, measured at the object's barycenter. The obliquity angle is the angle between the plane containing the object, the observer and the spin axis of the object, and the plane perpendicular to the plane containing

the observer, the object and the Sun. This angle is indicated as o in Fig. 9, which shows in a graphical way the meaning of the above angles. Finally, another angle ϕ describes the rotational phase of the object in its rotation around its axis. In practice, the values of all the above mentioned angles reduces to the computation of the *sub-observer* (normally called *sub-Earth*) and *sub-Solar* points, namely the latitude and longitude coordinates of the two points which are the intersections of the body's surface with the vectors from the object's barycenter to the observer and to the Sun, respectively.

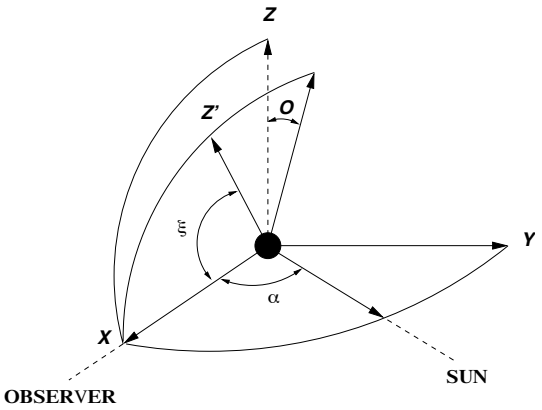

Fig. 9. Graphical explanations of the aspect (ξ) and the obliquity (o) angles. The angle α in this figure is the phase angle. Vector $\mathbf{Z}'$ is the direction of the positive spin.

Due to the variations of the observing circumstances at different epochs, lightcurves taken at different oppositions of the same object will generally exhibit a variation in their morphologies, and in particular of their amplitude. This is due to the fact that the aspect angle of an object is a function of the ecliptic longitude (or equivalently, the Right Ascension) at which it is observed at a given epoch. For instance, if we assume that the object has the shape of a triaxial ellipsoid with semi-axes $a > b > c$, spinning around the shortest axis c, the maximum lightcurve amplitude will be reached when the object is seen in equatorial view, when $\xi = 90°$. This view is in principle always reachable and corresponds to two well defined values of the Right Ascension of the object (separated by an angle of 180°), which depend on the spin axis orientation. Just to make the things more clear, to observe an object at $\xi = 90°$ means observing it when it reaches one of its two equinoxes.

We only remind that the choice that we make here of a triaxial ellipsoid shape with semi-axes $a > b > c$ is particularly suitable to illustrate the predictable magnitude variations. Triaxial ellipsoids seen at zero phase angle project in the sky an ellipse. The apparent surface S of this ellipse is given by the following relation:

$$S = \pi a^2 (A_1 \sin^2(\phi) + A_2)^{1/2} \tag{13}$$

where ϕ is the rotation angle of the object, assumed to be zero at lightcurve maximum (when the projected ellipse has the major semiaxis equal to a). A_1 and A_2 are given by:

$$A_1 = \left(\frac{c}{a}\right)^2 \left[\left(\frac{b}{a}\right)^2 - 1\right] \sin^2(\xi) \tag{14}$$

and

$$A_2 = \left(\frac{c}{a}\right)^2 \sin^2(\xi) + \left(\frac{b}{a}\right)^2 \cos^2(\xi) \tag{15}$$

It is easy to verify that, at the maximum and the minimum of luminosity, the projected areas of the ellipse are, respectively:

$$S_{max} = \pi a \cdot \sqrt{b^2 \cos^2(\xi) + c^2 \sin^2(\xi)} \tag{16}$$

and

$$S_{min} = \pi b \cdot \sqrt{a^2 \cos^2(\xi) + c^2 \sin^2(\xi)} \tag{17}$$

We may assume in first approximation that the received flux of scattered sunlight coming from the asteroid will be simply proportional to the apparent projected surface S, so that, by neglecting any realistic effect of light scattering on the surface, we can simply write $m = -2.5 \log(S) + c$, where c is a constant. As a consequence, it is easy to verify that, if we call A the lightcurve amplitude, namely the difference of magnitude between the maximum and the minimum brightness, when we are in equatorial view ($\xi = 90°$) we have that $A = -2.5 \log(a/b)$. This means that observations of a triaxial ellipsoid asteroid taken in equatorial view, something that is always possible to obtain sooner or later, in principle, provide also an estimate of the value of the a/b ratio.

The lightcurve amplitude progressively decreases as the aspect angle decreases from its maximum possible value of 90°. The minimum possible value of the aspect angle for a given object depends on the orientation of its spin axis. For an object whose spin axis lays on the ecliptic plane, a pole-on view becomes possible ($\xi = 0$), and in that geometric configuration the lightcurve amplitude in principle becomes zero and the object's magnitude does not change during the rotation. In that situation, the projected area will be $S = \pi ab$, which corresponds to the maximum possible value among all the possible projections of the triaxial ellipsoid, and then it corresponds also to the maximum possible brightness of the object. In general, however, the spin axis will be oriented in such a way as not to allow to reach a pole-on view.

Due to the fact that the lightcurve changes as a function of the aspect angle, having at disposal several lightcurves of an object obtained at different oppositions, it becomes in principle possible to derive the direction of its spin axis ("asteroid pole"). Different techniques have been developed for this purpose[65, 54]. Predictions concerning asteroid shapes and spin axis directions based on ground-based photometry have been found to be fairly accurate, according to the results of *in situ* investigations carried out by space probes [54].

One major advantage of observing from an orbiting platform like Gaia, with respect to traditional ground-based observations, is that from space it is easier to observe the objects even when they are far from opposition, since from space there are not the strong observing constraint related to the diurnal and seasonal cycles

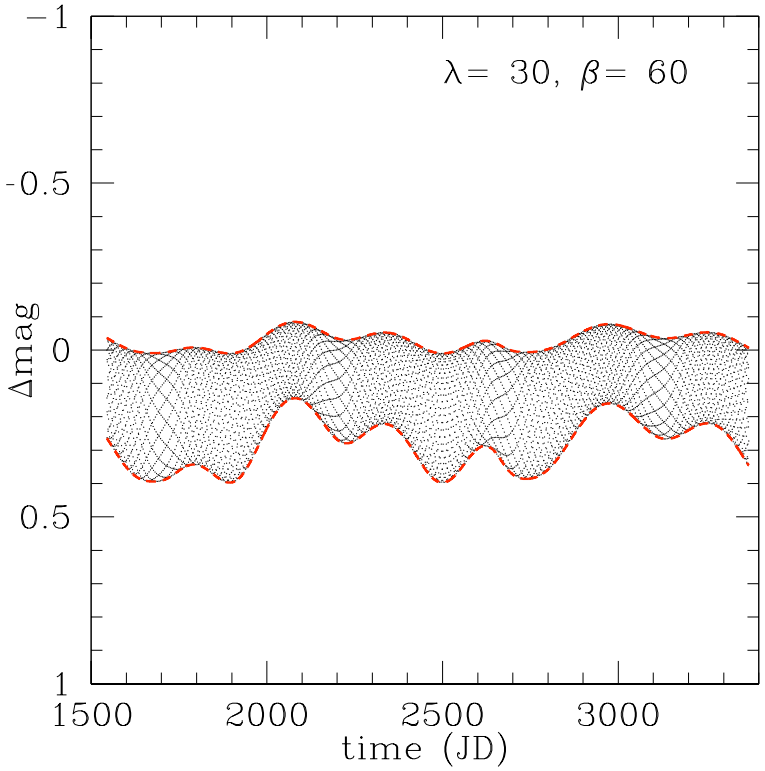

Fig. 10. The domain of possible values of magnitude (expressed as a difference with respect to the magnitude measured at a reference epoch) as a function of time (expressed in Julian Days) for a triaxial ellipsoid object having the same orbit of the asteroid (39) Laetitia. The axial ratios of the object are $b/a = 0.7$ and $c/a = 0.5$. The coordinates of the asteroid pole are given in the figure (λ being the ecliptic longitude and β the ecliptic latitude of the pole). The time interval covers 5 years, equal to the expected operational lifetime of Gaia.

of the Earth. In particular, from space the asteroids can be seen at small solar elongation angles, which are hardly achievable from the ground.

Each Main Belt asteroid will be typically observed tens of times during the five years of the planned operational lifetime of Gaia. The simulations indicate that each object will be detected over a wide variety of ecliptic longitudes. Correspondingly, Gaia will make a good sampling of the interval of possible aspect angles of each object. The same variety of aspect angles, needed to derive the orientation of the spin axis, may be sampled from the ground only over much longer times. As a consequence, Gaia will be very efficient in providing disk-integrated photometry

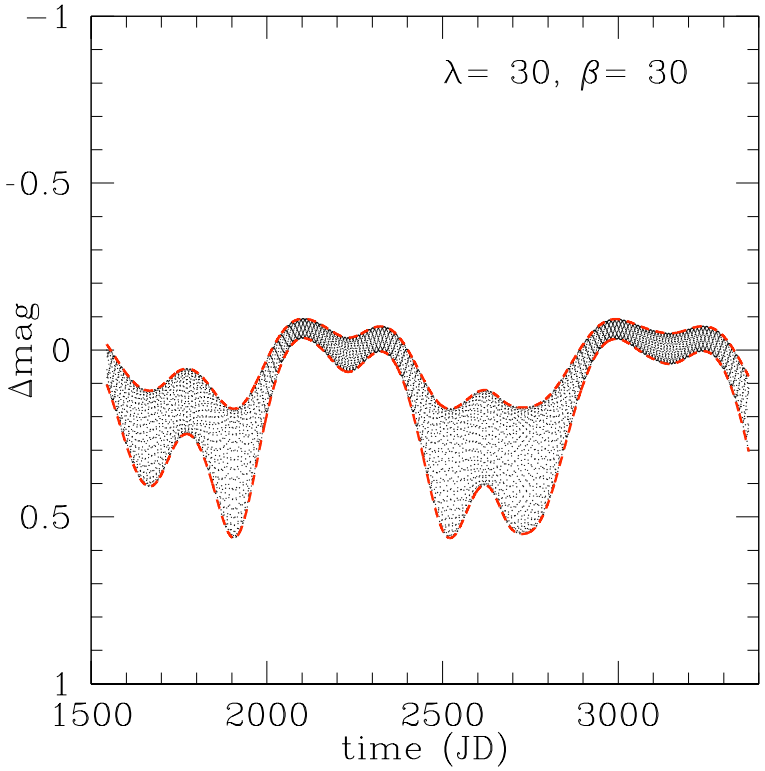

Fig. 11. The same as Fig. 10, but this time the ecliptic latitude of the asteroid's pole is $\beta = 30°$. Together with Fig. 12, these three figures give some idea of the role played by the latitude of the pole in determining the photometric behaviour of a triaxial ellipsoid object.

data sufficient to derive the poles of the asteroids in a relatively short time, as well as the sidereal periods and the overall shapes.

However, it must be noted that there is a fundamental difference with respect to the situation usually encountered in traditional ground-based asteroid photometry. In fact, Gaia will detect each object only during very short transits when it crosses the field of view at epochs determined by the rotational and precessional motion of the satellite, and by the orbital motion of the asteroid.

This means that Gaia photometry will not consist of full lightcurves, but only of a number of sparse, single photometric measurements lasting a few seconds. This would seem in principle a crucial limitation, but it is more than compensated by the high number of photometric measurements that will be recorded for each object (on the average, between 60 and 80 for main belt asteroids), and by the good accuracy of Gaia photometry.

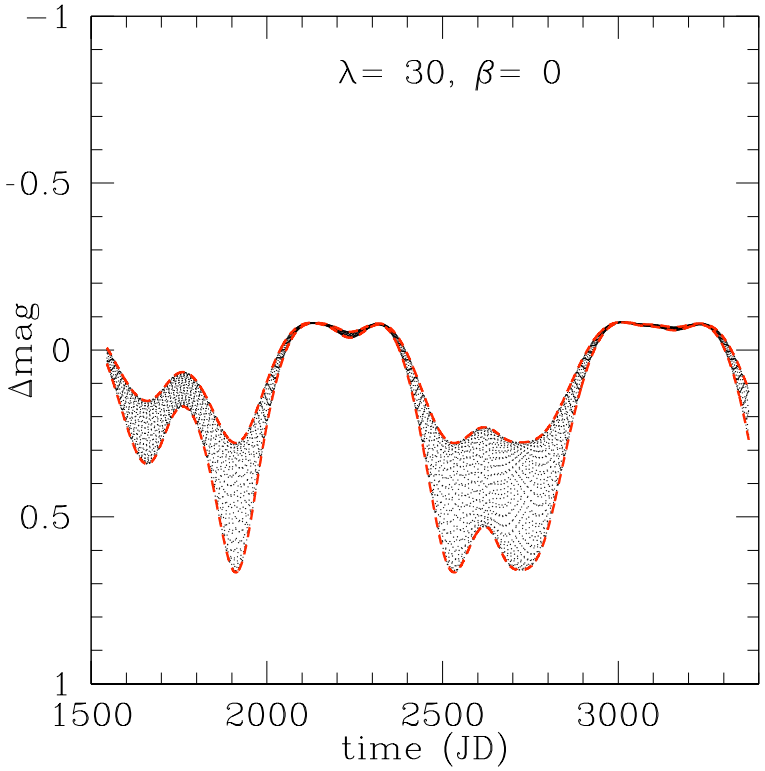

Fig. 12. The same as Fig. 10, but this time the ecliptic latitude of the asteroid's pole is $\beta = 0°$.

In particular, the photometric accuracy will depend on the brightness of the target and it is expected to be better than 0.01 mag for single detections of objects down to approximately $V = 20.0$.

As we have seen above, the magnitudes of the objects detected at different epochs will depend on several parameters: the most important ones being the sidereal period, the shape and the orientation of the spin axis, and the illumination circumstances, described by the phase angle. Additional variations may come in principle also from possible albedo variegation of the surfaces, but this is not expected to be very relevant for the majority of the objects. The possible existence of a non-negligible fraction of binary systems must also be taken into account, but for the moment we will not deal with this problem.

Gaia will obviously measure apparent magnitudes, that will be immediately converted to magnitudes at unit distance from both the Sun and the satellite (reduced magnitudes). When reducing photometric data, the epochs of observations

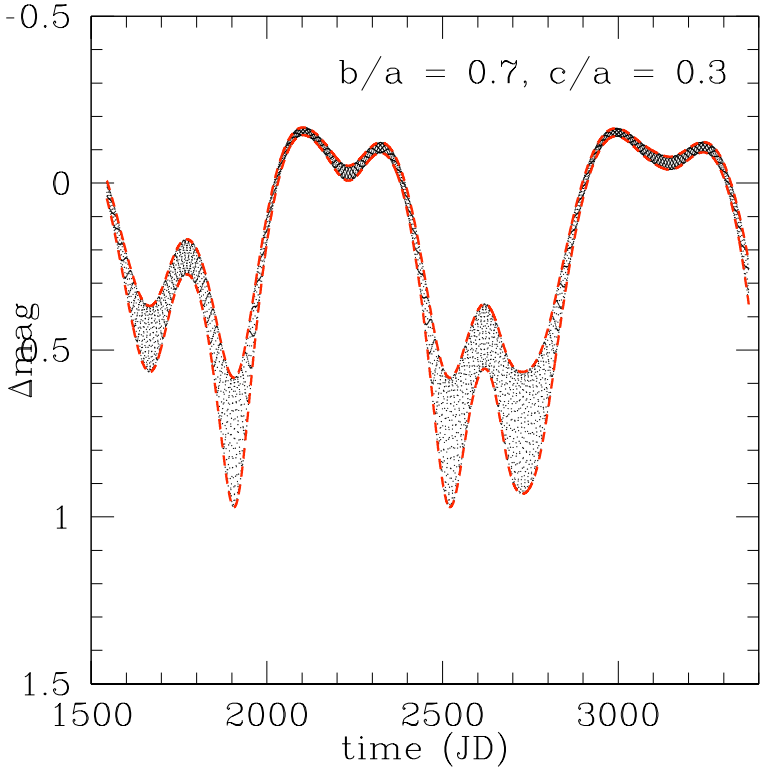

Fig. 13. The same as Fig. 10, but this time for an object having the same pole ($\lambda = 30°$, $\beta = 60°$), but a more elongated shape: $b/a = 0.7$, $c/a = 0.3$.

will also be corrected for light-time, being known the distance of the object at each detection.

Assuming now for sake of simplicity to deal with an object having a triaxial ellipsoid shape, orbiting around the Sun along a typical Main Belt asteroid orbit, it is possible to compute how the reduced magnitude is expected to vary as a function of time, depending on the coordinates of the pole. In particular, when making this exercise, it is convenient to work in terms of *differences* of reduced magnitude with respect to a reference observation (for instance, the first one in a series of different observations collected at different epochs). In this way, any potential error related to the constant appearing in the definition of magnitude ($m = -2.5\log(\Phi) + c$, where m is the magnitude, Φ is the received (normalised) flux and c is a constant depending on the chosen units) is automatically removed.

If, for sake of simplicity, we make also the assumption that the object is always observed at zero phase angle, it is easy to produce the plots shown in Fig. 10 - 14, which have been computed assuming that the object has the same orbit of

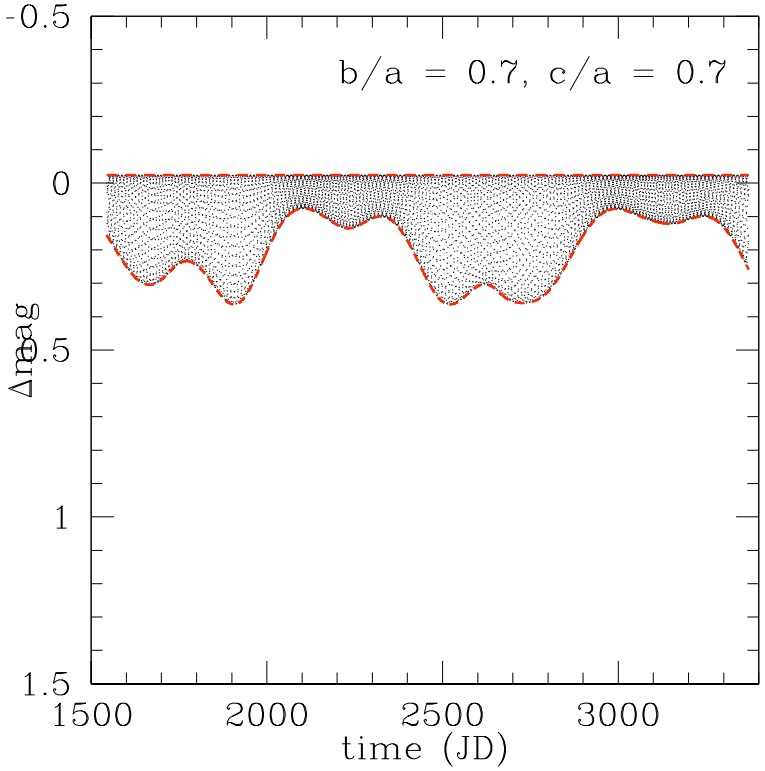

Fig. 14. The same as Fig. 13, but this time for an object having the same pole, but axial ratios: $b/a = c/a = 0.7$. The fact that $b = c$ has the effect of making constant the lightcurve maximum at all aspects.

asteroid (39) Laetitia, a typical main belt asteroid. Note that a choice for the object orbit must be done, because the aspect angle at any epoch depends both on the coordinates of the rotation pole and on those of the object itself, which is a function of its orbit.

The plots shown in Fig. 10 - 14 represent the domains in the time - Δm plane, Δm being the difference between the magnitude at time t and the magnitude at reference time $t = t_0$, occupied by the object during an interval of five years. In particular, the figures show how the domain of permitted Δm changes as a function of the object's shape (axial ratios) for a fixed pole of rotation, or, *viceversa*, as it changes by assuming a fixed shape, but varying the coordinates of the rotation pole. It must be noted that the above plots are used only to give a qualitative idea of the role played by shape and pole orientation in determining the possible range of photometric variation of an object, but they are not at all detailed representations of the real world.

In particular, the plots correspond to a very ideal situation in which the object has a perfect triaxial ellipsoid shape, and it is always seen at perfect Sun opposition. Thus, the effect on the apparent magnitude that arises from the fact of observing the object at different phase angles in different illumination conditions is not taken into account. Equally important, no realistic effect of light scattering is taken into account, and the magnitude is assumed to be purely due to the extent of visible illuminated area seen from the observer.

Of course, the real objects will only be sparsely observed by Gaia during the mission operational lifetime. As a consequence, what is more interesting is not the whole possible photometric domain where a given object can be seen during 5 years, but rather the way how the actual Gaia observations will sample the whole domain of photometric variation. To do this, one can take profit of detailed simulations of the mission, including observing circumstances of known asteroid detections, developed by a team including one of the authors of the present paper (PT).

Figure 15 shows the results of such an exercise. In particular, it shows how Gaia would sample the photometric variation of an ideal triaxial ellipsoid object having the same orbit of the asteroid (311) Claudia, a spin period $P = 19.15$ hours, axial ratios $b/a = 0.86$, $c/a = 0.71$, and pole ecliptic coordinates $\lambda_P = 49°$, $\beta_P = 51°$. As it can be seen, the sampling of the photometric variation seems fairly good. Even better, it is interesting to do the same computation, but showing the results in an ecliptic longitude - magnitude plot, as done in Fig. 16. (Note that expressing the coordinates in the equatorial reference frame, Right Ascension and Declination, would be totally equivalent). We recall that different ecliptic longitudes of the object correspond to different aspect angles. Fig. 16 shows therefore that an object having a typical main-belt orbit, like (311) Claudia, will be observed in a fairly wide variety of aspect angles. This is encouraging when trying to develop methods to use these sparse photometric data to achieve an actual data inversion, leading to the determination of objects' rotation properties and overall shapes.

Plots like the one shown in Fig. 16 are useful, because in principle a well sampled longitude - magnitude plot may provide *per se* a lot of information. In particular, we have seen that the maximum lightcurve amplitude is achieved in equatorial view, and directly provides an estimate of the b/a axial ratio, if we assume a triaxial ellipsoid shape. Moreover, the minimum lightcurve amplitude is reached at an ecliptic longitude corresponding to that of the asteroid pole. A minimum lightcurve amplitude close to zero means that the object may be seen nearly pole-on. Finally, a nearly flat maximum of the observed magnitude corresponds to an axial ratio b/c close to unity.

Of course, what is not known *a priori* when examining a longitude - magnitude plot like the one shown in Fig. 16 is the rotation period of the object. It is this parameter that determines the measured magnitude of the object at each single epoch of observation, which may be considered as a single snapshot of a continuous magnitude modulation superposed to the effects of the varying geometric observing circumstances.

In other words, the set of sparse photometric measurements that will be obtained by Gaia, as well as, it is important to note this, those from the ground based telescopes of the next generation of sky surveys like Pan-STARRS, can be considered as single points of a complex, time-extended hyper-lightcurve. The goal of the analysis of these data will be then that of being able to derive from them

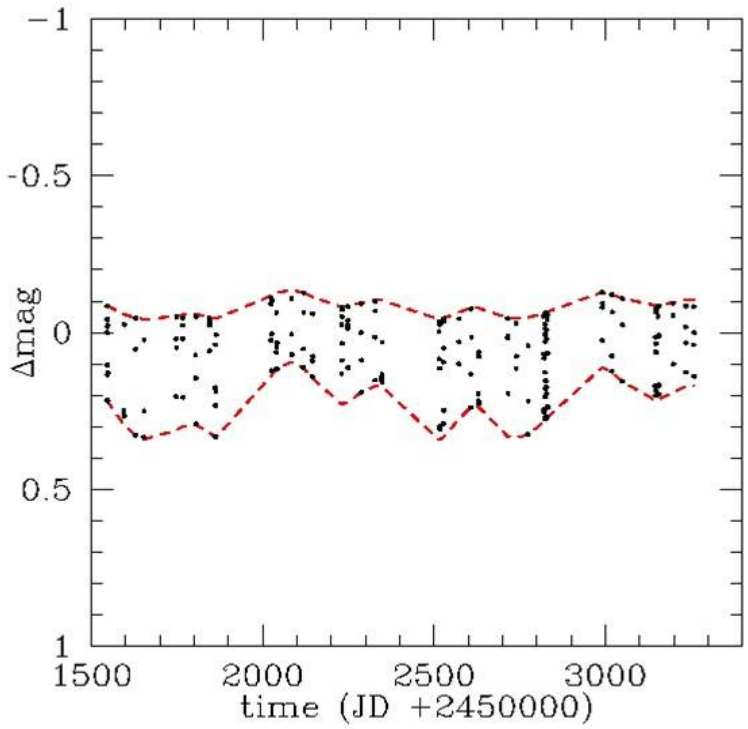

Fig. 15. Simulated observing circumstances of Gaia observations of a triaxial ellipsoid object having the same orbit of the main belt asteroid (311) Claudia, rotation period $P = 19.15$ hours, axial ratios $b/a = 0.86$, $c/a = 0.71$, and pole ecliptic coordinates $(49^\circ, 51^\circ)$. The predicted magnitudes as a function of time are plotted. The envelop represents the whole domain of photometric variation for such an object during the predicted operational lifetime of Gaia (5 years).

the main physical properties of the objects that are responsible of these observed hyper-lightcurves.

In particular, these is a list of parameters that should be determined by the photometric inversion:

- the asteroid's rotation period;
- the coordinates of the asteroid's pole, namely the intersection of the spin axis of the object with the celestial sphere. These two coordinates may be indifferently expressed in the equatorial or in the ecliptic system. Following the IAU convention [97] the ecliptic system should be preferred;

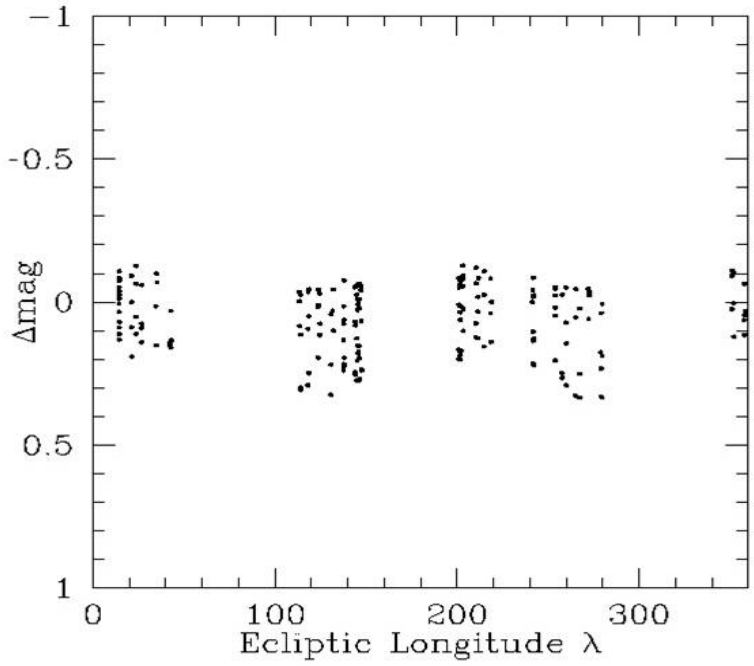

Fig. 16. The same as Fig. 15, but here the predicted magnitude is plotted against the ecliptic longitude of the object at the epochs of Gaia observations.

- some parameters describing the shape of the asteroid. In the case of a triaxial ellipsoid shape with semiaxes $a \geq b \geq c$, this reduces to two simple parameters, namely the axial ratios b/a and c/a;
- a parameter specifying the variation of the asteroid's brightness as a function of the phase angle. In practice, since Gaia will observe asteroids in a range of phase angles far from Sun opposition, and because the phase function is generally linear in the range 20-30 deg., the simplest approximation is to consider a linear magnitude–phase relation, described by one single slope parameter;
- a value specifying the rotational phase of the asteroid at a reference epoch, usually taken to be the epoch of the first recorded observation;

The above list corresponds therefore to a set of seven unknown parameters to be determined by the inversion, assuming that the objects have triaxial ellipsoid shapes. Of course, this particular shape choice is not the unique possibility that might be considered. Some explanation is then necessary, and is given in the next section.

6.3 Notes on the choice of a triaxial ellipsoid shape

Asteroids are small rocky bodies whose shapes are normally determined by solid-state forces rather than by self-gravitation. Asteroid images taken from short distances by space probes have generally revealed, mainly for the smallest visited objects, fairly irregular, "potato-like" shapes. Even objects of greater sizes, like (253) Mathilde, have revealed shapes strongly affected by the presence of giant concavities due to large impact craters. Moreover, in recent times there has been the development of methods of lightcurve and even sparse-data inversion, that have produced complex reconstructed shapes, that have been in several cases confirmed, directly or indirectly, by other pieces of independent evidence [54].

Based on the above evidence, the choice of approximating objects by means of triaxial ellipsoid shapes looks *a priori* very questionable. On the other hand, there are several reasons why this choice has been done for at least a preliminary inversion of the future Gaia data. Most of these reasons are strictly related to the need of reducing as much as possible the number of free parameters to be determined by the photometry inversion algorithm that will be described in the next section. Summarising, a list of reasons justifying the choice of a triaxial ellipsoid approximation is the following:

- In spite of being simple and depending upon only two parameters (the b/a and c/a axial ratios) triaxial ellipsoid shape are fairly flexible, and allow represent a fairly wide variety of shapes, from elongated "cigar-like" shapes, to flat disks, up to regular spheres.
- There are reasons to believe that, at least among the biggest asteroids, triaxial ellipsoid shapes might be a good approximation. The reason is that this is the equilibrium shape expected for re-accumulated objects having a large angular momentum. These objects, commonly called "rubble piles", are expected to exist, and correspond to the so-called LASPA (Large Amplitude Short Period Asteroids) objects, identified in the 80s ([32, 33]).
- Triaxial ellipsoid shapes have been successfully used by several authors in the past to compute asteroid rotation poles that have been confirmed also by other techniques [65].
- The shapes of impact fragments collected in laboratory experiments have been approximated in the past by triaxial ellipsoids [16]. The reason is that, when dealing with a variety of irregular fragments produced by energetic impact experiments, circumscribed triaxial ellipsoids turned out to be simple and sufficiently accurate to be used for building a reasonable statistics of the shapes of these fragments.
- One fundamental advantage of triaxial ellipsoid shapes is that they admit *analytical solutions* of the problem of computation of visible and illuminated areas as seen from an observer in any geometric configuration. This property is decisive for the choice of this kind of shape to be implemented in the kind of inversion algorithm that will be described in the following section.
- As we will see, the choice of triaxial ellipsoid shapes is justified *a posteriori* by the fact that it can be proven to be able to produce successful inversion not only of simulated objects having a wide variety of shapes and light scattering properties, but also of real objects previously observed during space missions in the past.

As a final remark, we note that using a model in which a triaxial ellipsoid shape is assumed to fit the objects, simply means that the corresponding inversion of available data will look for the triaxial ellipsoid shape that best fits the observations. One should be aware that this triaxial ellipsoid can well not be adequate to represent the fine details of the real shape, but this is not equivalent to state that the resulting inversion must be necessarily bad, in particular for the period determination. The goodness of the solutions must be checked *a posteriori* by extensive simulations and by applications of the inversion algorithm to real data. We also note that it might be over-ambitious to try to use sparse photometric data to get, in additions to spin periods and poles, also very detailed reconstruction of the shapes. We remind, for instance, that even the most advanced methods of shape reconstruction based on lightcurve data cannot deal with shape concavities in a straightforward way [54]. For this reason, even an apparently modest triaxial ellipsoid approximation can well prove to be useful to derive global shape estimations, and this may be convenient if this can be made with only a modest investment of CPU power, as we will see below.

6.4 Photometry inversion by means of a genetic algorithm

Before describing the details of the adopted algorithm for the inversion of sparse photometric data, it should be useful to point out that this is a problem that hardly can be attacked by means of a pure "brute force" approach based on the power of modern computers. The reason is that, although the number of unknown parameters is only seven (the rotation period, two pole coordinates, two axial ratios, one magnitude-phase linear slope, and one initial rotation phase), the number of possible combination of these parameters, corresponding to single possible solutions, is large, mostly due to the required accuracy in the spin period determination.

In fact, if one considers for instance the case of an object having a rotation period of 6 hours, the need to have the final photometric observations "in phase" within a not-so-small error of 0.8 in rotational phase, means that the spin period must be computed with an accuracy not worse that 10^{-5} hours. A brute force approach based on computing the best solution by building of grid of possible cases in the space of the seven unknown parameters would then lead to the need of performing a huge number of iterations, of the order of 10^{19}, as it is easy to verify taking into account the range of variability of the seven parameters (the period between 0 and tens of hours, the pole longitude between 0 and 360 degrees, the pole latitude between -90 and $+90$ degrees, the axial ratios between 0 and 1, the initial rotational phase between 0 and 0.5 (an ambiguity of 0.5 is permitted for this parameter), linear slope of the magnitude-phase relation between 0 and some tenths of magnitude per degree).

The above estimate means that the photometric inversion of each object would require an exceedingly big investment in CPU power. On the other hand, other approaches exist that may avoid the use of brute computing power, and may permit to save a lot of computing time.

Among these approaches, a one based on the development of a so-called *genetic algorithm* has been chosen for the processing of Gaia photometric data. Genetic algorithms are adaptive algorithms developed to solve some classes of problems that are particularly suited to being attacked using this kind of approach. Some

general ideas which are at the basis of the genetic algorithm approach are borrowed from natural sciences, and in particular from the processes of natural evolution of living species and survival of the fittest.

In particular, we can consider any possible solution of the problem of inversion of sparse photometric data as an individual "organism" characterised by its own "genome". The genome consists of a single value for each of the seven unknown parameters to be determined by the inversion. Any possible solution, therefore, is uniquely characterised by its own set of parameters (spin period, pole coordinates, axial ratios, slope of the magnitude-phase relation, and initial rotational phase), which can be seen as the "genes", or the "DNA" of the given solution.

Of course, different solutions can be more or less good. The range goes from completely bad solutions of the problem, up to excellent solutions, which may be accepted as the result of photometry inversion. The goodness of any given solution is assessed on the basis of its corresponding residuals with respect to a set of real (or simulated) observations. Better solutions give a better fit of the observational data, corresponding to smaller residuals $(O - C)$ between the observed data and those computed according to the given set of parameters. In the application to the Gaia problem, the parameter that has been used so far to quantify the goodness of a given solution is the following:

$$\epsilon = \sqrt{\frac{\sum_i (O_i - C_i)^2}{N_{obs}}} \tag{18}$$

where N_{obs} is the number of available observations, and O_i and C_i are the observed and calculated values of the ith observation, respectively.

The idea of the genetic approach is then to find a good solution of the inversion problem by taking an initial set of tentative solutions, randomly generated, and then let them "evolve" by mixing their genomes during a series of successive generations, until the correct solution of the problem emerges spontaneously. In other words, starting from an initial set of "parent" solutions randomly generated, and which are generally very bad, as one would expect *a priori* from a set of completely random attempts, an iterative process of production of new generations of solutions is started. The generation process consists in a random coupling of the parameters of two parent solutions, randomly selected, and/or in some random variation ("genetic mutation") of the "genome" of one single solution.

At each generation, a check is performed of the residuals generated by each newly born "baby" solution. If it is better than some of those solutions saved until that step, it enters the "top list", whereas the previously worst solution of the parent population is removed from the population.

In this way, after a number of the order of one million of "generations", a very good solution is usually found, which produces small residuals and basically solves the inversion problem. Due to the intrinsically random nature of this "genetic" approach, the right solution is not forcedly found always, but if the genetic algorithm is repeatedly applied to the same set of observed data (typically 20 times), then the right solution (giving the minimum residuals in different attempts) is usually found several times.

Based on the above description, it may be now clear why the assumption of a triaxial ellipsoid shape turns out to be very convenient using this approach. The

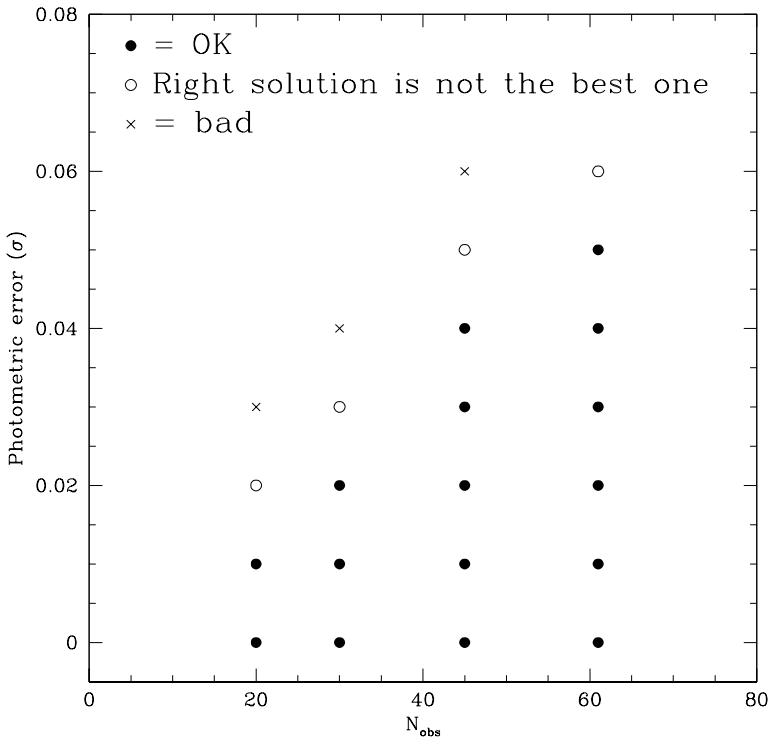

Fig. 17. Conditions of applicability of the photometry inversion method for triaxial ellipsoid shapes and simple geometric light scattering. The horizontal axis gives the number of available observations, while the vertical axis gives the photometric uncertainty of the observations (supposed for simplicity to be the same for each observation). The different symbols in the plot indicate whether the photometry inversion methods successfully finds the right solution, if it does not find a unique, right solution, or if it fails.

basic advantage is that each of the millions of computations of the brightness corresponding to the observing circumstances of each recorded observation can be made by using analytical formulae, instead of numerical computations of more complex shapes based on an approximation of the shape by means of plane facets, followed by the computation of the contribution of each facet to the total brightness. Such an approach, in principle feasible and more flexible, would lead in practice to a huge investment in CPU power and in much longer computing times. The apparent illuminated surface of a triaxial ellipsoid seen by any observer in any geometric configuration Observer - Asteroid - Sun can be instead computed by using analytical formulae, as shown by [90].

The performances of the adopted genetic algorithm for the inversion of sparse photometric data has been tested by means of a large number of numerical simulations, and by application to real data. In particular, simulations have been performed considering a large variety of situations for what concerns:

- the orbits of the simulated objects, to check whether orbital properties may have important consequences on the number of Gaia detections and on the variety of observing circumstances. In particular, the simulations have also dealt with near-Earth objects, taking into account that many objects of this type will be observed by Gaia, although the majority of detections will refer to main-belt asteroids;
- the rotation periods of the simulated objects;
- the spin axis direction;
- the object shapes. Both triaxial shapes characterized by a large variety of axial ratios, and more complex shapes, often taken from available observations (optical and radar) of real objects, have been simulated;
- different numbers of available observations, and different photometric uncertainties, in order to test the conditions of applicability of the inversion algorithm when the available data are scarce and/or the error bars of the data are large;
- different light scattering laws, ranging from pure geometric scattering to Lommel-Seeliger and Hapke scattering models.

For what concerns the last item in the above list, Fig. 17 shows the results of simulations of regular triaxial ellipsoid shapes in the simplified case of geometric light scattering (no limb darkening). Simulations produced cases with varying numbers of available observations, and different photometric uncertainties for each observation. As it can be seen, the results are strongly encouraging in these simplified cases, because they indicate that the inversion method should be applicable even in situations much worse than those expected to hold for Gaia data (numbers of observations of the order of 70, typical photometric uncertainties of the order of 0.01 mag). Even taking into account that the real objects will have surfaces scattering sunlight in a more complicated way, and non-ellipsoidal shapes, it seems nevertheless that the inversion method does a good job and it is not too much constrained by the number of data and their accuracy.

Figure 18 shows what the fit of simulated data can be in cases in which a significant photometric uncertainty of 0.03 mag is added to the computed magnitudes of a simulated triaxial ellipsoid body. As expected, there are not negligible $(O-C)$ residuals, but they are fully corresponding to what should be predicted *a priori*. The resulting inversion, in fact, turns out to be practically perfect in this case. This means a computed period solution within 0.00001 mag from the correct one, and pole coordinates within less than 2 degrees from the correct pole solution.

If simulations of triaxial ellipsoids without light scattering effect may seem too poor to assess the effectiveness of the photometry inversion algorithm, Fig. 19 is representative of what is encountered when much more realistic simulated cases are taken into account. The plot shows the simulated photometric data of an object having the same shape of (433) Eros as it has been derived from *in situ* observations by the NEAR-Shoemaker probe, and simulating a surface scattering the light according to a Hapke light scattering law with the usual parameters used to represent the photometric behaviour of real asteroids. In the same plot, the magnitudes computed—based on the result of the photometric inversion algorithm—are

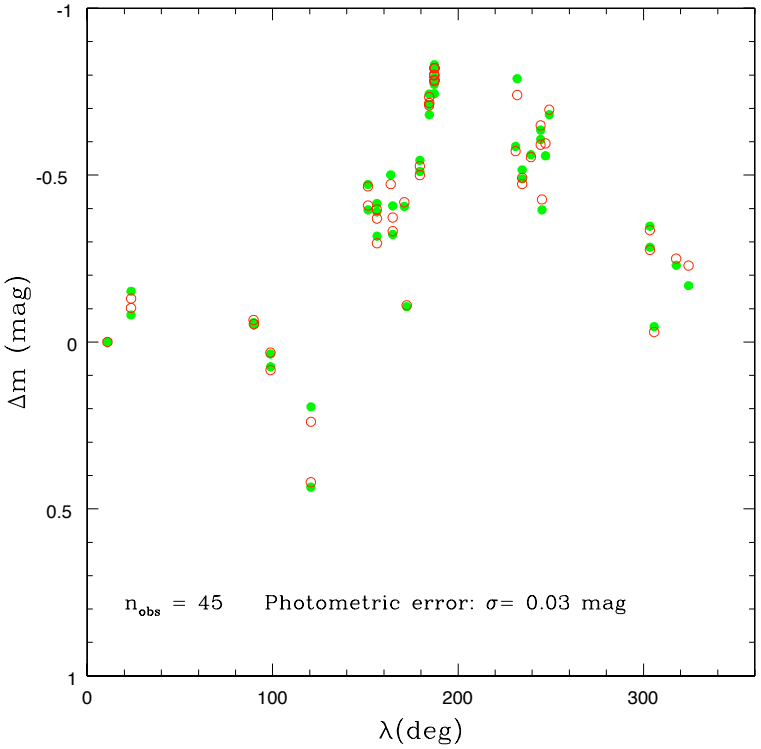

Fig. 18. Results of the inversion of a simulated triaxial ellipsoid asteroid with a fairly large superimposed photometric error of 0.03 mag. Filled symbols: simulated observations. Open symbols: corresponding computed brightness at each epoch of observation.

also showed for a comparison. As expected, there are large values of the $(O-C)$ residuals, like one should expect from a body as irregular as Eros (see Fig. 20) when approximated by a simple triaxial ellipsoid. In spite of the obvious oversimplification of the shape model used in the inversion algorithm, however, the solution turns out to be excellent, with the spin period being exact within a few thousandths of an hour, and the pole solution differing from the simulated one by less than 3 degrees; justifying our previous statement in Sect. §6.3. Even the very elongated, cigar-like shape of Eros is not badly reproduced by the shape solution, with b/a and c/a axial ratios both of the order of 0.4. This is not an isolated success of the inversion method. Equally good results have been obtained also for other complicated simulated shapes and scattering laws, including that of the asteroid (6489) Golevka, an Apollo asteroid observed by radar technique for which a detailed and highly non-convex shape model is available.

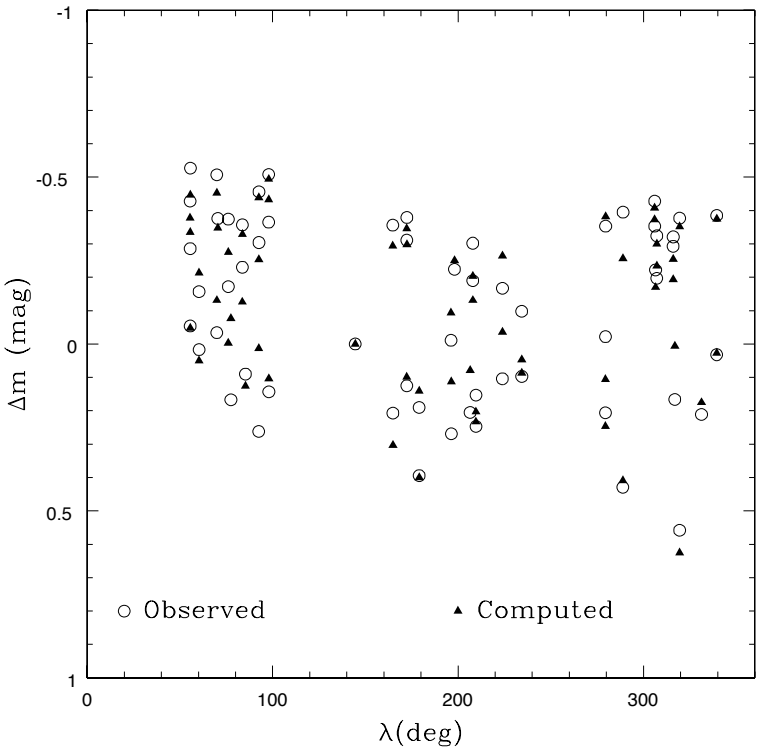

Fig. 19. The same as Fig. 18, but this time the simulated object had the shape of the irregular asteroid (433) Eros as resulting from the images taken by the NEAR-Shoemaker probe. In addition, the simulated surface was assumed to scatter sunlight according to a realistic Hapke scattering law.

The most important test so far performed of the effectiveness of the adopted photometry inversion algorithm has been the application to Hipparcos observations. We remind that the Hipparcos satellite is the immediate precursor of Gaia (see §2.1). What is important in the context of this discussion, is that Hipparcos obtained sparse photometric data for a limited number (48) of the brightest asteroids. Among these objects, many were observed only a few times, and/or the obtained data had large error bars. If we refer to the results shown in Fig. 17, only 26 objects satisfy the number of observations + error bar conditions that made inversion possible for simple simulated triaxial ellipsoid shapes without limb darkening. Among these 26 objects, moreover, some were just at the limit of acceptability.

A systematic analysis of these data has demonstrated that a successful inversion of Hipparcos data, in terms of successful determination of the orbital period and pole, has been obtained for 14 objects. In addition, inversion of the two big objects

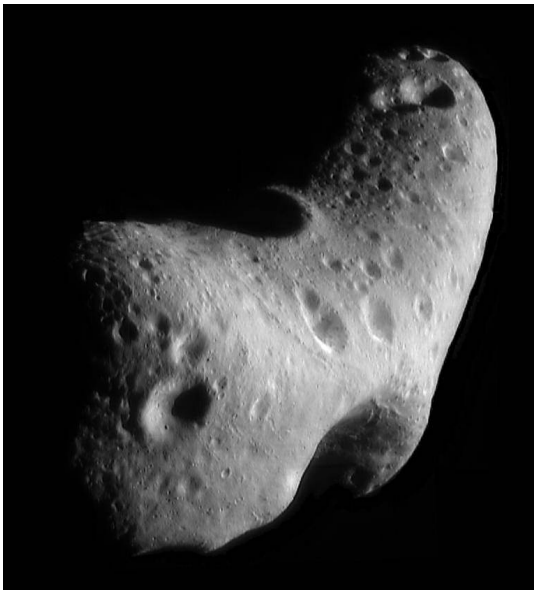

Fig. 20. A NEAR-Shoemaker image of asteroid (433) Eros. (*Courtesy of NASA*)

(1) Ceres and (4) Vesta were obtained, but with a resulting spin period equal to twice the correct value. These two results can well be explained by the fact that Ceres and Vesta are peculiar asteroids, whose photometric variation is due to albedo spots on the surface, and not to shape effects. Also the results of Hipparcos data inversion seem thus to indicate that the photometry inversion algorithm based on the genetic approach discussed in this section seems quite effective and reliable.

According to the results of these tests, it is reasonable to expect that the inversion of Gaia disk-integrated photometric data will lead to the determination of the spin properties and overall shapes for a number of the order of $10,000$ asteroids. Moreover, the triaxial shapes and pole coordinates obtained from photometry inversion will be used also to refine the determination of asteroid sizes as explained in §5.

7 The expected Gaia-based asteroid taxonomy

We have considered so far the photometric signal acquired in the broad Gaia photometric G band, and more specifically its temporal variation. As seen in §3.2 there are, after the crossing of the main astrometric field, two additional CCDs columns (RP and BP). These will provide low-resolution spectroscopy similar to multi-band colour-photometry measurements. One could again analyse variations due to the spin of the asteroids. We focus here on the information that can be obtained on the surface of the body, and the taxonomy of asteroids that can be derived.

The relevant spectro-photometric capability of Gaia will be used to obtain spectral reflectance data for a very large number of asteroids. As seen before, there should be a number of the order of 300,000 main belt asteroids that will exhibit apparent magnitudes brighter than 20 in V light when detected by Gaia. When passing through the BP and RP detectors of Gaia, the colours of these objects will be recorded. In particular, the whole range of wavelengths covered by the BP and RP detectors is from about 330 nm up to 1000 nm. This will make it possible to obtain spectro-photometric data covering about 20 bands in the above mentioned wavelength interval, producing a very valuable data-set of spectral reflectance data for asteroids. Of course, many objects will be faint, and, especially at short wavelengths, at some transits across the Gaia field of view the recorded fluxes will be below the detection limit. Moreover, in some cases the objects may move sufficiently fast as to be lost from the observing window before reaching the RP and BP detectors. Although detailed studies have not yet been produced at the moment, however, it seems that, taking profit of the fact that each object will be detected several times during the operational lifetime of Gaia (a number of detections of the order of 65 being typical for main belt asteroids), and some detections will be better than others since the objects will be brighter being at smaller geocentric distances, it is reasonable to expect that for a quite large fraction of the total number of detected bodies a complete coverage of the spectro-photometric behaviour from blue to red wavelengths will be obtained. These data will be very important because they will be used to derive a new taxonomic classification of a very big asteroid sample, much larger than any similar data-set currently available.

In particular, Gaia low-resolution spectral data will be obtained for objects over a wide range of sizes, and this will be important to analyze possible size-dependent effects on asteroid colours, related to the interplay of collisional and dynamical ages and effects of surface space weathering. For instance, it is known that the surfaces of young S-type asteroids that belong to the near-Earth population have spectral properties that are more similar to those of ordinary chondrite meteorites than those of larger, main belt objects orbiting belonging to the same taxonomic class.

From the point of view of taxonomy, Gaia will have a couple of excellent properties: first, this very large spectro-photometric data-base will be obtained using a unique, homogeneous photometric system, and not merging together data coming from different instruments. Second, and equally important, the spectral coverage will include the blue region of the reflectance spectrum. This is a very useful property, because the regions of the spectrum corresponding to the classical Johnson U and B colours, which were included in classical UBV spectro-photometric data-bases obtained many years ago by means of photoelectric photometers, are currently largely missed by the most recent spectroscopic surveys, like SMASS and SMASS2 [14].

One should consider, in fact, that the blue region of the reflectance spectrum is very important to distinguish between several groups of primitive, low-albedo bodies. Among the many thousands of asteroids that are expected to be classified based on the Gaia spectro-photometric data-base, a large fraction will consist of primitive, dark objects belonging to the so-called C super-class, which dominates the asteroid inventory in the outer regions of the asteroid belt. As opposite to spectroscopic surveys like SMASS and SMASS2, that were limited in practice to an interval of wavelengths between 0.5 and 0.95 μm, Gaia is expected to do a better job

in discriminating among different subclasses of the big C complex, and to determine the relative abundance of these different subclasses.

A typical example of an important class of asteroids that has been lost in recent taxonomies is the F class. This objects have low albedos, are generally more abundant in the outer belt, but they exhibit a local overabundance in the inner belt, possibly associated with a dynamical family (Polana [21]). Interestingly, F objects have been found to exhibit unusual polarimetric properties [6] and may also have some relations with comets, since comet Wilson-Harrington was classified as an F asteroid, before its cometary nature was discovered, and also the near-Earth object (3200) Phaeton, which is known to be associated with the Geminid meteor shower, was also classified as an F-type [6].

The Gaia taxonomy will be an important tool for studying the overall compositional gradient of the material which accreted into the planetary bodies in our Solar System [18]. Moreover, the availability of spectral reflectance data and taxonomic classification will also be important for future studies of the identification of asteroid dynamical families. The reason is that classical family searches have been based so far on the distribution of the objects in the space of proper elements. Since many families tend to overlap in this space, spectroscopic data may add a new dimension to the problem, and should be very useful to discriminate among members of different families overlapping in the space of proper orbital elements [19].

We note that new taxonomic classifications of the minor bodies of the Solar System based on spectral reflectance data will be obtained in the next years also by the next generation of dedicated ground-based surveys like Pan-STARRS and/or the LSST. The Gaia-based taxonomy, however, in spite of the existence of such "competitors", will "come for free", being an automatic sub-product of the BP and RP detections. Taking into account the above-mentioned coverage of the B region of the spectrum, and the general link with other, unique results that will be produced by Gaia asteroid observations, it is certain that Gaia taxonomy will be a very useful addition to the extremely important scientific value of the Gaia mission for asteroid science. For instance, it will be possible to link immediately the obtained average density determinations for about 100 objects with the taxonomic classification of the same objects, a very important result to interpret taxonomy in terms of overall composition of the objects. In this respect, also the determination of Gaia albedos of the same objects will be extremely important to sketch an overall interpretation paradigm of such a wealth of physical information.

8 Dynamical model improvement with Gaia

We have seen before in $4, that the Gaia mission will provide the orbits of a large number of asteroids with high accuracy. Not only will the observations be precise on the CCD (no refraction, no personal equation, well calibrated measure through one single instrument independently of the northern/southern hemisphere, etc.) but mostly all positions are referred to a very homogeneous reference frame (materialised by QSOs and primary reference stars), avoiding many systematic errors. Such refined orbits (for at least over the period of the Gaia observations) will enable to detect and/or measure small and subtle effect, either dynamical,

relativistic, or non gravitational. We will see some aspects for the determination of asteroids mass, test of general relativity and linking of reference frames. Because we have to wait to acquire the real Gaia data all results given below are hence obtained from simulations of the observations, and they mostly concern the precision of parameters estimation. Combining on one side the image simulation on the focal plane and a centroiding precision (§5.4) to the Gaia scanning law and asteroids ephemerides on the other side, one gets the useful data to derive the quantities presented below.

8.1 Asteroid mass

As we will see later (§ 10), monitoring the orbits of binary and multiple systems will provide their total mass, and in some circumstances, the mass of each component. The other way to derive the mass of an asteroid is to measure the mutual gravitational perturbation during a close encounter [118, 51, 76, and references therein]. This can be done from the perturbations of asteroids on Mars, or asteroids-asteroids perturbations. Indeed this generally involves a large massive asteroid influencing several mass-less target asteroids, although target asteroids can in some encounters act as perturber too. Given the high precision with which Gaia can derive the orbit of an asteroid (see Fig. 21), one can detect small effects affecting the orbit, in particular small perturbations during close encounters. It is clear that the effect can be detected only if the astrometric observations are obtained before *and* after the encounter itself. The more general and straightforward problem would be to integrate the equations of motions (and variational equations) of the dynamical system at once. This means a N-body integration with N of the order of 300,000 plus the eight planets, relativistic effects, the effect of the oblate Sun and a ring of asteroids, etc. The step size would need to be automatic and would be governed by the encounters. However such high CPU consuming algorithm is not necessary in our more hierarchical problem, where many asteroid orbits can be considered as perturbed two-body solutions. In fact the gravitational effect of a given asteroid i on a planet or an asteroid j is in most cases negligible and should not be computed, not only to decrease the CPU time but also to avoid unnecessary numerical noise. It is hence better to perform the integration by taking into account only relevant perturbations, and thus derive a list of potential perturbers. These perturbing asteroids are to be added to the classical perturbing major planets that are systematically taken into account in the perturbing function [75]. Note also that a perturbing asteroid can still be a target for another one, but the size of the N-body system is decreased by several orders of magnitude. So, the first step is to provide the list of targets for each large asteroid and inversely the list of perturbers to include for a given asteroid. In the second step, one computes the partial derivatives for the additional unknown masses. Note that when the error on the mass is large, the problem is likely to be non-linear. In the other case one starts with a linear least-squares treatment of the problem. It has been shown in [74] that Gaia will derive the mass of about 150 asteroids with a relative precision better than 50% (see Fig. 21). Since the number of targets is often large, systematic effects are reduced, so that Gaia will increase the *precision* of the mass determination, but mostly its

accuracy[8]. Some of the targets can be poorly observed with the Gaia scanning law,

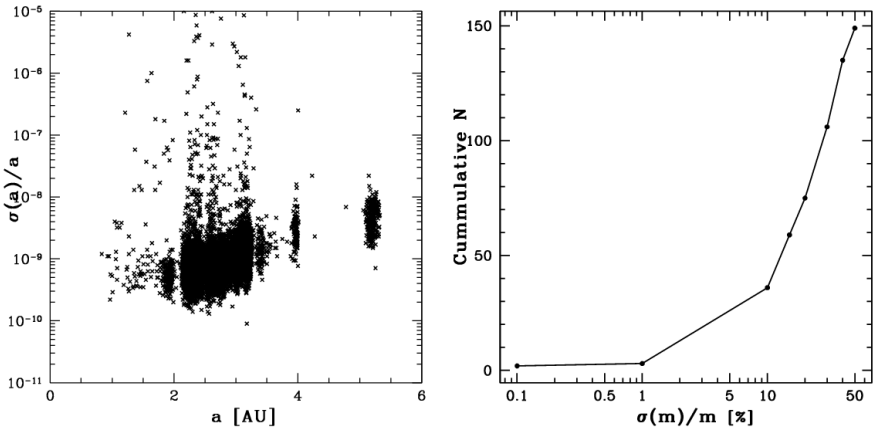

Fig. 21. Left: Orbit improvement; relative precision obtained on the semi-major axis from the 5 years of Gaia observations. Right: Precision of asteroid mass determination with Gaia from gravitational perturbation during close encounters.

or the encounter can take place close to the beginning or the end of the 5 years mission. In the latter case, having only half of the data is totally useless; so it could be interesting to complement the space-base data with additional ground-based astrometry. These should however be of good precision and over a limited time span to reduce the effects of systematic errors. Again, conservative simulations have shown that additional masses can be derived from such data combination [78].

The mass of Ceres and Vesta will surely be known with higher accuracy from the future Dawn mission, and they will help to validate the method. Some of the targets are also binary asteroids which will provide additional calibrations. Interestingly other asteroids in the list of Gaia mass determination have currently no mass determination, or act as large perturber on Mars [74]. Since the present limitation on the ephemerides of inner planets arise from the poor knowledge on the asteroids mass, Gaia will bring some improvement. Combining the measures of mass and size-shape-volume provides another fundamental physical parameter, the bulk density. With the aid of ground-based high-angular resolution observations this quantity will be obtained with high precision for about 60 targets, covering many taxonomic

[8] Note the semantic. Broadly, the precision corresponds to the dispersion or variance of a quantity around the mean or expectancy, while the accuracy will give the error between the true and mean. A parameter estimation or determination can be of very high precision, in particular when obtained from a large the number of observations, but in severe error if there are uncorrected bias in either the observations of the model. An illustration can be given by a badly build ruler where the graduation starts at 1 not 0, the precision of the measure is about 0.5 mm which is fair, but all measures are systematically wrong by 1 cm, hence inaccurate.

classes, and enabling to test possible links between density and taxonomy. We know for instance that rubble-pile asteroids or highly fractured ones can have substantial porosity making this link non trivial [12].

Global solution

Let us stress that—in contrast to previous works on mass determinations—these estimations are obtained while treating the problem globally: all targets for a perturber are treated simultaneously and cross-perturbers terms are also taken into account. The system of observational equations takes the form of a sparse diagonal-column bloc-matrix:

$$\mathbf{P}\cdot\begin{pmatrix} \mathbf{A_1} & 0 & \cdots & \cdots & \mathbf{G_1} & \mathbf{M_1} \\ 0 & \mathbf{A_2} & 0 & \cdots & \mathbf{G_2} & \mathbf{M_2} \\ \vdots & & \ddots & & \vdots & \vdots \\ 0 & \cdots & \cdots & \mathbf{A_N} & \mathbf{G_N} & \mathbf{M_N} \end{pmatrix}\cdot\begin{pmatrix} d\mathbf{q_1} \\ d\mathbf{q_2} \\ \vdots \\ d\mathbf{q_N} \\ d\mathbf{g} \\ dm_1 \\ \vdots \\ dm_p \end{pmatrix} = \begin{pmatrix} d\boldsymbol{\lambda}_1 \\ d\boldsymbol{\lambda}_2 \\ \vdots \\ d\boldsymbol{\lambda}_N \end{pmatrix} \tag{19}$$

where:

- N is the total number of asteroids ($\approx 300\,000$);
- $\mathbf{P}$ projection matrix to transform heliocentric (barycentric) position vector $\mathbf{x}$ to observed quantities λ (or RA, Dec);
- $\mathbf{A_i}$ is the Jacobian matrix ($n_i \times 6$) of the partial derivatives with respect to the initial conditions for asteroid i, $\left[\frac{\partial \mathbf{x}}{\partial \mathbf{q_o}}\right]_i$;
- $\mathbf{q_i}$ is the vector of corrections to the 6 initial conditions for asteroid i;
- $\mathbf{G_i}$ is the Jacobian matrix for asteroid i ($n_i \times n_{par}$) of the partial derivatives with respect to global parameters common to all asteroids $\left[\frac{\partial \mathbf{x}}{\partial \mathbf{g}}\right]_i$;
- $\mathbf{dg}$ is the vector of the n_{par} global parameters;
- $\mathbf{M_i}$ is the Jacobian matrix for asteroid i ($n_i \times p$) of the partial derivatives with respect to the mass corrections relevant to asteroid i. It is again a sparse matrix;
- dm_j is the mass correction for massive asteroid j perturbing asteroid i. As said before the list of perturber has been previously selected from a simulation of close encounters [76, 77].

This system is inverted for all parameters together and combining various target asteroids simultaneously.

Other small effects – Estimated and/or considered parameters

The photocentre offset corresponds to the difference—projected on the sky—between the centre of gravity of the body (the one to be considered in the equations of motion) and the point derived from some centroiding giving for instance the mode of the light distribution on the focal plane [62, 43]. For a sphere observed at full phase there is no difference as long as the light distribution is radially symmetric. Of course, if the phase is important the difference will be large; it scales with the

apparent size of the body and its surface properties light scattering and albedo variegation. Such effect is generally taken into account for planets and large planetary satellites [72] since it amounts to several mas. Considering only the phase i and the size of the object which assumed to be spherical (of apparent diameter ϕ) and with no albedo markings on its surface, one can write:

$$\delta\lambda_p = C(i)\ \sin(i/2)\phi/2 \tag{20}$$

where the displacement $\delta\lambda_p$ is given in the direction of the Sun. The function $C(i)$ depends on the scattering properties of the surface; for a perfect and hypothetical Lambertian sphere one has $C(i) \sim \frac{3}{4} + \frac{3}{32}i^2 + o(i^3)$, which generally yields an estimation of the *maximum* offset. This offset is also noticeable in the Hipparcos data for the largest asteroids [44]. With the high precision measure from Gaia, it will be of importance for a larger number of objects. There are three different cases depending on the size of the target, and our knowledge of its size, shape, and brightness distribution. If the body is small, the effect can be *negligible*; if the object is bright and large, the effect can be modelled with enough accuracy or some parameters can even be *estimated* from the inversion of the system of Eq. 19 itself [44]. Dynamical (state-vector initial conditions) and physical parameters (size, shape, ...) can be derived simultaneously for a combination of both astrometric and photometric data [53], however as long as they remain largely de-coupled one can also proceed iteratively with separate estimations of shape and light scattering properties from the photometry and size estimations from the astrometry. However, there remains the third and intermediate case where the effect (generally systematic, see below) is neither negligible nor can it be fully modelled or estimated for instance from incomplete knowledge of the shape and light scattering at the surface of the body [55]. In this case there will be additional random noise in the modelled photocentre offset which, in turn, will decrease the accuracy of other parameters estimation, this can be handled through consider covariance matrix [106]. The LLS problem to solve can be written as $\mathbf{A_x}.\mathbf{x} + \mathbf{A_c}.\mathbf{c} = \mathbf{b}$, where only $\mathbf{x}$ is the unknown vector to be estimated; the consider vector $\mathbf{c}$ of input parameters is assumed to be known but with some *a priori* uncertainty, e.g. $\boldsymbol{\sigma}^{\mathbf{2}}(\mathbf{c}) = \sigma^{\mathbf{2}}.\mathbf{I}$. Clearly, both the LLS solution for $\mathbf{x}$ and its variance/covariance matrix will depend on the choice of $\mathbf{c}$ and associated *a priori* variance/covariance matrix. Such procedure also allows to yield the sensitivity of the estimated parameter $\mathbf{x}$ with respect to the consider parameter $\mathbf{c}$.

One should note that the photocentre offset is a *systematic* effect, always directed toward the direction of the Sun, hence typically in the ecliptic plane for an asteroid. Being systematic, such effect should not be compared to the precision of a single observation in the error budget, but to the precision foreseen for global parameters, which—compared to the observation precision—scales as $N^{-1/2}$, and more specifically to their correlations. As analysed in [101, 43] for the Hipparcos data, the photocentre offset effect mimics a global rotation along the ecliptic pole. The situation is very similar to another systematic effect due to thermal inertia of the body, the Yarkovsky effect.

In addition to the perturbations already mentioned, one can consider non-gravitational forces acting on the dynamic of the body (out-gazing comet, asteroid, meteoroid, particle, ...) such as Pointing-Robertson or solar pressure. Here we consider the Yarkovsky drag which is a thermal effect. An asteroid is not a perfectly reflecting body and is re-emitting part of the solar energy in the thermal infrared.

Due to thermal inertia (and the asteroid rotation) this re-emission has some lag in time; to illustrate this consider for instance the hottest time in the day: it is not at solar noon but a couple of hours later in the day. Thus the photons are re-emitted in a direction different from the (radial) reception direction. Taking the balance of energy one sees that the force created can be decomposed by one part in the radial direction and by another part in the tangent direction, and hence create some additional non-gravitational force or acceleration (see Fig. 22). This effect that was previously considered for small particles such as meteoroids has been detected on larger bodies, first on the LAGEOS satellite [94] and later for asteroids [95, 121]. For a fast rotating body or a non-spinning one there is no diurnal effect. The Yarkovsky effect scales with the object size, its thermal inertia (or equivalently thermal conductivity), and last its distance to the Sun. The general trend effect is most noticeable in the NEOs population [23]. From its astrometric measurements alone, Gaia will not be able to derive all physical parameters involved in the Yarkovsky effect, but for some NEOs can derive one scaling parameter. This means that if the diameter and spin state are well known, the thermal inertia can be derived for a half dozen of bodies [74]. Again when not completely negligible such systematic effect can affect other parameters estimations, such as those involved in the local test of general relativity.

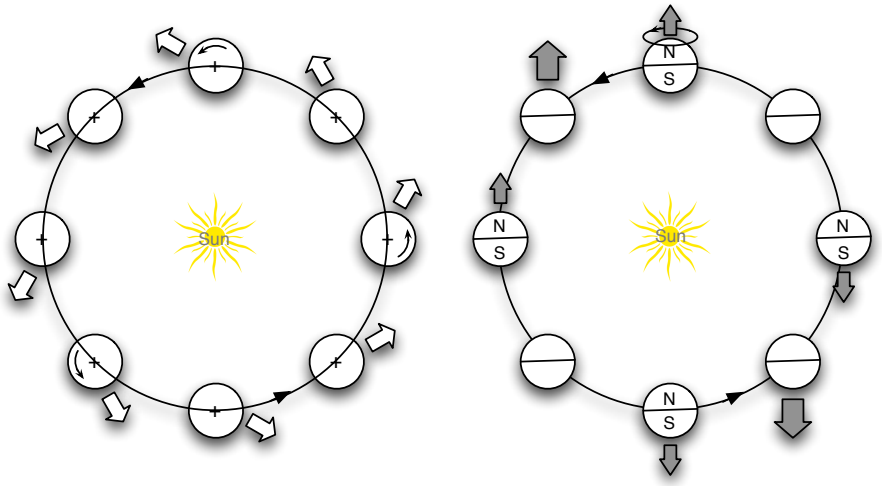

Fig. 22. The diurnal (left) and seasonal (right) Yarkovsky effects. Depending on the prograde (resp. retrograde) spin axis direction the force will secularly decrease (resp. increase) the semi-major axis of the asteroid (diurnal). In case of zero obliquity (purely seasonal) one always has $da/dt \leq 0$. (Credits GSFC NASA).

8.2 Local tests of general relativity & Reference frame link

There are three historical and fundamental tests that assessed with some success[9] the theory of General Relativity of Einstein (1916): precession of the perihelion of Mercury, light deflection by the Sun, and gravitational red-shift. A fourth can be added to that list that arrived later: the radar-echo delay, also called Shapiro effect. Last, let us note the importance of the work of Schwarzschild who derived—under given hypotheses—an exact solution to the equations enabling to predict quantitatively these effects.

It was known since Le Verrier in the middle of 19^{th} Century that the (Newtonian-Euclidian) planetary theories from celestial mechanics couldn't match with the precession of the perihelion of Mercury's orbit around the Sun of 43"/cy. No satisfactory explanation could be given until the theory of General Relativity that nicely predicts this very effect. Alternative theories to the GR do exist; a particular class of *metric theories* can be linearized and grouped in a parameterized formalism when gravity is weak and massive bodies move slowly $v \ll c$, the parameterized post-Newtonian formalism [125]. This expansion, in its 'first' order[10] corresponds to the classical Newtonian gravity, on in its 'second order', to post-Newtonian corrections [71]. Among the parameters of this formalism, γ reflects the light deflection and β the relativistic precession of the perihelion, they are both equal to one in general relativity. Test of general relativity, at least when dealing with phenomena in the Solar System, usually consist to measure the deviation to the canonical value predicted by GR for these PPN parameters [123, 124].

Excluding the part due to planetary perturbations that can be modelled precisely, the precession of the perihelion of the orbit of a solar system body is governed by the relativistic effect and an additional effect due to the oblateness of the Sun, given by its quadrupole moment J_2. Within the PPN formalism, the secular term for the argument of the perihelion ω is given by:

$$\begin{aligned} \Delta\omega &= \Delta\omega_{|PPN} + \Delta\omega_{|J2} \\ &= \left[\frac{6\pi m_\odot}{a^{5/2}\,(1-e^2)}\,\Gamma + \frac{6\pi R_\odot^2}{4}\,\frac{5\cos^2 i - 1}{a^{7/2}\,(1-e^2)^2}\,J_2 \right] (t - t_0) \\ &= \frac{3 m_\odot}{a\,(1-e^2)} \left[\Gamma + \frac{R_\odot^2}{4\,a\,m_\odot}\,\frac{(5\cos^2 i - 1)}{(1-e^2)}\,J_2 \right] n\,(t - t_0) \end{aligned} \tag{21}$$

where $m_\odot = GM_\odot/c^2 \approx 1.48\,\mathrm{km}$, $\Gamma = \frac{2+2\gamma-\beta}{3}$, a is in AU, t in year, n in rad/year, and last, $\Delta\omega$ is in radians. Neglecting the contribution due to the Sun, the relativistic effect from the general relativity is $\Delta\varpi = \Delta\omega = 6\pi m_\odot\,[a\,(1-e^2)]^{-1}\,\lambda_p$ [rad/cycle], which for Mercury yields a precession rate of 43"/cy. However it clearly appears from the equation above that the effect of the Sun and the relativistic effect are linearly coupled, and one cannot derive both unknown parameters from one single value of the precession of one planet. On the other hand,

[9] The two experiments for the light deflection during the Solar eclipse of 1919 were not free of some errors, but nevertheless gave a result close enough to the prediction to convince Eddington and Dyson, and further the scientific community. The precession for Mercury's perihelion matches the observations but the part due to the oblateness of the Sun is not well known.

[10] All small parameters are expanded simultaneously.

having different bodies spanning a larger range of eccentricities and semi-major axis, improves the separation of the unknowns; moreover there is an additional effect on the precession of the ascending node $\Delta\Omega = \Delta\Omega_{|J2}$ that arrises from the Sun only, while there is no particular relativistic effect on that argument.

The asteroids act as test particles in the gravity field of the Sun, having hence orbits that are well defined by Gaia enables—in theory—to derive both parameters separately. Performing simulations of the motions and Gaia observations of synthetic populations of NEAs [48] again yields a variance analysis. Since the actual known population of NEAs is not complete to apparent magnitude 20, we should not restrict ourselves to the known population only, but estimate also the NEAs yet to be discovered before Gaia. Heuristic samples have been produced following the (un-correlated) distribution in orbital elements and absolute magnitudes derived by [10]. For each possible set of Gaia observations we have determined the variance matrix for the unknown parameters including Γ and J_2 either simultaneously or separately.

Similarly one can add as global parameter a possible variation of the gravitational constant G, a problem similar to Gyldén-Mestschersky problem [68], also present in the analysis of Lunar-Laser Ranging data and planetary ephemerides [126, 88]. One should note that depending on the definition of the osculating elements, the results for the variation can differ [56, 41]. In addition one can also perform a link of reference frames. All computed positions are given with respect to a frame *defined* by the equations of motions and associated parameters (time scale, masses, etc.): the dynamical reference frame. This frame is materialised by the positions of solar system objects. All observed positions, in contrast, are given wrt a frame *defined* as kinematically non-rotating. This frame is materialised by the distant QSOs (extra-galactic, quasi-stellar objects) and next by reference stars for which the motion is well modelled. Both reference frames are non-rotating, either dynamically or kinematically; nevertheless a global rotation might subsist. In any case the reference plane and origin of longitudes in this plane are conventional and completely independent in each frame; in the case of the ICRF (the reference frame in used defined by the QSO from VLBI astrometry) it is close to the FK5 J2000 mean equator and equinox but the x axis does not point exactly in the direction of the vernal point. Again, all accurate observations of solar system objects can act as reference point to derive the rotation vector $\mathbf{W} = \mathbf{W_0} + \dot{\mathbf{W}}\,(t - t_0)$, i.e. both the rotation for the link to the dynamical reference frame W_0 at some given reference epoch t_0, and a possible test of rotation rate $\dot{\mathbf{W}}$. One sees from Table I that the rotation rate will be derived with a precision similar to the one of the Gaia optical ICRF reference frame itself.

9 Orbit determination and improvement

9.1 Introduction - A historical perspective

Determination or more exactly the representation of orbits is an old problem starting, after Babylonian tables, with the epicycles, and later with the work of Kepler who derived the correct form of orbits with the conics [100]. Another ancient aspect connected to this topic is the determination of the orbits of comets which

Table I. Standard deviation ($1\,\sigma$) for various global parameters derived simultaneously by Gaia. The rotation and rotation rate vector components are given in the ecliptic J2000.

	β	J_2	$\dot{G}/G$	$\mathbf{W_o}$	$\dot{\mathbf{W}}$	Ref.
	–	–	yr^{-1}	μas	μas.yr^{-1}	
Gaia	5×10^{-4}	2×10^{-8}	2×10^{-12}	2-2-5	1-1-2	[48]
LLR	2×10^{-4}	–	9×10^{-13}	–	100	[126]
EMP	1×10^{-4}	3×10^{-8}	1×10^{-13}	–	–	[88]
INPOP	–	2×10^{-8}	–	–	–	[34]

$1\mu\mathrm{as/yr} \sim 5\times10^{-12}\mathrm{rad/yr}$

shows some interest, or more recently the orbits and motion of meteoroids and meteor streams[11]. As noted by Gauss in his fundamental "*Theoria Motvs*[12]" preface [37, 36, 38], the problem for the comets (and now, for the asteroids too) is different from that for the planets for which many observations can or have already been gathered. In fact this amount of data collected principally by Tycho Brahe led Kepler to find his eponym laws; now, in the case of the small bodies, the problem to solve is different: we know the orbit has to be an ellipse or an hyperpola and we want to derive its parameters with only few data in hand. As shown by the historical examples of Olbers, and Halley for his famous comet[13], and also Piazzi, Gauss, von Zachs for Ceres, the practical significance to the determination of an orbit is to be able to compute the ephemeris and hence to be able to track the object in the telescope (consider nowadays typical $\approx 10'$ large/small fields of view) at its next apparition. If not, the body can be lost, necessitating some painful effort to catch it again; one illustrative example is given by the long-lost asteroid 719 Albert, discovered in 1911, it was re-discovered as 2000 JW8 in year 2000, about 9 decades later. With modern archives data-mining techniques [111] it becomes also interesting to be able to go back into the past and see whether additional data already exists.

Before the discovery of asteroids and the particular work of Gauss, the history of orbit determination was closely related to comets. Indeed comets were intriguing and furtive objects yet bright and showing large motion in the sky; but even their parallax remained for long unknown. Many attempts to derive their orbits were unsuccessful, mainly because the exact nature of the curve was not known[14], and

[11] Interestingly, it appears that comets were associated to meteors—in the etymological sense—by ancient philosophers [2].

[12] *Theoria Motvs Corporvm Cœlestivm in Sectionibvs Conicis Solem Ambientivm. Autore Carlo Friderico Gauss.*

[13] Nowadays comets are named after their discoverer, it was not the case at the time of Halley.

[14] Tycho Brahe having observed the comet of 1577 noted it could not be on a circular orbit, hence differing from the planets.

Fig. 23. G. Piazzi (1746–1826) on the left showing—not Gauss but—his newly discovered minor planet Ceres Fernandinea; and C. F. Gauß (1777–1855) on the right in a portrait (extract) painted well after the Ceres story (he was 24 at that time).

often assumed to be a straight line. Newton proposing in his "*Principia*" (1686, book III, prop. XLI) a geometric method based on a description by a parabola with the Sun at the focus, paved the way to future successes. While we shall note some contributions from Euler, Lambert and Lagrange in the field, the comet of Halley—or comet of 1759—is the first case for which an orbit and precise prediction was computed. Halley, following the work of Newton, identified in 1705 from the computation of the *parabolic* orbital elements, the apparent periodicity and successive returns of this celestial body (meaning the orbit is an elongated ellipse rather than a parabola). Next, from the calculation of the planetary perturbations on the comet provided by Clairaut (1762), it was possible to give accurate enough predictions for the 1759 apparition with all its spectacular outcome and a begining of a new era in the cometary science. The oldest apparition attested in observation goes back to 240 BC, in China, possibly 467 BC [27, and reference therein]. We will end this short historical review by mentioning the later work of Olbers, and by far mostly used technique for deriving the orbits of comets. Contemporary to Olbers, Gauss recognised the advances obtained by Newton for the orbit determination of comets: "The great Newton himself, the first geometer of his age [...] he came out of this contest also the victor", but added however that having one of the unknown removed (either eccentricity, or semi-major axis for the parabola) advantageously reduced the complexity of the problem (there are more equations than unknowns and no transcendental equations). The problem of the determination of an asteroid's orbit generally resides in the determination of the elliptic elements having several topocentric observations of the target spread over a limited interval of time (say a few weeks). In many situations in the solar system—and in contrast to a

full N-body problem—the Keplerian two-body problem studied by Newton gives a satisfactory approach; which can be, if needed, iteratively developed to higher degree of accuracy later-on by considering the small perturbations. The two-body problem is of importance also because it has a complete solution in closed form. In the following we shall focus mainly on orbits of asteroids, possibly as test particles in our Solar System, and sometimes massive bodies that show mutual perturbations or gravitational perturbations on Mars and/or other inner planets. We will at some point consider a perturbed two-body problem (the mass and attraction of the Sun is preponderant, the attraction of the planets act as small perturbation) with small additional gravitational forces. We will not develop the case of comets, for which well known non-gravitational acceleration can be important, neither will we discuss here the problem of the orbit determination of meteoroids or meteors, see [27, chap. 12]. We will not discuss the case of range and range-rate data although it is of major importance in modern data for NEAs and space vehicles. We will focus mainly on the problem of orbit determination for an asteroid given classical telescopic RA and/or Dec data.

The most impressive work performed on the determination of the orbit of asteroid was performed by a great mathematician and astronomer: Carl Friedrich Gauss[15]. It took some time to Gauss to publish[16] his work in the "*Theoria Motvs*" (1809), where he explains and exposes his method with great details but certainly with additional refinements that were not used in the original work applied to the Ceres case. Indeed the illustrative example of the orbit determination is given not for asteroid (1) Ceres but for (3) Juno [38, Book II, Sect. I]; Ceres is also treated with the additional observations obtained in 1805. One can note a few technical details that maybe are of no more use today: little use of rectangular coordinates, use of manipulations to carry out calculations with the aid of logarithms, use of a fictitious place of the Earth in the plane of the ecliptic to decrease the effect of unknown parallax, and reduction of time of observations to the meridian of Paris... After the discovery of the asteroid (or minor planet[17]) Ceres by the astronomer Piazzi at Palermo observatory in January 1801 (see Fig. 23), a large excitation arose to be able to predict its next apparition. Ceres[18] was observed starting from its discovery until the beginning of February down to a solar elongation of 70 degrees, corresponding to a relatively short arc of 3 degrees over 40 days. Being suspected to be a star, then a comet, it appeared clear at the discovery time that its orbit was more likely planetary. With his pioneering work and correspondence with astronomers, Gauss was able to predict Ceres' next apparition in December 1801 with a small 0.1 deg error as observed by Von Zach, and next Olbers one year after

[15] Karl Friedrich Gauß for the German spelling, this can be helpful for bibliographic research.

[16] It also took some time to have the text translated, 1857, 1859, and 1864 for the English, Russian, and French version respectively. The collected works of Gauss were published starting from 1862.

[17] The discovery of Piazzi is in some sense remarkable, he did find—depending on the nomenclature in use—the first planetoid, the first minor planet, the first asteroid, the first dwarf planet, and possibly [66] the first trans-Neptunian that was injected into the inner solar system!

[18] Originally called Ceres Fernandinea by Piazzi, referring to the King Ferdinand III of Sicily.

its discovery. This was better than any other predictions, and assessed the success of Gauss' method and collaborator observers[19]. The case of Ceres at discovery is given from his correspondence in the collected works, Band VI [35], with the data from 02/01, 22/01, and 11/02 1801. These dates are not too much separated in time and one moreover has $t_2 \approx 1/2\,(t_2 + t_3)$. The presentation of the method of orbit determination is generally separated in two parts, as was done by Gauss; in a first time one develops relation in the orbit and in space from positions or position and velocity, and in a second time one derives the method starting from 3 or more geocentric observations.

9.2 Orbit determination

Since the pioneering book of Gauss, several textbooks summarise the problem of the determination of an orbit, (elliptic or parabolic), and the evolution with time up to the modern ones allowing the use of fast computing machine [80, 81, 113, 87, 27, 30, 93]. Considering the two-body problem in the rest of this section, there are two classical problems encountered in celestial mechanics and astrodynamics computation of the position and velocity at a given time of a body given the orbital elements, or, inversely, obtain the orbital elements given the initial position-velocity conditions or state-vector [93]. The latter form is of particular interest since it says that the (heliocentric or barycentric) orbit is completely defined from the knowledge of such (heliocentric) state-vector. Another possibility to fully characterise the orbit is to have two (heliocentric) radius vectors, at any two different epochs (excluding however data separated by half periods, or colinear vectors). These are the basis of the methods for the determination of orbits developed by Gauss and Laplace. They are in fact very similar as pointed out by H. Poincaré in his preface of the Leçons[20] from Tisserand ([114]). The problem of Laplace and Gauss are indeed very similar but technically different and have encountered various success depending on the practical aspects to solve. Both Gauss and Laplace approximations will provide reliable results, possibly with different convergence speed. One can also note here that some practical refinement have been proposed by various authors (in particular [92] for the method of Gauss, or [64] for the method of Olbers). Actually, Gauss method is most widely used (it was already the case before modern computers [89]), although Laplace can be applied with modern CCD observations that allow to estimate the apparent motion of the body e.g. [15] it remains dependent on the precision with which one is able to derive the second derivatives of the right ascension and declination [27]. A comparison of the practical aspects with modern computations can be found in [17] (who also introduce a less famous method developed by the Italian astronomer Mossotti). The conclusion of their simulation runs is that Gauss method gives in general (more than twice times) better results (when compared to the reference orbital parameters a, e, i) than the one of Laplace.

All methods for deriving the orbit of an elliptic motion necessitate to solve non linear problems, involving transcendental functions, hence with no close form or general algebraic solution. Approximations are thus needed which generally also imply that observations are not too far apart but neither too close to encounter

[19] All these names are now associated to asteroids: 999 Zachia, 1000 Piazzia, 1001 Gaussia, and 1002 Olbersia.

[20] Note that only the methods of Olbers and Gauss are developed in these Leçons.

degeneracy of the problem. Gauss method supplant the one of Lagrange, in fact Gauss showed that it is more convenient to reduce the problem to two unknowns x, y involved in two equations $X = Y = 0$ as simple as possible. He also gave a method to compute the ratio of sector to triangle (Sect. 9.3), one of the fundamental quantities used. These classical methods require 3 (or more) observations, hence sufficient equations to derive the 6 unknowns of the problem. One other method of interest has been developed—in the case where only two topocentric observations are available—by Väisälä (in addition to the determination of a circular orbit, e.g. [112, 27]). If the orbital plane is close to the ecliptic the—classical—method fails, Gauss also considered this case and give the extension to find the orbit from four observations. Before starting the orbit computation itself one can also want to correct the observations (apparent directions given in, say, the true frame of the date, though today such frame will have to be replaced by the CIP and its non rotating origin) for various classical effects of (stellar) aberration, precession/nutation, parallax. These being in any case small, can often be ignored on the first step.

We give in the following a sketch of Gauss' method of orbit determination. Let us before reproduce a remark extracted from the preface of the French translator (E. Dubois [36]) of Gauss' work: "Or il est bien probable que la zone située entre Mars et Jupiter n'est pas encore suffisemment explorée et que le chiffre de 79 auqel on est arrivé, sera encore augmenté. Qui sait ce que réserve l'avenir !!... Bientôt alors les astronomes officiels n'y pourront plus suffire, si des calculateurs dévoués à l'astronomie et à ses progrès ne leurs viennent aussi en aide de ce coté[21]". Well, the future actually gave an increase by several orders of magnitudes of objects in that zone (and a few more in the Trojan and Trans-neptunian region) which number is still increasing exponentially; we shall ask again what will the future hold for us with ongoing surveys like Pans-STARRS, LSST and others?

9.3 Gauss method – a sketch

The general scheme of Gauss method is to reduce the problem to a system of two equations $X = Y = 0$ involving two variables x, y; one sets these two variables for two of the observations, derives the orbital parameters, and tests whether the equations are satisfied for the third observation. Generally they won't, so the next step is to derive the (small) corrections λ, μ to apply to x, y from the knowledge of the first order derivatives of $\partial(X, Y)/\partial x, \partial(X, Y)/\partial y$ and repeat the process until convergence to a solution that will satisfy all three observations together is reached. Actually Gauss does not give one, but five methods with additional extensions [38, Book II, Sect. I, 124–129], and comparison to the observed geocentric position itself is not always necessary. The first, and more natural, process given by Gauss is to take for the two variables x, y the geocentric distances (or the logarithm of these distances projected on the equator) for the first and last observations. From there on derives the heliocentric position vectors of the target, the orientation of the orbital plane in the inertial reference frame, and—from the timing and longitudes

[21] It is likely that the zone between Mars and Jupiter is not yet sufficiently explored and that the number of 79 that has been reached, will still be increased. Who knows what the future will hold for us!!... Soon official astronomers will not suffice, if some computers devoted to astronomy and its progress do not come to their rescue also on that side.

in this plane—all other elliptical elements. Computing the values for the third - middle - observation will yield two equations, that, for the computed orbit to be a solution, should satisfy $X = Y = 0$. Another variable that could be tested is the time difference for the third - middle - observations, but this is not as precise. The most common process is to take as unknown the heliocentric and geocentric distances of the asteroid at the second observation.

The f and g series and sector to triangle ratio

A Keplerian orbit is fully characterised from the knowledge of the 6 elliptic orbital elements, or also from the initial conditions of the equations of motion $\mathbf{r}_o, \dot{\mathbf{r}}_o$ at some reference epoch t_o. Gauss also showed that it can equivalently be derived from the knowledge of two heliocentric radius vectors $\mathbf{r}_1, \mathbf{r}_2$ at time t_1 and t_2.

The so-called f and g series are of fundamental use in such problems of preliminary orbit determination and approximation. Following [25, 30, 93] we shall introduce them broadly here. Starting with the equation of motion:

$$\frac{d^2\mathbf{r}}{\mathbf{dt^2}} + \mu \frac{\mathbf{r}}{r^3} = 0 \tag{22}$$

and introducing a transformation of time $\tau = \mu^{1/2}\, t = k\, t$, one can write:

$$\frac{d^2\mathbf{r}}{\mathbf{d}\tau^{\mathbf{2}}} + \frac{\mathbf{r}}{r^3} = 0 \tag{23}$$

and

$$\mathbf{r} = f(\tau)\, \mathbf{r}_o + g(\tau) \left(\frac{d\mathbf{r}}{d\tau}\right)_o \tag{24}$$

Expressing $\mathbf{r}$ in Taylor expansion from the starting position $\mathbf{r}_o$, and expressing also the derivatives $d^n\mathbf{r}/d\tau^n$ from Eq. (23) one gets the f, g series:

$$\begin{aligned} f &= 1 - \frac{\tau^2}{2\, r^3} + \frac{\tau^3}{2\, r^4} \frac{dr}{d\tau} + o(\tau^4) \\ g &= \tau \left(1 - \frac{\tau^3}{6\, r^3} + \frac{\tau^3}{4\, r^4} \frac{dr}{d\tau} + o(\tau^4)\right) \end{aligned} \tag{25}$$

note that g is given, without particular reason..., to order $O(\tau^4)$. On another hand, by introducing the eccentric anomalies, one can also derive a closed form for f and g:

$$\begin{aligned} f &= 1 - \frac{a}{r_0}\Big(1 - \cos(E - E_0)\Big) \\ g &= \tau - \frac{a^{3/2}}{\mu^{1/2}}\Big((E - E_0) - \sin(E - E_0)\Big) \end{aligned} \tag{26}$$

where E is the eccentric anomaly. Introducing the true anomalies v in the orbital plane, one can write one of Gauss' fundamental relations giving the ratio of sector to triangle:

$$y = \frac{\sqrt{a\,(1 - e^2)}\,\tau}{|\mathbf{r}_o \times \mathbf{r}|} \tag{27}$$

another formulation, not reproduced here, will give a similar—yet more complex—relation with the eccentric anomalies. This ratio can be obtained from continuous fraction of Hansen:

$$y = 1 + \frac{10}{9}\,\frac{h}{1 + \frac{\frac{11}{9}\,h}{1+\frac{\frac{11}{9}\,h}{1+\cdots}}} \tag{28}$$

involving the quantity $h = h(r, r_o, \tau)$.

Starting from the knowledge of the two radius vectors $\mathbf{r}_1, \mathbf{r}_2$ at time t_1 and t_2, Gauss provides—from the ratio of sector to triangle relation—a formulation to compute f, g from the Eqs. (26) above. We can now write:

$$\dot{\mathbf{r}}_2 = (\mathbf{r}_1 - f\,\mathbf{r}_2)/g \tag{29}$$

and consider that the orbit is fully characterised from the knowledge of the state vector $(\mathbf{r}_2, \dot{\mathbf{r}}_2)$ at time t_2.

9.4 Orbit determination from 3 positions

Since we are looking for a Keplerian orbit, all three position vectors $\mathbf{r}_i$ at time t_i are coplanar, so that one can write:

$$\mathbf{r}_2 = \frac{[\mathbf{r}_2, \mathbf{r}_3]}{[\mathbf{r}_1, \mathbf{r}_3]}\,\mathbf{r}_1 + \frac{[\mathbf{r}_1, \mathbf{r}_2]}{[\mathbf{r}_1, \mathbf{r}_3]}\,\mathbf{r}_3 \tag{30}$$

where the coefficients of this liner relation are exactly the ratio of the era of the triangles formed by the respective vectors. Taking in to account now Kepler's law of era, Gauss showed that one can get iteratively an approximation of the triangles era $[\mathbf{r}_1, \mathbf{r}_3]$ from the elliptic sectors era $(\mathbf{r}_1, \mathbf{r}_3)$ with high precision. Expressing the areas from the vectors cross products, and making use of the f, g series (§9.3), one will get an approximation for their formulation:

$$\begin{aligned} c_1 &\equiv \frac{[\mathbf{r}_2, \mathbf{r}_3]}{[\mathbf{r}_1, \mathbf{r}_3]} = \frac{g_3}{f_1 g_3 - f_3 g_1} \\ c_3 &\equiv \frac{[\mathbf{r}_1, \mathbf{r}_2]}{[\mathbf{r}_1, \mathbf{r}_3]} = \frac{-g_1}{f_1 g_3 - f_3 g_1} \end{aligned} \tag{31}$$

Putting:

$$\begin{aligned} \tau_1 &= k\,(t_3 - t_2) \\ \tau_2 &= k\,(t_3 - t_1) \\ \tau_3 &= k\,(t_2 - t_1) \end{aligned} \tag{32}$$

and expressing the f, g coefficient with the modified time, one has:

$$\begin{aligned} c_1 &= \frac{\tau_1}{\tau_2}\left(1 + \frac{\tau_2^2 - \tau_1^2}{6\,r_2^3}\right) + o(\tau^3) \\ c_3 &= \frac{\tau_3}{\tau_2}\left(1 + \frac{\tau_2^2 - \tau_3^2}{6\,r_2^3}\right) + o(\tau^3) \end{aligned} \tag{33}$$

which equation still involves three unknowns. Examination of these relations show that taking for the time of the second observation $t_2 = 1/2(t_1 + t_3)$ will derive this

approximation with higher precision. Writing the simple triangle vectorial relation Sun, Earth and asteroid position at t_i:

$$\mathbf{r}_i = \mathbf{R}_i + \boldsymbol{\rho}_i \tag{34}$$

where $\mathbf{r}_i, \boldsymbol{\rho}_i$ are the heliocentric and geocentric positions of the asteroid, and $\mathbf{R}_i$ is the heliocentric position of the Earth, one obtains the system of three equations:

$$\rho_2 - c_1\rho_1 - c_3\rho_3 = c_1\mathbf{R}_1 + c_3\mathbf{R}_3 - \mathbf{R}_2 \tag{35}$$

and after some manipulation, one finally obtains a relation involving only $\mathbf{r}_2, \boldsymbol{\rho}_2$ of the form:

$$\boldsymbol{\rho}_2 = A + B/r_2^3 \tag{36}$$

and similar for others ρ_i, r_i.

This provides one equation involving the two unknowns ρ_2, r_2. Simple geometry of Eq. (34) at t_2 yields an additional one:

$$r_2^2 = \mathbf{R}_2^2 + 2\,\mathbf{R}_2 \cdot \boldsymbol{\rho}_2 + \rho_2^2 \tag{37}$$

This system of two equations and two unknowns can be solved numerically. Gauss however, either reduced the system to a single equation of the eighth degree, or to a transcendental equation. Having solved for r_2 and ρ_2 yields the other ρ_i, and next all $\mathbf{r_i}$. From the three position vectors at the three dates, or equivalently $\mathbf{r_2}$ and $\dot{\mathbf{r}}_\mathbf{2}$ at t_2, the orbit is fully determined (see §9.3).

Starting from a first good approximation, it is an iterative method which improves the results at each step. In the next iterations the values for the triangles ratio c_1, c_3 given above to $o(\tau^3)$ will be improved. There are several ways to do so, Gauss developed his use of the sector to triangle ratio §9.3, and no new equations are to be used. Making use of Kepler's law of era, the ratio of triangles can be expressed as a function of the ratio of sectors:

$$c_1 \equiv \frac{[\mathbf{r}_2, \mathbf{r}_3]}{[\mathbf{r}_1, \mathbf{r}_3]} = \frac{(\mathbf{r}_2, \mathbf{r}_3)}{(\mathbf{r}_1, \mathbf{r}_3)}\,\frac{y_2}{y_1} = \frac{\tau_1}{\tau_2}\,\frac{y_2}{y_1} \tag{38}$$

where now the modified time should include corrections for light-time travel, etc. As noted by Gauss himself, three iterations are generally sufficient. This basic method is very performing when the angular observations are close together (but neither too much, to the point they would correspond to a single observation), the case for which Gauss designed his algorithm(s). Gauss also give conditions for the method to work [38, Book II, Sect. I, 130]. If the observations are spread over a large interval of time, the method is less well suited and might not converge. One can instead use the 'double r-iteration' technique [30] or very similarly the 'statistical ranging' technique (Sect. §9.5). In that case one simply takes randomly—with some initial guess on the nature of the object, NEA, MBA, etc.—two values for the geocentric distance at two of the observations. This defines all two radius vectors and one possible orbit. The 'double r-iteration' will iteratively correct the initial guess for the distances to converge to a solution, the statistical ranging will more simply proceed to straight trial/error Monte Carlo sampling of possible values.

The method of Laplace - briefly

In the method of Laplace one writes the first and second derivatives of the position vector $\mathbf{r}$ considering that the observations can provide the corresponding derivatives for the observed apparent direction. Let us write the heliocentric position vector of Eq. (34):

$$\mathbf{r}_i = \mathbf{R}_i + \rho_i \mathbf{u}_i \quad ; \quad |\mathbf{u}_i| = 1 \tag{39}$$

Putting this expression in the equations of motion (22), one has a system of four unknowns $(r, \rho, d\rho/dt, d^2\rho/dt^2)$, the quantities for the Earth being given by the ephemerides[22]. One again will write the additional Eq. (37) from the triangle. The system can be reduced to an equation of an eighth-degree resultant (as with Gauss' method) involving only r_2 for the observation at time t_2. This is solved numerically by successive approximation. The characteristics of the solution have been studied by Charlier [87, chap. 3-21] who gave a geometrical interpretation for the various roots from a strophoid curve. The first and second derivative of $\dot{\mathbf{u}}$ are often derived from an expansion instead of being measured, this is also given by Laplace. The approximation of the geocentric distance will not be obtained as accurately than with Gauss method.

9.5 Other methods

Before developing the linear case that is well adapted to refinement of asteroids' orbit with large number of observations, of good quality and over large space and time span, we will briefly present non linear techniques than can be of interest for different purposes, in particular when convergence of the linearization method is not obtained, or when the problem remains highly non linear and/or non gaussian. Some of semi-linear or statistical inversion methods are presented in [11]; we also note with particular emphasis a filtering method already discussed some time ago [29]. Some of the methods making use of descent gradient or filters will still need some linearization parts and/or some relatively good initial guess of the solution. They do not exactly correspond to the case of what we have defined here as orbit determination, because they can fail if the initial conditions taken are too far from the true—and completely unknown—one. Another quite different approach is to tackle the problem of parameter estimation from the other side by some trial/error process: take one set of parameters randomly (either elliptic or equinoctial elements, or state vector, ...) and test if it is a solution (that is, including some possible error). One illustration can be given, in the one-dimensional case, by the dichotomy method for finding the real root of some monotone function $f(x) = 0$. Here one will sample the $\mathbb{R}$ space randomly, with however some additional improvement from the fact that $x_i \leq x \leq x_{i+1}$, where $f(x_i).f(x_{i+1}) \leq 0$. Some other methods rely on Monte Carlo technique, MCMC or Bayesian statistical inversion [61], or also genetic algorithms. In this case the full space-phase of the unknowns is sampled *with some adapted strategy* or algorithm to find the solution(s) in terms of χ^2 values. These techniques are fully generic and well adapted to modern computation

[22] To be found in the "Connaissance des Temps" for the Leçon of F. Tisserand, the "Astronomical Almanach" for Roy, or at URL http://ssd.jpl.nasa.gov and http://www.imcce.fr, here.

facilities including possibilities of parallel computations. The genetic algorithm has been introduced before in §6.4 for deriving unknown parameters from the measured photometric data, they are also used recently in orbit determination of extra-solar planets from measured radial velocities [82, 24]. Statistical ranging [119] is another algorithm of statistical inversion that provides the full set of orbits from Monte Carlo technique. This method is particularly well adapted to the case where observations are scarce and cover short arcs. It is very similar in nature to the method described before for the orbit determination when two positions at two dates are known. Given two observed geocentric directions $\mathbf{u}_i$ at two dates t_1 and t_2 (generally close in time) one will now span the range of plausible geocentric distances ρ_i for both observations to construct two heliocentric positions $(\mathbf{r}_i = \rho_i \mathbf{u}_i + \mathbf{R}_i,\ t_i)$. Once the candidate orbit is computed from these two positions, it is tested whether it fits all available observations. This process is repeated in a Monte Carlo run until sufficient successful trials have been obtained for sampling the actual distribution of the orbital elements. The algorithm is combined to Bayesian approach involving *a priori* knowledge of the unknown quantities, this yields the full probability density of the solution. Obviously, when the number of observations becomes large, spanning a large range in time for several orbits, and the problem can be linearized locally; any trial/error methods will become not only much less efficient, but useless compared to classical linear least-squares.

9.6 Orbit improvement

The previous section was dealing with the orbit *determination*, i.e. find the orbital elements of the newly discovered asteroid, with little information and few measures, while nothing is known on its actual characteristics (distance to Sun or Earth, eccentricity, etc.). The previous method was based on the assumptions that the observations were not too much separated in time and/or space. When more data are acquired and over a larger time-span compared to the orbital period, one shall get a better idea of these elements. Having at our disposal some initial guess of the orbit, we will now look for orbit *improvement* (or differential correction of orbit); this is the aim of the second part of Gauss' book, where he also puts the basis of the least squares method that we are going to present briefly. There are several methods for orbit improvement, the most commonly used being the linear least squares (LLS) from differential correction that will converge rapidly to the least squares solution. If the system is highly non-linear one might use a general least-squares method (e.g. Levenberg-Marquat). In both cases, the solution is the one that will minimise the L^2 norm of the residuals[23], and the confidence regionConfidence region around this solution will be an $n-$axial ellipsoid obtained from a local linear approximation. Last, in more general cases where the problem to invert is non-linear and the input data are not of the same distribution, one can obtain maximum likelihood estimators (MLE) other than the least-squares solution.

We will hereafter develop the LLS method for orbit improvement of asteroids, and briefly discuss another approach from statistical inversion. We also implicitly assume the object is an asteroid, and do not consider here the cases of satellites of

[23] One can also, in case of poor robustness of the least-squares solution, consider other norms such as the L^1 one.

the Earth, planetary satellites, or comets, for which different adapted methodologies have been developed.

9.7 Linear system – LLS

Starting from the equations of motion, and writing the Taylor expansion to first order for the barycentric (resp. heliocentric) position vector denoted by $\mathbf{x}(t)$ (resp. $\mathbf{r}$):

$$\begin{aligned}\mathbf{x}(\mathbf{q_o} + d\mathbf{q_o}, p_1 \cdots p_m, t) &= \mathbf{x}(\mathbf{q_o}, p_k, t) + d\mathbf{x} \\ &= \mathbf{x}(\mathbf{q_o}, p_k, t) + \frac{\partial \mathbf{x}(t)}{\partial \mathbf{q_o}}\, d\mathbf{q_o} + o(dq_o^2)\end{aligned} \tag{40}$$

where the position/velocity state vector $\mathbf{q_o} = [\mathbf{x}(\mathrm{t_o}), \dot{\mathbf{x}}(\mathrm{t_o})]$ gives the initial conditions at t_o of the system, the one obtained from the orbit determination in §9.2, and where p_k are other dynamical parameters such as the perturbing planets and asteroids masses, etc. The computed geocentric directions[24] of the object $\mathbf{u}(t_i) = (\alpha_i, \delta_i, t_i)$ are derived from the barycentric (resp. heliocentric) position of Eq. (40) $\mathbf{u}(t) = \langle \mathbf{x}(t - \tau) - \mathbf{x}_{\mathrm{E}}(t) \rangle$, where τ accounts for the light-time travel and $\mathbf{x}_{\mathrm{E}}$ is the position of the Earth .

9.8 Partial derivatives

After correcting these directions for aberration, light deflection, precession/nutation, etc., one can compare them to the observed directions and derive the differences $O - C$ vector $(\Delta\alpha_i \cos\delta_i, \Delta\delta_i, t_i)$. Further, by neglecting all terms of the order of $o(dq_o^2)$ for the small corrections $|d\mathbf{q_o}| \ll 1$, one writes the linear system to solve:

$$O - C \equiv \mathbf{b} = \mathbf{P} \,.\, \left[\frac{\partial \mathbf{x}(\mathrm{t})}{\partial \mathbf{q_o}}\right] .\, \mathrm{d}\mathbf{q_o} \tag{41}$$

where the expression of $\mathbf{P}$ defining the projection from 3D to the nD observational space is left to the reader (see e.g. [13]). The 3x6 Jacobian matrix

$$\mathbf{J} = \left[\frac{\partial \mathbf{x}(\mathrm{t})}{\partial \mathbf{q_o}}\right] \tag{42}$$

has now to be computed. One can distinguish three different ways to compute such quantity in general, depending whether a) nothing is known about the function and only tabulated values are available, b) one can approximate the partial derivative computation to obtain analytical closed-form formulations, and c) we know the function to integrate and compute the variational equations. The first case also corresponds to the case where the variational equations might be to complex to derive and/or integrate.

[24] We restrict the discussion to classical telescopic observations, but these could be other quantities as e.g. range and range rate with radar, laser ranging, or any other technique, and from other positions in space than the geocentre as well.

a. **Finite difference**. The variant or finite difference method is practical for numerical computation, either by using the cartesian form or the elliptical elements for the initial conditions. It is obtain from the limit definition of a derivative:

$$\frac{\partial f(\mathbf{q})}{\partial h} = \lim_{h \to 0} \frac{f(\mathbf{q}+h)}{h}$$

by:

$$\frac{\partial f(\mathbf{q_o}, t)}{\partial h_i} = \frac{f(\mathbf{q_o} + h_i, t) - f(\mathbf{q_o} - h_i, t)}{2h_i} + o(h_i^3) \tag{43}$$

where the small variation h_i is applied to each element of the initial conditions $\mathbf{q}_o$ separately. With this formulation correct to the third order of the small parameter, one has to perform in general 3 numerical integration or ephemerides computation for $\mathbf{q}$, $\mathbf{q}_o + h_i$, and $\mathbf{q}_o - h_i$. One can reduce this number to two numerical integration with an approximation correct to only $O(h_i)$. The value of the quantity h_i has to be defined by the experience of the user; too small it increases numerical errors, too large it reduces the precision of the approximation. A practical value can be find by successive tests until the results of the partial derivative computation remains robust. It will in general be sufficient to use the same step for all objects and all observation dates.

b. **Two-body, analytical.** The analytical formulation with elliptic elements is given in [87, chap7] [13, chap. 9] and [27, chap. 11], it is also given with cartesian elements in [27] and [30]. They are obtained from the derivation of the two-body problem. We reproduce here without details the matrix for the more general use as given by [13], it is given as a function of corrections to the elements $d\mathbf{q} = (dl_o + dr, dp, dq, e.dr, da/a, de)$, and the position and velocity $(\mathbf{x}, \dot{\mathbf{x}})$ at time t:

$$d\mathbf{x}(t) = \left[\frac{\dot{\mathbf{x}}}{n} \; ; \; \mathbf{P} \times \mathbf{x} \; ; \; \mathbf{Q} \times \mathbf{x} \; ; \; \frac{1}{e} \left(-\frac{\dot{\mathbf{x}}}{n} + \mathbf{R} \times \mathbf{x} \right) \; ; \; \mathbf{x} - \frac{3}{2} t \, \dot{\mathbf{x}} \; ; \; H \, \mathbf{x} + K \, \dot{\mathbf{x}} \right] \tag{44}$$

The quantities H, K are given by:

$$\begin{aligned} H &= \frac{r - a(1+e^2)}{a\, e(1-e^2)} \\ K &= \frac{r\, \dot{r}(r + a(1-e^2))}{a^3 n^2\, e(1-e^2)} \end{aligned} \tag{45}$$

and the vectors $\mathbf{P}, \mathbf{Q}, \mathbf{R}$ are given by the rotation, transformation from the conventional equatorial frame to the frame associated to the orbital plane and orbit periastron:

$$[\mathbf{P}; \mathbf{Q}; \mathbf{R}] = \mathcal{R}_{\mathbf{z}}(-\mathbf{\Omega}).\mathcal{R}_{\mathbf{x}}(-\mathbf{I}).\mathcal{R}_{\mathbf{z}}(-\omega) \tag{46}$$

so that the variation of the angles $(d\Omega, dI, d\omega)$ are represented by new variables (dp, dq, dr) given in Fig. 24 representing an infinitesimal rotation along the directions of the periastron, the direction directly perpendicular in the orbital plane, and the direction of the orbital pole, respectively.

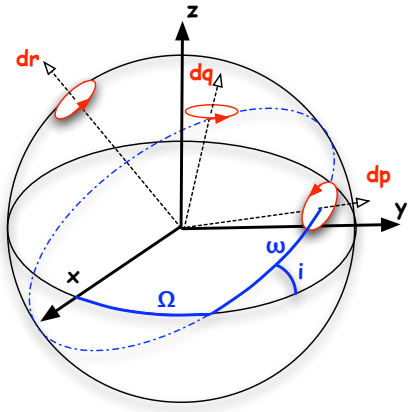

Fig. 24. Elements for the infinitesimal rotation associated to the asteroid orbit.

c. **Variational equations**. The variational equations are well adapted to the perturbed two-body problem and are computed during the numerical integration of the equations of motion themselves. The reader may have noticed that we did not yet explicitly mentioned the system to solve[25]: the equations of motion. In the case of a test particle orbiting a massive central body of mass $M_\odot$, and perturbed by N planetary bodies (planets, dwarf planets, asteroids, etc.) of masses M_i, we can write the equation of motion for the heliocentric position:

$$\ddot{\mathbf{r}} = -GM_\odot \frac{\mathbf{r}}{r^3} + \sum_{i=1}^{N} GM_i \left(\frac{\mathbf{r}_i - \mathbf{r}}{|\mathbf{r}_i - \mathbf{r}|^3} - \frac{\mathbf{r}_i}{r_i^3} \right) \tag{47}$$

Because of its properties one can write the differentiation:

$$\frac{d}{dt^2}\left(\frac{\partial \mathbf{r}}{\partial \mathbf{q}_o}\right) = \frac{\partial \ddot{\mathbf{r}}}{\partial \mathbf{q}_o}.$$

The 3x6 Jacobian matrix $\mathbf{J}$ can hence be obtained by integrating the system

$$\ddot{\mathbf{J}} = \frac{d}{dt^2}\mathbf{J} = \left[\frac{\partial \ddot{\mathbf{r}}}{\partial \mathbf{r}}\right] \mathbf{J} \tag{48}$$

and where now $[\partial \ddot{\mathbf{r}}/\partial \mathbf{r}]$ is given in closed-form and depends on the dynamical system to consider. For our perturbed two-body problem one gets the second order derivatives [8]:

$$\frac{\partial \ddot{\mathbf{r}}}{\partial \mathbf{r}} = -GM_\odot \nabla \left(\frac{\mathbf{r}}{r^3}\right) - \sum_{i=1}^{N} GM_i \nabla \left(\frac{\mathbf{r}_i - \mathbf{r}}{|\mathbf{r}_i - \mathbf{r}|^3} \right) \tag{49}$$

with the operator ∇ on vector $\mathbf{s}$:

[25] It was only implicitely used in method (b), but in its simple algebraic form for the 2 body approximation.

$$\nabla\left(\frac{\mathbf{s}}{s^3}\right) = -\frac{3}{s^5}\begin{pmatrix} s_1^2 - s^2/3 & s_1\,s_2 & s_1\,s_3 \\ s_2\,s_1 & s_2^2 - s^2/3 & s_2\,s_3 \\ s_3\,s_1 & s_3\,s_2 & s_3^2 - s^2/3 \end{pmatrix} = \frac{1}{s^3}\left(\mathbf{I} - \frac{3}{s^2}\mathbf{s}\cdot\mathbf{s}'\right) \tag{50}$$

and where both $\mathbf{I}$ the identity matrix, and the outer product $\mathbf{s}\cdot\mathbf{s}'$ are 3x3 matrices. One can extend such formulation to other perturbative forces and accelerations, and also to the more general N-body problem [8]. The initial conditions associated to the system in Eq. (48) are given by $J_{11} = J_{22} = J_{33} = \dot{J}_{14} = \dot{J}_{25} = \dot{J}_{36}$ and $J_{ij} = 0$ elsewhere. The additional equations (49) having been written, one has to solve simultaneously from numerical integration (e.g. some typical methods for ODEs integration: Bülirsch & Stoer, Adams Moulton, Radau, RK-k, ..., cf. [31]) the system of Eqs. (47) and (48), which will provide simultaneously the ephemerides and the partial derivatives.

Note that the effect of perturbing forces or perturbing bodies are not directly considered in cases (a) and (b), but through the computation of the position of the target only. This is particularly true for the analytical formulation of Brouwer & Clemence [13] given here, which formulation is somewhat hybrid since the position and velocities can also—and should—be computed not analytically, but from a numerical integration of the perturbed problem). In the case of the perturbed two-body problem, i.e. all forces of the perturbing planets are small and the asteroid does not influence the positions of the planets (no cross-terms), the formulations (b) and (c) remains fully tractable. In the case of a fully N-body problem, more cross terms and equations that have to be integrated appear in formulation (c).

9.9 Observational equations

The partial derivatives $\mathbf{J}$ being computed one can derive the solution and associated errors by classical linear algebra and matrices computations. The observational equations:

$$O - C \equiv \mathbf{b} = \mathbf{P}\,.\,\mathbf{J}\,.\,\mathrm{d}\mathbf{q_o} = \mathbf{A}\,.\,\mathrm{d}\mathbf{q_o} \tag{51}$$

give the observed and measured quantities as a function of the foreseen corrections $d\mathbf{q}_o$. The unweighted[26] least square solution to this linear system is given by:

$$\overline{d\mathbf{q}_o} = (\mathbf{A}'\mathbf{A})^{-\mathbf{1}}\,\mathbf{A}'\,.\,\mathbf{b} \tag{52}$$

and the variance-covariance matrix $\boldsymbol{\sigma}^2(d\mathbf{q}_o)$ for the errors and correlation is the inverse of the normal matrix $(\mathbf{A}'\mathbf{A})^{-1}.\boldsymbol{\sigma}^2(\mathbf{b})$. In the simplest case of one asteroid orbit to improve, this involves a 6x6 matrix inversion. In the more general case were more unknowns (initial conditions to the Cauchy problem and addition dynamical, physical, and instrumental parameters) have to be derived different techniques can be adapted such as Cholesky or QR algorithms for dense matrix; in the case of sparse matrices and iterative processes the conjugate gradient, which consist in minimising the quadratic form $f(\mathbf{x}) = (\frac{1}{2}\mathbf{x}'\,\mathbf{A}'\mathbf{A}\,\mathbf{x} - \mathbf{b}'\mathbf{A}\,\mathbf{x})$ will be preferred [91, 39]. Here we

[26] One can weight the equations to better take into account different observations noise by multiplying $\mathbf{A}$ and $(O-C)$ by the diagonal weight matrix $\sqrt{\mathbf{p}} = [1/\sigma_i]_D$ where σ_i is the standard deviation of the observed quantity at time t_i as estimated by the observer.

will focus on another method, based on the singular value decomposition (SVD), that is not optimal in terms of computation speed, but that is robust, and is well adapted to the case of degenerate and/or rank deficient problems. The SVD also deals with non square matrix, which is the case here when the number of observations exceeds the number of unknowns. Having a $m \times n$ matrix $\mathbf{A}$, $m \geq n$, of observational equations one can write the SVD decomposition [91]:

$$\mathbf{A} = \mathbf{U} \,.\, \mathbf{W} \,.\, \mathbf{V}' \tag{53}$$

where $\mathbf{U}$, $m \times n$, is orthogonal to the left $\mathbf{U}'\mathbf{U} = \mathbf{1}$, $\mathbf{V}$, $n \times n$, is orthogonal $\mathbf{V}'\mathbf{V} = \mathbf{V}\mathbf{V}' = \mathbf{1}$, $\mathbf{W} = [w_i]_{\mathrm{D}}$, $n \times n$, is diagonal, and the w_i are called the singular values[27] of matrix $\mathbf{A}$. The solution of our LLS problem is given from:

$$\overline{d\mathbf{q}_o} = \mathbf{V} \,.\, [1/w_i]_{\mathrm{D}} \,.\, \mathbf{U}' \,.\, \mathbf{b} \tag{54}$$

which does not necessitate to explicitly compute the normal matrix, neither to invert any matrix. Obviously if one of the singular value is zero the above expression is not defined, or in other words the determinant of the normal matrix ($\mathbf{A}'\mathbf{A}$) is null too and there is no *unique* solution. Similarly if one singular value is small ($0 < w_i/w_{max} \ll 1$) the matrix is ill-conditioned. This is encountered, for instance, in case of degeneracy of the problem or of high correlation between two (or more) unknown parameters, showing that given the available data they cannot be determined separately but only one (or more) linear combination can be derived. In such case the matrix can be considered to be rank deficient, and the solution retained—among all possible one—will be the one of minimal norm. The dimension of the kernel corresponds to the number of zero singular values, and a vector basis of this sub-space is given by the vectors of $\mathbf{V}$ corresponding to these zero singular values. In practice the SVD has one advantage, since in that case one simply sets to zero all small singular values, without any other modification to the computation software. The solution so obtained is the one of minimal norm, but the solution to the general problem is not unique and is given by $d\mathbf{q} = \overline{d\mathbf{q}_o} + \sum_{k=1,K} \alpha_k \mathbf{v}_k$, where K is the dimension of the (quasi)kernel and $\mathbf{A} \,.\, \mathbf{v_k} \approx \mathbf{0}$. To ensure the validity of the assumption that a singular value is zero one can test whether $\mathbf{A} \,.\, \mathbf{v_k} \approx \mathbf{0}$, and also that the residuals $\mathbf{v} = \mathbf{b} - \mathbf{A} \,.\, \overline{\mathbf{dq_o}}$ do not statistically differ, for instance from its L^2 norm, from the one obtained from the full inversion. Let us also mention the possible introduction of so called 'consider covariance matrix' which contains additional variance/covariance information on the model. This is useful when some parameters $\mathbf{c}$ were set in the observational or dynamical linearized model, which parameters cannot be estimated from the data at hand but that however are known with some uncertainty $\boldsymbol{\sigma}^2(\mathbf{c})$. The uncertainty of these assumed model parameters can increase the formal error of the unknowns [106].

Finally, independently of the method used to compute the partial derivatives of Eq. (42), and next to solve the linearized system of Eq. (51), one has a correction to apply to the initial conditions $\mathbf{q_o}$ that improves the asteroid's orbit and fits—to the least-squares sense—all available data. However the linearization of the equations is valid as long as the corrections are small. Additional iterations will be performed until the corrections to be applied are statistically non significant.

[27] The singular values of $\mathbf{A}$ are related to the eigenvalues of the positive symmetric normal matrix $\mathbf{A}'\mathbf{A}$, $\lambda_i = w_i^2$.

The least-squares estimator (LSE) is only under certain given conditions (often satisfied) equal to the maximum likelihood estimator (MLE). We do not discuss here methods of generalised least squares (GLS) that apply to non linear systems, these are iterative too, they also need to have a starting point close to the true solution, and last they generally provide a biased solution. In a linear model $\mathbf{Ax} = \mathbf{b} + \epsilon$, where ϵ is the error, the Gauss-Markov theorem states that if the errors are centred $E(\epsilon) = 0$, and also un-correlated and of same variance $\epsilon\epsilon' = \sigma^2\mathbf{I}$ (homoscedasticity); then among all estimators without bias, the LSE is the most *precise*, i.e. of minimum variance.

9.10 Confidence region

In the previous sections we have derived a solution, an orbit, that fits the data. If one chooses to weight the equation with some particular rule, or equivalently to suppress some data, or to apply another norm than the L^2, the results will be different. If the sensitivity of the solution is high with respect to these changes, the robustness of the solution is poor and should be taken with caution. Moreover the observational data are not free of stochastic (and possibly systematic) errors as recognised by Legendre (1806), their noise can be considered to follow a centred Gaussian distribution $\epsilon \in \mathcal{N}(0, \sigma)$ (as did C. F. Gauss in his pioneering work). So, as for any physical measure, one has to ask how accurate and precise (see note 8) is the solution obtained? It is known for instance that in the case of the orbit of planet Neptune [113] or comet Lexell (Le Verrier again!) [115], that the orbital elements are in rather strong error when compared to those that can be derived with large number of observations, but they nevertheless reproduce the available data well, and possibly were they the most probable solution. One will hence associate to any solution a confidence region. Other discussion and aspects to the orbit determination and improvement methods connected to observations of various type of asteroids can be found in [11] and [106] for satellites. In the case of a linear system, the observation noise being assumed to be Gaussian, the resulting LSE will follow a Gaussian distribution. The variance-covariance matrix $(\mathbf{A}'\mathbf{A})^{-1}$ defines the n-dimensional probability density function (p.d.f.) of the solution. Let us remind that the multivariate Gaussian distribution is entirely defined by the variance and co-variance of the parameter. This is associated to an ellipsoid, or to a quadratic form. One can hence decompose this matrix in the space of the proper elements $(\mathbf{A}'\mathbf{A})^{-1} = \mathbf{P}'.\mathbf{D}.\mathbf{P}$ where the matrix $\mathbf{P}$ gives the orientation of the principal axis of the ellipsoid in the frame of the physical parameters, and where the diagonal matrix gives the standard deviation 1σ of the parameters in the eigenspace. Also all probabilities or confidence region can be obtained from the 1σ value; for instance $P(|x - \mu| \leq 1\sigma) = 0.68268$; $P(|x - E(x)| \leq 3\sigma) = 0.99730$. In the non-linear case GLS, or if the observational noise is non-Gaussian, the LSE will provide one solution but little or no indication on its distribution or error. One can derive an error bar locally from a linear approximation, but if the error is large this estimation of the error or standard deviation can fail, giving raise to the question "What is the error on your error?". The χ^2 for a multivariate distribution can be complex, and can be sampled around this solution by Monte Carlo run or by use of the technique given in [3, 59, 122]. Depending hence on the problem to solve, one will have very different topology for the probability distribution that—only in

the case of the multivariate Gaussian of the linear case—will be summarised in a simple way from the variance-covariance matrix (see Fig. 25).

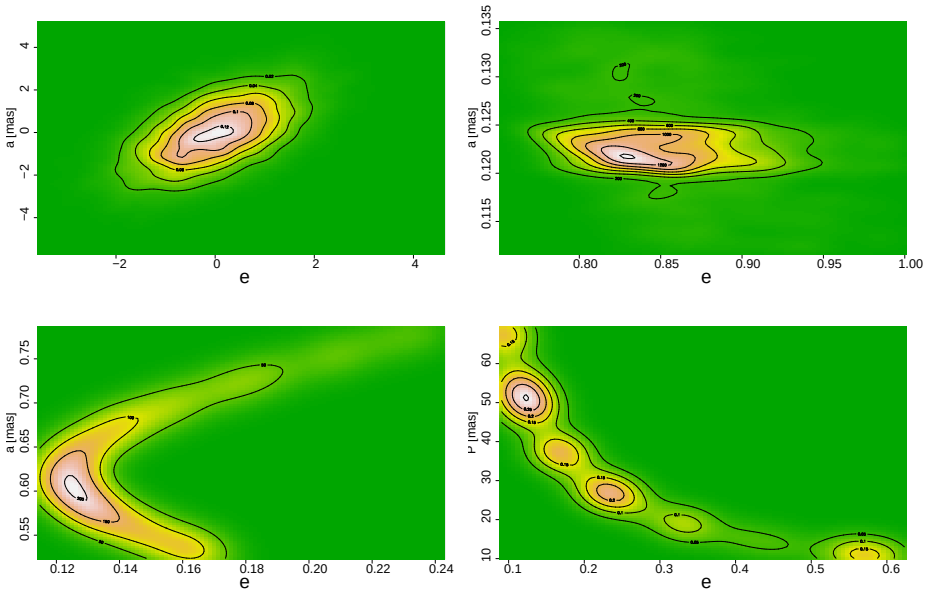

Fig. 25. Examples of 2D-projections from a multivariate orbital element distributions for the different cases of linear (top-left), semi-linear (top-right) and non-linear (bottom) problems of orbit determination/improvement.

10 Binary stars and asteroids

We discuss in the following section the case of astrometric observation of binary and multiple systems (stars, asteroids, etc.). The star ζ UMA, Mizar, was the first one found accidentally to appear as a *double star* through a refractor by Italian astronomer G. Riccioli[28] in 1650, well before E. Halley noticed to the attention of the Royal Society that stars do have proper motions (1718). Later, the German-born English astronomer Sir W. Herschel—the one that discovered Uranus and some of its moons with his stupendous telescopes, the one also that coined the denomination 'asteroid'—while cataloguing double stars, discovered their motion around one another, defining them as binary stars (1802,1803) [1]. Since the time of Herschel, such observations and measures of *binary stars'* relative positions, in opposition to *optical double* that happen only by chance to be close on the sky from projective

[28] Riccioli might have been preceded by B. Castelli in 1617, reporting to Galilei about Mizar "una delle belle cose che siano in cielo".

effect, are of high value. Of course they confirm that gravitation is universal and not only present for bodies orbiting around the Sun, for the orbits of satellites around their planets, but also for objects outside of our Solar System. Another very important impact is that it is possible to derive—with good accuracy—a fundamental parameter of the system otherwise inaccessible: the mass. The story for the asteroids in the solar system is not much different starting with some supposition of their existence with no clear evidence [65], to the accidental discovery of the satellite of the asteroid Ida by the space probe Galileo, and next to detection from ground based observations [67, and references therein]. Satellites of asteroids are found in the Near-Earth asteroid population as well as in the main-belt, the Trojans, Centaurs and the trans-Neptunian region. The typical mass ratio, orbital period and separation of these systems are generally different between the various populations, indicating different mechanism of formation (e.g. but not exclusively neither definitely, YORP spin-up for the NEOs, catastrophic collision in the main-belt, chaos assisted capture for the TNOs, ...).

In the zoology of denominations of stellar multiple and binary systems depending on their nature and techniques of observations, we will consider two particular cases: resolved and astrometric binaries.

- *Resolved binaries*, also previously called visual binaries, are systems for which each component is clearly detected or separated in the telescope, either in the visible domain or in other wavelength[29];
- *Astrometric binaries* are, similarly to most of the presently detected extra-solar planets, systems for which only one component is visible (the brightest) but the reflex motion of the photocentre shows a wobble with respect to the barycenter.

There are several techniques of orbit determination, graphical, semi-graphical, analytical, that were adapted to different cases and to different observations techniques. We will develop hereafter the one of Thiele [109], an analytical one that provides the true orbit from three observations. Before that, let us briefly mention the graphical method of Zwiers [87], that derives the true orbit after having drawn the observed and apparent one. In this method one will measure one important parameter characterising the orbit: the areal velocity constant; in order to do so, one shall cut in some paperboard the elliptical sectors and simply weight them on a balance to derive $C' = \rho^2 \dot{\theta}$; this sounds straightforward indeed, but surely not much in use today! In the following we will focus on the orbit determination of a pair once it has been discovered, and/or only few sparse and scarce data is available. In a first approach all orbits can be considered to be Keplerian (2-body problem). We will derive, from statistical inversion, not only one single solution but the (usually broad) bundle of orbits that fit to the data, and subsequently their density distribution.

10.1 Resolved binary – Thiele-Innes

In the case of a resolved binary, one has at his disposal the relative position of the two components, at the different epochs of observations. This position is often given in polar coordinates (North up and position angle counted positive from North to East) or more recently in cartesian coordinates. Assume now we have

[29] The reason why the terminology visual was abandoned because of a possible confusion with the 'visible domain'

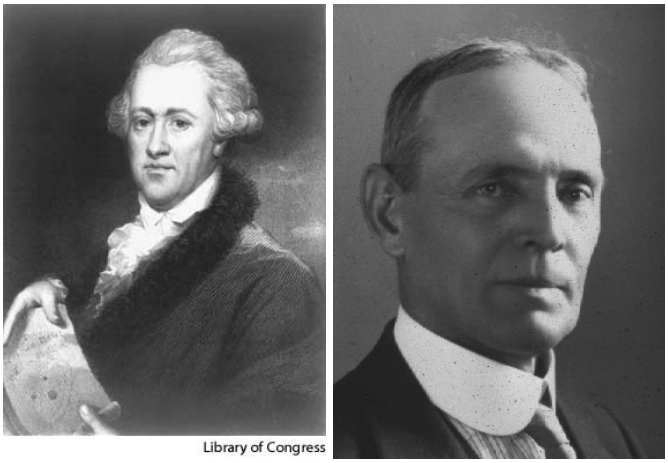

Fig. 26. Two famous binary stars observers from older and modern time. Sir W. Herschel (1738–1822) on the left , and R. G. Aitken (1864–1951) on the right.

such cartesian coordinates for n observations (t_i, x_i, y_i); $i \in [1..n]$ at time t_i. The objective or problem is to find a solution orbit, i.e. derive the orbital parameters of the orbit that fits the data. In case of under-constrained problem there is no unique solution. In the case of over-constrained problem, there is no exact solution, and we will look for a solution that fits the data in a way statistically acceptable. Based on the 'statistical ranging' technique of [120], a method of statistical orbit determination of binary systems has been constructed [49]. This later technique differs from the more recent one used in [40] since it makes use of the well known Thiele-Innes algorithm [109]. The Thiele, Innes, van den Bos algorithm [1, 42, and references therein] provides, when it exists, the Keplerian solution starting from three observational positions, and one assumed orbital period (or conversely the constant of areal velocity). Following [1], and putting:

$$X = \cos E - e$$

$$Y = \sqrt{1 - e^2}\, \sin E \tag{55}$$

one can write the relative position of the secondary:

$$\begin{aligned} x &= A\,X + F\,Y \\ y &= B\,X + G\,Y \\ z &= C\,X + H\,Y \end{aligned} \tag{56}$$

where the last equation corresponds to the radial (non-observed) quantity which—in contrast to stars—will be of particular use for solar system objects. This last linear system is also convenient to compute the relative position in space at any given epoch and makes use of the Thiele-Innes constants (A, B, F, G, C, H) instead of the usual elliptic elements:

$$A = a\,(\cos\omega \cos\Omega - \sin\omega \sin\Omega \cos i)$$

$$\begin{aligned} B &= a\,(\cos\omega \sin\Omega + \sin\omega \cos\Omega \cos i) \\ C &= a\,\sin\Omega \sin i \\ F &= a\,(-\sin\omega \cos\Omega - \cos\omega \sin\Omega \cos i) \\ G &= a\,(-\sin\omega \sin\Omega - \cos\omega \cos\Omega \cos i) \\ H &= a\,\cos\Omega \sin i \end{aligned} \tag{57}$$

Here the angles are referred to the tangent plane and one origin axis in this plane (see [1] for more details). By considering two observations p and q, the double area of the triangle is given by:

$$\Delta_{p,q} = x_p y_q - x_q y_p = (AG - BF)\,(X_p Y_q - X_q Y_p)$$

it can be related to the eccentric anomalies, yielding the fundamental equation of Thiele:

$$t_q - t_p - \mathcal{C}^{-1}\Delta_{p,q} = n^{-1}\,[(E_q - E_p) - \sin(E_q - E_p)] \tag{58}$$

Starting with three observations at time (t_1, t_2, t_3), and a given orbital period, one can then solve a system of three equations

$$\begin{aligned} t_2 - t_1 - \mathcal{C}^{-1}\Delta_{1,2} &= n^{-1}\,[u - \sin u] \\ t_3 - t_2 - \mathcal{C}^{-1}\Delta_{2,3} &= n^{-1}\,[v - \sin v] \\ t_3 - t_1 - \mathcal{C}^{-1}\Delta_{1,3} &= n^{-1}\,[u + v - \sin(u + v)] \end{aligned} \tag{59}$$

involving the unknown areal constant $\mathcal{C}$ and the two differences in eccentric anomalies $u = (E_2 - E_1)$ and $v = (E_3 - E_2)$, from which one eventually gets:

$$\begin{aligned} e\,\cos E_2 &= \frac{\Delta_{23}\cos(E_2 - E_1) + \Delta_{12}\cos(E_3 - E_2) - \Delta_{13}}{\Delta_{12} + \Delta_{23} - \Delta_{13}} \\ e\,\sin E_2 &= \frac{\Delta_{23}\sin(E_2 - E_1) - \Delta_{12}\sin(E_3 - E_2)}{\Delta_{12} + \Delta_{23} - \Delta_{13}} \end{aligned} \tag{60}$$

and the values for e and E_2, next E_1 and E_3, and corresponding mean anomalies from Kepler equation, time of periastron passage, then the values of X and Y from Eqs. (55), and finally the Thiele-Innes constants and elliptical elements. Note that the solution from this algorithm is almost obtained in closed form. The Keplerian equation is used and remains transcendental, but the numerical solution is easily obtained (at least for reasonable eccentricities of our—supposed—elliptic orbits). The system (59) of three unknowns is non linear but can be solved with Brown's method with good convergence whatever the starting point in $[0, 2\pi]$ and $\mathcal{C} = -1$ whatever the system under consideration, Main Belt Binary, Trans-Neptunian Binary, brown dwarf, etc.

Once the orbital elements are known one can compute subsequent positions for future as well as for past epochs. As said before, Eqs. (56) will readily provide such positions, but Thiele-Innes constants are related to one particular tangent plane. This plane is invariant for distant stars[30], but not for a solar system object where, after several months or years, the observer can observe the same system from an opposite direction. One can take into account this parallax in the Thiele-Innes

[30] Parallax in this case will introduce, as for the precession, small corrections to add linearly to the nominal solution.

constants from a transformation from one plane-of-sky to another one from a linear relation:

$$\begin{pmatrix} A' & F' \\ B' & G' \\ C' & H' \end{pmatrix} = \mathbf{P} \cdot \mathbf{A} \begin{pmatrix} A & F \\ B & G \\ C & H \end{pmatrix} \tag{61}$$

where

$$\mathbf{A} = \begin{pmatrix} -\sin\alpha_E & -\cos\alpha_E \sin\delta_E & \cos\alpha_E \cos\delta_E \\ \cos\alpha_E & -\sin\alpha_E \sin\delta_E & \sin\alpha_E \cos\delta_E \\ 0 & \cos\delta_E & \sin\delta_E \end{pmatrix} \tag{62}$$

is a transformation matrix from the POS (α_E, δ_E) to some conventional reference frame (ecliptic, equatorial, ...) independent of the system. Matrix $\mathbf{P}$ is simply an inverse rotation to some other direction (α'_E, δ'_E). Last, the apparent orbit (x', y') in this new POS is given by:

$$\begin{aligned} x' &= A'\,X + F'\,Y \\ y' &= B'\,X + G'\,Y \\ z' &= C'\,X + H'\,Y \end{aligned} \tag{63}$$

where (X, Y) are obtained from Eq. (55), and the radial coordinate z' is optional. We can note here that Eqs. (58) involving the classical Thiele-Innes constants (A, B, F, G) do not depend on the sign of the inclination i, so that there are two symmetric true orbits that project to the same apparent one. The coefficient in the new POS, in contrast, depend on the inclination and will not project to the same apparent trajectory, as will be discussed in a following section $10.3.

10.2 Monte Carlo

The previous algorithm provides one single solution starting from three positions or observations. This is not sufficient or satisfactory for at least two reasons:

- The observations are not free from errors, and one also needs to provide the confidence regionConfidence region around this nominal solution, including the fact that the solution might not be unique. Since the problem to solve is highly non linear, the error on the orbital parameters should not be Gaussian even from an observational noise that follows a normal distribution. A Monte Carlo (i.e. random) run will provide such information [61, 107].
- There are in general more than three observations and one wants to derive the most likely solution (e.g. in the sense of least squares) and also the bundle of orbits that fits the observations with associated probability. Bootstraping or Jack-knife without replacement will provide the bundle of orbits.

This goal can be achieved from statistical inversion with a trial/error Monte Carlo technique. At each step of the Monte Carlo computation one chooses a set of three of the observations for the (semi-) analytical computation of the orbit, and additionally one chooses an orbital period generally following a uniform distribution with no particular prior. The computed orbit is then tested for fitting all other available observations. Such statistical inversion will provide the bundle of orbits and their distribution as well as prediction of the position to other epochs and error propagation estimates. All retained solutions are mathematically satisfactory in the

sense that they fit the available relative positions data. One can then add additional filter by taking into account either an *a priori* distribution of the orbital element, or prior knowledge on the mass if some other satellite has been better observed, and more efficiently a limit on the total mass (or density) obtained, which in some cases can be physically unrealistic; making it readily adapted to a Bayesian analysis approach.

Note that one can introduce the observational error directly from a normal distribution, but also as uniform distribution with subsequent normalisation filter to be applied to the final set of solutions. Note also that the spurious symmetric solution can generally be removed if the parallax is large enough as in the case of an MBB. Using the Monte Carlo approach also enables one to analyse the propagation of errors to past or future epochs. In the latter case it is possible to derive the best epoch to observe a Trans-Neptunian binary (TNB) and remove the spurious solution (see Fig. 27). Indeed, there generally remains 4 intersections of the two symmetric orbits (i.e. intersection of the apparent trajectory *at the same date*) which observations would not enable to separate the spurious from the true one. This is of particular importance for at least two reasons: prediction of mutual phenomena, and test of formation models. Knowing the true inclination of the orbit enables one to predict the mutual phenomena (eclipses/occultation between the primary and secondary) that are of high value to better constrain many of the system's components physical parameters [110, 9]. Let us add that, similarly to equinoxes, such phenomenon occurs twice during a revolution of the binary system around the Sun, approx. every 150 years, hence extremely rare! The second reason why the inclination is an important parameter to know unambiguously is that different models of formation of binary systems exits [79, 127, and references therein] which do not give the same prediction. In particular the angular momentum can show an asymmetric distribution which can be tested from a measure of the relative frequency of prograde/retrogade orbits [60].

10.3 A summary

We can now resume the complete algorithm in the following sequence:

1. choose randomly 3 observations among the n available. These should nevertheless belong to a same group or run of observations, not to two very different tangent planes;
2. add stochastic error from the observational noise model ($\varepsilon \in \mathcal{N}(0,\, \sigma)$) with Box-Müller method [91, chap. 7], or prefer a more general uniform distribution that will ease further normalization or introduction of any other noise distribution;
3. choose one orbital period from stochastic distribution (e.g. $P \in \mathcal{U}\,[P_{min},\, P_{max}]$);
4. compute the orbit and Thiele-Innes coefficients from the algorithm described in the previous paragraph. In fact there are two fully symmetric orbits;
5. compute the positions for both symmetric orbits for all other $n-3$ observations, including parallax and other precession effects;
6. test if the resulting $O-C$ for all these positions is acceptable with respect to the observational noise
   − if no: return to step #1;
   − if yes: accept the solution with all parameters, and return to step #1.

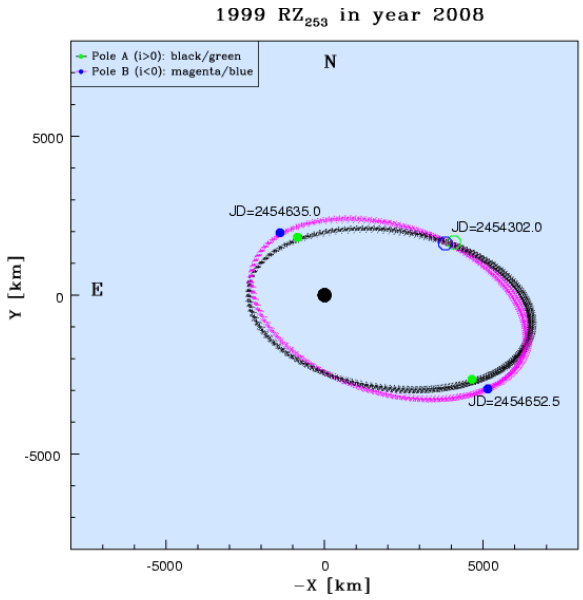

Fig. 27. Two apparent orbits bundle for the TNB Borasisi (ex. 1999 RZ_{253}) corresponding to the two symmetric solutions that fit equally well the data obtained 4 years before. The predicted positions at three different dates are also indicated. It is clear that at the epoch $JD = 2\,454\,302.0$ the orbits (not only the apparent trajectories) intersect, making it again impossible to distinguish the spurious from the true solution.

Because a subset of the observations sample is chosen, one can make use of the jack-knife technique for automatically detecting outlier points. Moreover, since only the orbital period is chosen arbitrarily, this Monte Carlo run is most efficient leaving a one-dimensional space to explore instead of the initial, more general and "brute force", 7-dimension problem to solve. Another possibility is to use the statistical ranging approach [120, 40]; in this case one has to chose two arbitrary relative distances for two different observations epoch. This increases the dimension of the problem, though still to practicable application. Having only *one* parameter of the space-phase to be explored (the orbital period) when all other orbital parameters are easily derived, the algorithm practical and fast in terms of CPU. At the beginning of the process one might have no indication of he orbital period and should span a large interval, e.g. [0, 100] days, depending on the system to be analysed (MBB, TNB, binary star, ...), or on another hand, one might reduce the interval to scan if the position angle of the secondary has almost span an entire cycle. As a matter of illustration, a bundle of $\approx 7\,500$ orbits, with 4% efficiency in the trial/error throw (period range $P \in [10; 70]$ days), has been obtained for the data analysis of the trans-Neptunian (136108) Haumea's second satellite Namaka, with no particular optimisation, in 40 s real time on a personal laptop.

10.4 Astrometric binary

Let us briefly mention in this last paragraph a subset of problem closely related to resolved or visual binaries: the astrometric binaries. The first detection of such systems was made by Bessel [7] from his analysis of the abnormal proper motions of Sirius and Procyon. Luminosity, as he said, is not a straight propriety of stellar mass[31]. Astrometric binaries are binary system for which both components are not observed separately (either the secondary is to faint to be detected in the instrument, or similarly it is too close to the bright primary), but instead one observes the photocentre of the system. This photocenter differs periodically from the centre of mass with an amplitude that depends on the mass ratio for the position of the barycenter, the brightness distribution and ratio for the position of the photocentre, and the inclination of the orbit [116, 1]. What is observed is not the Keplerian orbit a but the photometric orbit α which are related by:

$$f = \alpha/a + \beta \quad ; \quad \beta = (1 + 10^{0.4\Delta V})^{-1} \tag{64}$$

where f is the fractional mass, β the fractional light. The photometric orbit is thus scaled from the Keplerian one by $(f - \beta)$. In the case of a stellar system one will consider particular mass-luminosity relation [42], a key parameter that links mass and luminosity. In the case of solar system objects; considering that both components are spherical with same albedo and there is no strong phase effect, the relative position of the barycenter and photocentre is given as a function of mass ratio $0 < q \leq 1$:

$$\alpha = \left(\frac{1}{1 + q^{-2/3}} - \frac{1}{1 + q^{-1}} \right) a \tag{65}$$

It can be seen from the equations above, that there is no astrometric signal in the two extreme cases $q = 0$ and $q = 1$, the peak being at $q \sim 0.15$. One can put this additional parameter in the Monte Carlo run for resolved binaries, having now two dimensions (P, q) to explore which remains tractable. In the case of asteroids, and if one solution orbit exists, one will end-up with a possible separation that will have to be compared to prior knowledge. If the separation is relatively large it can plausibly be a binary system, if the 'separation' is small, it will likely be a non-symmetric single object.

In contrast to the situation in the main-belt (and assumed as such by us) where multiple systems involve mostly small moonlet, or in the Near-Earth region where separations are small making them difficult to distinguish from a single body, the trans-Neptunian and Centaur binaries can have much larger separation and mass ratio, well in the detection range for modern astrometric observations. The other parameter of importance in this study is the orbital period which can be large [86]. Given the ratio of known (resolved) binaries in TNO population, one could follow the statement of Bessel for stars [63] and wondering how many targets should be suspicious of being binaries in our outer Solar System?

11 Conclusion

Starting with the Hipparcos catalogue birthday, we have reviewed in this lecture the different aspects of the Gaia mission, its payload, its instruments and observations,

[31] Let us add that it seems to be the same for the matter in the Universe...

and the results to be expected from the direct observations of asteroids. From the highly accurate astrometry and photometry gathered over the five years mission duration, Gaia will provide a breakthrough in our knowledge of these bodies and subsequently on the formation of the Solar System and its dynamical evolution. Gaia will provide a wealth of data and results from the direct observations (photometric in many bands from the low-resolution spectra, astrometric and imaging; the high resolution spectroscopy is very marginal) of asteroids and small bodies of the Solar System. We will have a clearer view of their dynamical and physical characteristics, for an incredibly and yet unprecedented number of objets of different kinds. One of the high impact is obtained from the large number of targets observed, from which one will get simultaneously sharp information and large statistical analysis, all programs that could not be achieved by a single team from ground-based observations, or a space probe rendez-vous, and surely not over such short time span of observations.

Moreover Gaia will also provide a new area in asteroids and small bodies science from astrometric catalogue of stars. The current—and severe—limitation to the use of the Hipparcos or Tycho2 astrometric catalogues in the reduction of photographic or CCD plates is their poor numbers of star or low density: there are tiny chances to have one Hipparcos star in a typical 12'x12' field of view, but this is useless because at least three are needed. The situation will be considerably improved with Gaia, so that next generation post-Gaia era astrometry will have a gain of one order of magnitude in the classical astrometric reductions. Surveys that go to deeper magnitudes (Pan-STARRS, LSST, ...) will dramatically benefit of the Gaia astrometric catalogue. Similarly the computations of both asteroids and stars ephemeris will be increased, yielding much more accurate stellar occultation predictions for different kinds of bodies, MBAs to TNOs, with our without atmospheres, and again a huge step in our understanding in the physical characteristic of small and faint bodies that were even not observable with Gaia.

Acknowledgments

The authors wish to thank Marco Delbò (OCA, Nice) and Serge Mouret (IMCCE, Paris) for their various contributions and help, thanks to undergraduate students who also took part to the project, and the members of the Gaia-CU4/SSO and Gaia-REMAT at large. We also acknowledge Marc Fouchard (IMCCE, Paris) for his careful reading of the manuscript and improving the quality of the text. Let us express our gratitude to the editors and also organisers of this school in Bad Hofgastein (Austria).

Acronyms

AF	Astrometric Field
BP/RP	Blue/Red Photometry
CCD	Charge-Coupled Device
CTE	Charge Transfer Efficiency
PSF	Point Spread Function
RVS	Radial Velocity Spectrometer
SM	Sky Mapper
TDI	Time Delayed Integration
GLS	General Least Squares
GR	General Relativity
LLS	Linear Least Squares
mas	milli-arcsecond
MCMC	Monte Carlo Markov Chain
MLE	Maximum Likelihood Estimator
O-C	Observed-minus-Calculated
ODE	Ordinary Differential Equation
p.d.f.	probability distribution function
PPN	Parameterized Post-Newtonian
SNR	Signal-to-noise ratio
SVD	Singular Value Decomposition
TI	Thermal inertia
FK5	Fundamental Katalog, 5th version
ICRF	International Celestial Reference Frame
IAU/UAI	International Astronomical Union – Union Astronomique Internationale
LSST	Large-Aperture Synoptic Survey Telescope
MBA	Main Belt Object
MBB	Main Belt Binary
NEO	Near-Earth Object
QSO	Quasi Stellar Object
SSO	Solar System Object
SSSB	Small Solar System Bodies
TNB	Trans-Neptunian Binary
TNO	Trans-Neptunian Object

References

1. R. G. Aitken. *The binary stars*. New York: Dover Publication, 1964, 1964.
2. F. Arago. *Les comètes*. Astronomie Populaire. A. Blanchard, Paris;, livre xvii, nouveau tirage edition, 1986. (1st ed. 1858).
3. Y. Avni. Energy spectra of X-ray clusters of galaxies. *Astrophysical Journal*, 210:642–646, December 1976.
4. J. Bange. An estimation of the mass of asteroid 20-massalia derived from the hipparcos minor planets data. *Astronomy & Astrophysics*, 340:L1–L4, 1998.
5. Y. V. Batrakov, Y. A. Chernetenko, G. K. Gorel, and L. A. Gudkova. Hipparcos catalogue orientation as obtained from observations of minor planets. *Astronomy & Astrophysics*, 352:703–711, 1999.

6. I. N. Belskaya, Y. G. Shkuratov, Y. S. Efimov, N. M. Shakhovskoy, R. Gil-Hutton, A. Cellino, E. S. Zubko, A. A. Ovcharenko, S. Y. Bondarenko, V. G. Shevchenko, S. Fornasier, and C. Barbieri. The F-type asteroids with small inversion angles of polarization. *Icarus*, 178:213–221, November 2005.
7. F. W. Bessel. Extract of a letter from on the proper motions of Procyon and Sirius. *M.N.R.A.S.*, 6:136–141, December 1844.
8. G. Beutler. *Methods of celestial mechanics*. Astronomy and Astrophysics Library. Berlin: Springer. In cooperation with Leos Mervart and Andreas Verdun, 2005.
9. R. P. Binzel. Hemispherical color differences on Pluto and Charon. *Science*, 241:1070–1072, August 1988.
10. W. F. Bottke, A. Morbidelli, R. Jedicke, J. M. Petit, H. F. Levison, P. Michel, and T. S. Metcalfe. Debiased Orbital and Absolute Magnitude Distribution of the Near-Earth Objects. *Icarus*, 156:399–433, 2002.
11. E. Bowell, J. Virtanen, K. Muinonen, and A. Boattini. Asteroid Orbit Computation. *Asteroids III*, pages 27–43, 2002.
12. D. T. Britt, D. Yeomans, K. Housen, and G. Consolmagno. Asteroid Density, Porosity, and Structure. In *Asteroids III, W. F. Bottke Jr., A. Cellino, P. Paolicchi, and R. P. Binzel (eds), University of Arizona Press, Tucson*, pages 485–500, 2002.
13. D. Brouwer and G. M. Clemence. *Methods of celestial mechanics*. New York: Academic Press, 1961.
14. S. J. Bus and R. P. Binzel. Phase II of the Small Main-Belt Asteroid Spectroscopic SurveyThe Observations. *Icarus*, 158:106–145, July 2002.
15. O.. Bykov. Initial orbit determinations of neo-2005 with pulkovo amp-method. In *MEOTUS Conf., Paris, France*, 2006.
16. F. Capaccioni, P. Cerroni, M. Coradini, P. Farinella, E. Flamini, G. Martelli, P. Paolicchi, P. N. Smith, and V. Zappala. Shapes of asteroids compared with fragments from hypervelocity impactexperiments. *nature*, 309:832–834, June 1984.
17. A. Celletti and G. Pinzari. Four Classical Methods for Determining Planetary Elliptic Elements: A Comparison. *Celestial Mechanics and Dynamical Astronomy*, 93:1–52, September 2005.
18. A. Cellino. Minor Bodies: Spectral Gradients and Relationships with Meteorites. *Space Science Reviews*, 92:397–412, April 2000.
19. A. Cellino, S. J. Bus, A. Doressoundiram, and D. Lazzaro. Spectroscopic Properties of Asteroid Families. *Asteroids III*, pages 633–643, 2002.
20. A. Cellino, P. Tanga, A. Dell'Oro, and D. Hestroffer. Asteroid science with Gaia: Sizes, spin properties, overall shapes and taxonomy. *Advances in Space Research*, 40:202–208, 2007.
21. A. Cellino, V. Zappalà, A. Doressoundiram, M. di Martino, P. Bendjoya, E. Dotto, and F. Migliorini. The Puzzling Case of the Nysa-Polana Family. *Icarus*, 152:225–237, August 2001.
22. Y. A. Chernetenko. Orientation of the hipparcos frame with respect to the reference frames of the DE403/LE403 and DE405/LE405 ephemerides based on asteroid observations. *Astronomy Letters*, 34:266–270, April 2008.
23. S. R. Chesley, D. Vokrouhlický, S. J. Ostro, L. A. M. Benner, J.-L. Margot, R. L. Matson, M. C. Nolan, and M. K. Shepard. Direct Estimation of Yarkovsky Accelerations on Near-Earth Asteroids. *LPI Contributions*, 1405:8330, 2008.

24. W. D. Cochran, M. Endl, R. A. Wittenmyer, and J. L. Bean. A Planetary System around HD 155358: The Lowest Metallicity Planet Host Star. *Astrophysical Journal*, 665:1407–1412, August 2007.
25. R. Deutsch. *Orbital dynamics of space vehicles.* Prentice-Hall International Series in Space technologies. Prentice Hall Inc., 1963.
26. R. P. di Sisto and R. B. Orellana. Determinación de posiciones de asteroides utilizando el catálogo Hipparcos. *Boletin de la Asociacion Argentina de Astronomia La Plata Argentina*, 43:8–13, 1999.
27. A. D. Dubyago. *The Determination of Orbits.* New York: The Macmillan Company, 1961, 1961.
28. D. W. Dunham, E. Goffin, J. Manek, M. Federspiel, R. Stone, and W. Owen. Asteroidal occultation results multiply helped by Hipparcos. *Memorie della Societa Astronomica Italiana*, 73:662–+, September 2002.
29. R. Dvorak and C. Edelman. Statistical method for the determination of asteroid and satellite orbits. *Astronomy & Astrophysics*, 77:320–326, August 1979.
30. P. R. Escobal. *Methods of orbit determination.* New York: Wiley, 1965.
31. P. Exertier and D. Coulot. L'Intégration Numérique en Calcul d'Orbites. Technical report, Cours de l'Ecole GRGS 2002, http://igsac-cnes.cls.fr/documents/gins/GINS_Doc_Algo_V4.html, 2002.
32. P. Farinella, P. Paolicchi, E. F. Tedesco, and V. Zappalà. Triaxial equilibrium ellipsoids among the asteroids. *Icarus*, 46:114–123, 1981.
33. P. Farinella, P. Paolicchi, and V. Zappalà. The asteroids as outcomes of catastrophic collisions. *Icarus*, 52:409–433, 1982.
34. A. Fienga, H. Manche, J. Laskar, and M. Gastineau. INPOP06: a new numerical planetary ephemeris. *Astronomy & Astrophysics*, 477:315–327, January 2008.
35. C. F. Gauss. Carl Friedrich Gauss' Werke Hereausgeber von der Königl. Gesellschaft der Wissenschaften zu Göttingen. *Astronomische Nachrichten*, 57:53–54, 1862.
36. C. F. Gauss. *Théorie du mouvement des corps célestes parcourant des sections coniques autour du soleil / trad. du "Theoria motus" de Gauss ; suivie de notes, par Edmond Dubois.* Paris : A. Bertrand, 1855; trad. E.-P. Dubois; in 8., 1864.
37. K. F. Gauss. *Theoria motvs corporvm coelestivm in sectionibvs conicis solem ambientivm.* Hambvrgi, Svmtibvs F. Perthes et I. H. Besser, 1809., 1809.
38. K. F. Gauss. *Theory of the motion of the heavenly bodies moving about the sun in conic section / translated and with Appendix by C. H. Davis.* New York: Dover, 1963, 1963.
39. G. H. Golub and C. F. van Loan. *Matrix computations.* Baltimore : Johns Hopkins University Press, 1996. (Johns Hopkins studies in the mathematical sciences), 1996.
40. W. M. Grundy, K. S. Noll, J. Virtanen, K. Muinonen, S. D. Kern, D. C. Stephens, J. A. Stansberry, H. F. Levison, and J. R. Spencer. (42355) Typhon–Echidna: Scheduling observations for binary orbit determination. *Icarus*, 197:260–268, September 2008.
41. P. Gurfil and S. Belyanin. The gauge-generalized Gyldén–Meshcherskii Problem. *Advances in Space Research*, 42:1313–1317, October 2008.
42. W. D. Heintz. *Double stars /Revised edition/*, volume 15 of *Geophysics and Astrophysics Monographs.* Reidel Publishing Company, 1978.

43. D. Hestroffer. *Astrométrie et photométrie des astéroïdes observés par le satellite Hipparcos. Apport à l'élaboration d'un système de référence dynamique.* PhD thesis, Paris Observatory, France, 1994.
44. D. Hestroffer. Photocentre displacement of minor planets: analysis of HIPPARCOS astrometry. *Astronomy & Astrophysics*, 336:776–781, 1998.
45. D. Hestroffer and J. Berthier. Determination of the PPN beta and Solar quadrupole from Asteroid Astrometry. In *ESA SP-576: The Three-Dimensional Universe with Gaia*, pages 297–300, January 2005.
46. D. Hestroffer and F. Mignard. Photometry with a periodic grid. I. A new method to derive angular diameters and brightness distribution. *Astronomy & Astrophysics*, 325:1253–1258, 1997.
47. D. Hestroffer, B. Morando, E. Hog, J. Kovalevsky, L. Lindegren, and F. Mignard. The HIPPARCOS solar system objects catalogues. *Astronomy & Astrophysics*, 334:325–336, 1998.
48. D. Hestroffer, S. Mouret, J. Berthier, and F. Mignard. Relativistic Tests from the Motion of the Asteroids. In H. Kleinert, R. T. Jantzen, and R. Ruffini, editors, *The Eleventh Marcel Grossmann Meeting. On recent developments in theoretical and experimental general relativity, gravitation and relativistic field theories*, November 2008.
49. D. Hestroffer and P. Tanga. Asteroids from Observations to Models. In J. Souchay, editor, *Dynamics of Extended Celestial Bodies and Rings*, volume 682 of *Lecture Notes in Physics, Berlin Springer Verlag*, pages 89–+, 2006.
50. D. Hestroffer, B. Viateau, and M. Rapaport. Minor planets ephemerides improvement. from joint analysis of hipparcos and ground-based observations. *Astronomy & Astrophysics*, 331:1113–1118, 1998.
51. J. L. Hilton. Asteroid Masses and Densities. In *Asteroids III, W. F. Bottke Jr., A. Cellino, P. Paolicchi, and R. P. Binzel (eds), University of Arizona Press, Tucson*, pages 103–112, 2002.
52. E. Hoeg and C. Fabricius. Sampling in the new MBP. Technical report, GAIA Technical Report, GAIA-CUO-139, 2004.
53. M. Kaasalainen, D. Hestroffer, and P. Tanga. Physical Models and Refined Orbits for Asteroids from Gaia Photometry and Astrometry. In *ESA SP-576: The Three-Dimensional Universe with Gaia*, pages 301–+, January 2005.
54. M. Kaasalainen, S. Mottola, and M. Fulchignoni. Asteroid models from disk-integrated data. In *Asteroids III, W. F. Bottke Jr., A. Cellino, P. Paolicchi, and R. P. Binzel (eds), University of Arizona Press, Tucson*, pages 139–150, 2002.
55. M. Kaasalainen and P. Tanga. Photocentre offset in ultraprecise astrometry: Implications for barycentre determination and asteroid modelling. *Astronomy & Astrophysics*, 416:367–373, March 2004.
56. C. Kholchevnikov and M. Fracassini. Le problème des deux corps avec G variable selon l'hypothèse de Dirac. *Conf. Oss. Astron. Milano-Merate, Ser. I, No. 9, 50 p.*, 9, 1968.
57. J. Kovalevsky. *Astrométrie moderne*, volume 358 of *Lecture Notes in Physics, Berlin Springer Verlag.* Springer Verlag, 1990.
58. J. Kovalevsky. *Modern Astrometry.* Astronomy and astrophysics library. Springer, Berlin, New York:, 2nd edition, 2002.
59. M. Lampton, B. Margon, and S. Bowyer. Parameter estimation in X-ray astronomy. *Astrophysical Journal*, 208:177–190, August 1976.

60. E. A. Lee, S. A. Astakhov, and D. Farrelly. Production of trans-Neptunian binaries through chaos-assisted capture. *M.N.R.A.S.*, 379:229–246, July 2007.
61. T. Leonard and S. J. John. *Bayesian Methods*, volume 4 of *Cambridge series in Statistical and Probabilistic Mathematics*. Cambridge University Press, 1999.
62. L. Lindegren. Meridian observations of planets with a photoelectric multislit micrometer. *Astronomy & Astrophysics*, 57:55–72, 1977.
63. S. L. Lippincott. Astrometric search for unseen stellar and sub-stellar companions to nearby stars and the possibility of their detection. *Space Science Reviews*, 22:153–189, July 1978.
64. M. Lœwy. *Détermination des orbites des comètes*. Gauthier-Villars, Paris, 1872.
65. P. Magnusson, M. A. Barucci, J. D. Drummond, K. Lumme, and S. J. Ostro. Determination of pole orientations and shapes of asteroids. In *Asteroids II*, pages 67–97, 1989.
66. W. B. McKinnon. Could Ceres be a Refugee from the Kuiper Belt? *Asteroids, Comets, Meteors 2008 held July 14-18, 2008 in Baltimore, Maryland. LPI Contributions*, 1405:8389, 2008.
67. W. J. Merline, S. J. Weidenschilling, D. Durda, J.-L. Margot, P. Pravec, and A. D. Storrs. Asteroids *do* have satellites. In *Asteroids III, W. F. Bottke Jr., A. Cellino, P. Paolicchi, and R. P. Binzel (eds), University of Arizona Press, Tucson*, pages 289–312, 2002.
68. J. Mestschersky. Über die Integration der Bewegungsgleichungen im Probleme zweier Körper von veränderlicher Masse. *Astronomische Nachrichten*, 159:229–242, September 1902.
69. F. Mignard. Overall Science Goals of the Gaia Mission. In *ESA SP-576: The Three-Dimensional Universe with Gaia*, pages 5–+, January 2005.
70. F. Mignard, A. Cellino, K. Muinonen, P. Tanga, M. Delbò, A. Dell'Oro, M. Granvik, D. Hestroffer, S. Mouret, W. Thuillot, and J. Virtanen. The Gaia Mission: Expected Applications to Asteroid Science. *Earth Moon and Planets*, 101:97–125, December 2007.
71. C. W. Misner, K. S. Thorne, and J. A. Wheeler. *Gravitation*. San Francisco: W.H. Freeman and Co., 1973, 1973.
72. D. Morrison and M. S. Matthews. *Satellites of Jupiter*. Space Science Series, Tucson: University of Arizona Press, 1982, edited by Morrison, David; Matthews, Mildred Shapley (ass.), 1982.
73. L. V. Morrison, D. Hestroffer, D. B. Taylor, and F. van Leeuwen. Check on JPL DExxx Using HIPPARCOS and TYCHO Observations. *Highlights in Astronomy*, 11:554+, 1998.
74. S. Mouret. *Investigations on the dynamics of minor planets with Gaia*. PhD thesis, Observatoire de Paris, 2007.
75. S. Mouret, D. Hestroffer, and F. Mignard. Asteroid mass determination with the Gaia mission. In G. B. Valsecchi and D. Vokrouhlický, editors, *IAU Symposium*, volume 236 of *IAU Symposium*, pages 435–438, 2007.
76. S. Mouret, D. Hestroffer, and F. Mignard. Asteroid masses and improvement with Gaia. *Astronomy & Astrophysics*, 472:1017–1027, September 2007.
77. S. Mouret, D. Hestroffer, and F. Mignard. Asteroid mass determination with the Gaia mission. *IAU Symposium*, 248:363–366, 2008.
78. S. Mouret, D. Hestroffer, and F. Mignard. Asteroid mass determination with the Gaia mission. A simulation of the expected precisions. *Planet. Space Sci.*, 56:1819–1822, November 2008.

79. K. S. Noll, W. M. Grundy, E. I. Chiang, J.-L. Margot, and S. D. Kern. Binaries in the Kuiper Belt. In *The Solar System Beyond Neptune*, pages 345–363, 2008.
80. T. Oppolzer. *Lehrbuch zur Bahnbestimmung der Kometen und Planeten*. W. Engelmann, Leipzig, 1882.
81. T. Oppolzer. *Traité de la détermination des orbites des Comètes et des Planètes*. Gauthier-Villars, Paris; E. Pasquier trad., 1886.
82. F. Pepe, A. C. M. Correia, M. Mayor, O. Tamuz, J. Couetdic, W. Benz, J.-L. Bertaux, F. Bouchy, J. Laskar, C. Lovis, D. Naef, D. Queloz, N. C. Santos, J.-P. Sivan, D. Sosnowska, and S. Udry. The HARPS search for southern extra-solar planets. VIII. μ Arae, a system with four planets. *Astronomy & Astrophysics*, 462:769–776, February 2007.
83. M. A. C. Perryman, K. S. de Boer, G. Gilmore, E. Høg, M. G. Lattanzi, L. Lindegren, X. Luri, F. Mignard, O. Pace, and P. T. de Zeeuw. GAIA: Composition, formation and evolution of the Galaxy. *Astronomy & Astrophysics*, 369:339–363, 2001.
84. M. A. C. Perryman and ESA, editors. *The HIPPARCOS and TYCHO catalogues. Astrometric and photometric star catalogues derived from the ESA HIPPARCOS Space Astrometry Mission*, volume 1200 of *ESA Special Publication*. ESA, 1997.
85. M.A.C. Perryman. *Astronomical Applications of Astrometry: A Review Based on Ten Years of Exploitation of the Hipparcos Satellite Data*. Cambridge University Press, 2008.
86. J.-M. Petit, J. J. Kavelaars, B. J. Gladman, J. L. Margot, P. D. Nicholson, R. L. Jones, J. W. Parker, M. L. N. Ashby, A. Campo Bagatin, P. Benavidez, J. Coffey, P. Rousselot, O. Mousis, and P. A. Taylor. The Extreme Kuiper Belt Binary 2001 QW_322. *Science*, 322:432–434, October 2008.
87. L. Picart. *Calcul des orbites et des éphémérides*. Paris : Octave Doin et fils ; Encyclopédie scientifique, 1913.
88. E. V. Pitjeva. Relativistic Effects and Solar Oblateness from Radar Observations of Planets and Spacecraft. *astronomy Letters*, 31:340–349, 2005.
89. H. Poincaré. Mémoires et observations. Sur la détermination des orbites par la méthode de Laplace. *Bulletin Astronomique, Serie I*, 23:161–187, 1906.
90. A. Pospieszalska-Surdej and J. Surdej. Determination of the pole orientation of an asteroid - The amplitude-aspect relation revisited. *Astronomy & Astrophysics*, 149:186–194, August 1985.
91. W. H. Press, S. A. Teukolsky, W. T. Vetterling, and B. P. Flannery. *Numerical recipes in FORTRAN. The art of scientific computing*. Cambridge: University Press, —c1992, 2nd ed., 1992.
92. R. Radau. Mémoires et observations. Sur la détermination des orbites. *Bulletin Astronomique, Serie I*, 2:5–15, 1885.
93. A. E. Roy. *Orbital motion*. IoP, Bristol and Philadelphia, fourth edition edition, 2005.
94. D. P. Rubincam. Yarkovsky thermal drag on LAGEOS. *JGR*, 93:13805–13810, 1988.
95. D. P. Rubincam. Yarkovsky thermal drag on small asteroids and Mars-Earth delivery. *JGR*, 103:1725–+, January 1998.
96. F. Safa. A summary of the Gaia spacecraft design. Technical report, GAIA Technical Report, GAIA-CH-TN-EADS-FS-001-1, 2006.

97. P. K. Seidelmann, B. A. Archinal, M. F. A'Hearn, A. Conrad, G. J. Consolmagno, D. Hestroffer, J. L. Hilton, G. A. Krasinsky, G. Neumann, J. Oberst, P. Stooke, E. F. Tedesco, D. J. Tholen, P. C. Thomas, and I. P. Williams. Report of the IAU/IAG Working Group on cartographic coordinates and rotational elements: 2006. *Celestial Mechanics and Dynamical Astronomy*, 98:155–180, July 2007.
98. M. Shao. SIM: the space interferometry mission. In R. D. Reasenberg, editor, *Proc. SPIE Vol. 3350, p. 536-540, Astronomical Interferometry, Robert D. Reasenberg; Ed.*, volume 3350 of *Presented at the Society of Photo-Optical Instrumentation Engineers (SPIE) Conference*, pages 536–540, July 1998.
99. M. Shao. Science overview and status of the SIM project. In W. A. Traub, editor, *New Frontiers in Stellar Interferometry, Proceedings of SPIE Volume 5491. Edited by Wesley A. Traub. Bellingham, WA: The International Society for Optical Engineering, 2004., p.328*, volume 5491 of *Presented at the Society of Photo-Optical Instrumentation Engineers (SPIE) Conference*, pages 328–+, October 2004.
100. B. Simon. How kepler determined the orbit of the earth around the sun (French Title: Comment kepler a determiné l'orbite de la Terre autour du Soleil). *Observations et Travaux*, 62:23–25, June 2006.
101. S. Söderhjelm and L. Lindegren. Inertial Frame Determination Using Minor Planets. a Simulation of Hipparcos-Observations. *Astronomy & Astrophysics*, 110:156–162, 1982.
102. R. C. Stone, D. G. Monet, A. K. B. Monet, F. H. Harris, H. D. Ables, C. C. Dahn, B. Canzian, H. H. Guetter, H. C. Harris, A. A. Henden, S. E. Levine, C. B. Luginbuhl, J. A. Munn, J. R. Pier, F. J. Vrba, and R. L. Walker. Upgrades to the Flagstaff Astrometric Scanning Transit Telescope: A Fully Automated Telescope for Astrometry. *Astronomical Journal*, 126:2060–2080, October 2003.
103. P. Tanga and M. Delbo. Asteroid occultations today and tomorrow: toward the GAIA era. *Astronomy & Astrophysics*, 474:1015–1022, November 2007.
104. P. Tanga, M. Delbò, D. Hestroffer, A. Cellino, and F. Mignard. Gaia observations of Solar System objects: Impact on dynamics and ground-based observations. *Advances in Space Research*, 40:209–214, 2007.
105. P. Tanga, D. Hestroffer, M. Delbò, J. Frouard, S. Mouret, and W. Thuillot. Gaia, an unprecedented observatory for Solar System dynamics. *Planet. Space Sci.*, 56:1812–1818, November 2008.
106. B. D. Tapley, B.E. Schutz, and G.H. Born. *Statistical Orbit Determination*. Elsevier Academic Press, 2004.
107. A. Tarantola. *Inverse Problem Theory. Methods for Model Parameters Estimation*. SIAM, Philadelphia, 2005.
108. E. F. Tedesco, P. V. Noah, M. Noah, and S. D. Price. The Supplemental IRAS Minor Planet Survey. *Astronomical Journal*, 123:1056–1085, 2002.
109. T. N. Thiele. Neue Methode zur Berechnung von Doppelsternbahnen. *Astronomische Nachrichten*, 104:245–254, 1883.
110. D. J. Tholen, M. W. Buie, R. P. Binzel, and M. L. Frueh. Improved orbital and physical parameters for the Pluto-Charon system. *Science*, 237:512–514, July 1987.
111. W. Thuillot, J. Berthier, J. Vaubaillon, F. Vachier, J. Iglesias, and V. Lainey. Data mining for the improvement of orbits of the NEOs. In *IAU Symposium*, volume 236 of *IAU Symposium*, August 2006.

112. F. Tisserand. Mémoires et observations. Sur la détermination des orbites circulaires. *Bulletin Astronomique, Serie I*, 12:53–59, 1895.
113. F. Tisserand. *Traité de mécanique céleste. Perturbations des planètes d'après la méthode de la variation des constantes arbitraires*, volume 1. Gauthier-Villars, Paris; 2nd edition, 1960. (1st ed. 1889).
114. F. Tisserand and J. Perchot. *Leçons sur la détermination des orbites.* Gauthier-Villars, Paris, 1899.
115. G. B. Valsecchi. 236 years ago... In G. B. Valsecchi and D. Vokrouhlický, editors, *IAU Symposium*, volume 236 of *IAU Symposium*, pages D17+, 2007.
116. P. van de Kamp. Unseen astrometric companions of stars. *Annual Review of Astronomy and Astrophysics*, 13:295–333, 1975.
117. F. van Leeuwen. *Hipparcos, the New Reduction of the Raw Data.* Astrophysics and Space Science Library. Vol. 350 20 Springer Dordrecht, 2007.
118. B. Viateau. *Apport des observations faites à Bordeaux à l'amélioration des orbites des astéroïdes. Utilisation de ces orbites.* PhD thesis, PhD Thesis, Observatoire de Paris (in French), January 1995.
119. J. Virtanen. *Asteroid orbital inversion using statistical methods.* PhD thesis, University of Helsinki, Finland, 2005.
120. J. Virtanen, K. Muinonen, and E. Bowell. Statistical Ranging of Asteroid Orbits. *Icarus*, 154:412–431, 2001.
121. D. Vokrouhlicky. Diurnal Yarkovsky effect as a source of mobility of meter-sized asteroidal fragments. I. Linear theory. *Astronomy & Astrophysics*, 335:1093–1100, July 1998.
122. J. V. Wall and C. R. Jenkins. *Practical Statistics for Astronomers.* Cambridge University Press, November 2003.
123. C. M. Will. The Confrontation between General Relativity and Experiment. *Living Reviews in Relativity*, 9, March 2006.
124. C. M. Will. The Confrontation Between General Relativity and Experiment. In A. Oscoz, E. Mediavilla, and M. Serra-Ricart, editors, *EAS Publications Series*, volume 30 of *EAS Publications Series*, pages 3–13, 2008.
125. C. M. Will and K. J. Nordtvedt. Conservation Laws and Preferred Frames in Relativistic Gravity. I. Preferred-Frame Theories and an Extended PPN Formalism. *Astrophysical Journal*, 177:757–774, November 1972.
126. J. G. Williams, S. G. Turyshev, and D. H. Boggs. Progress in Lunar Laser Ranging Tests of Relativistic Gravity. *Physical Review Letters*, 93(26):261101–1–261101–4, December 2004.
127. J. S. Young, J. E. Baldwin, R. C. Boysen, C. A. Haniff, D. Pearson, J. Rogers, D. St-Jacques, P. J. Warner, and D. M. A. Wilson. Measurements of the changes in angular diameter of mira variables with pulsation phase. In *IAU Symp. 191: Asymptotic Giant Branch Stars*, volume 191, pages 145+, 1999.